

## **Production, Processing and Assembly of Carbon Nanotubes**

by  
Huazhi Geng

A dissertation submitted to the faculty of the University of North Carolina at Chapel Hill  
in partial fulfillment of the requirement for the degree of Doctor of Philosophy in the  
Curriculum in Applied and Materials Sciences.

Chapel Hill  
2006

Approved by  
  
Adviser: Professor Otto Zhou  
  
Reader: Professor Sean Washburn  
  
Reader: Professor Lu-Chang Qin  
  
Reader: Professor Olin D. Velev  
  
Reader: Professor Jie Liu

© 2006  
Huazhi Geng  
ALL RIGHTS RESERVED

## ABSTRACT

Huaizhi Geng: Production, Processing and Assembly of Carbon Nanotubes  
(Under the direction of Professor Otto Zhou)

This dissertation reports the development of a method to achieve continuous production of carbon nanotubes. The as produced carbon nanotubes were purified and further processed to tune their properties. Then dielectrophoresis as a versatile technique was used to manipulate and assemble carbon nanotubes into functional structures.

In the processing part, purified carbon nanotubes are treated with strong acid then annealed at different temperatures. Combined TEM and NMR studies show that tips of SWNTs in bulk quantities can be uniformly opened by oxidation and closed by vacuum annealing at a surprisingly low temperature. The results provide a guideline on how the SWNTs should be processed for potential energy storage applications.

In the assembly part, first, the results of a systematic study on the interactions of CNTs suspended in media of various viscosities and ionic conductivities with an AC field of different frequencies were reported. Then the feasibility of utilizing the dielectrophoresis for controlled assembling of functional CNT structures was explored. Finally, the automated process of assembling CNT fibrils unto sharp probes was realized and a precise control over the process was especially studied.

## **ACKNOWLEDGMENTS**

First of all, I would like to thank Dr. Otto Zhou, for being a great teacher and advisor, for constant support and encouragements on my study and research. It is him who introduced me to the field and whose enthusiasm has been a daily source of inspiration. It is also his continuous encouragement, great consideration and patience that make this work possible.

It has been a privilege to work with so many talented people in Dr. Zhou's research group. I am grateful to several formal and current group members. They are, Dr. B. Gao, Dr. L. Fleming, Dr. H. Shimoda, Dr. J. Zhang, Mr. Q. Qiu , Dr. S. Oh., Ms. R. Rajaram, Ms. X. Calderon and Mr. D. Bordelon.

Finally, I want to thank the people who are such an integral part of my life, my husband Xuebin Yang and my parents, for their unconditional love, understanding, and patience. They have been terrific.

## TABLE OF CONTENTS

<b>Chapter 1 Introduction.....</b>	<b>1</b>
1.1 Structure and properties of CNTs.....	1
1.1.1 Structure of CNTs.....	1
1.1.2 Properties of CNTs.....	4
1.2 Applications of CNTs.....	6
1.2.1 Nanoprobes and Sensors.....	7
1.2.2 Field Emitters.....	9
1.2.3 Other Applications.....	12
1.3 Conclusions and dissertation overview.....	13
1.4 References.....	15
<b>Chapter 2 Synthesis of carbon nanotubes .....</b>	<b>19</b>
2.1 Introduction.....	19
2.2 Summary of currently used synthesis methods.....	19
2.2.1 Arc Discharge.....	20
2.2.2 Laser Ablation.....	21
2.2.3 Chemical Vapor Deposition.....	24
2.3 The method of Laser-CVD.....	26
2.3.1 The idea of Laser-CVD.....	26

2.3.2 Experiment and Results.....	27
2.4 Summary.....	32
2.5 References.....	33
<b>Chapter 3 Processing of Carbon Nanotubes.....</b>	<b>36</b>
3.1 Introduction.....	36
3.2 Purification and Cutting of carbon nanotubes.....	37
3.2.1 Purification of carbon nanotubes.....	37
3.2.2 Cutting of carbon nanotubes.....	40
3.2.3 Properties of acid treated carbon nanotubes.....	44
3.3 Regraphitization of carbon nanotube by high temperature annealing.....	47
3.3.1 HRTEM analysis .....	48
3.3.2 Gas absorption experiment and Results.....	49
3.4 Summary.....	52
3.5 References.....	53
<b>Chapter 4 Manipulation and assembly of CNTs by Dielectrophoresis.....</b>	<b>55</b>
4.1 Introduction.....	55
4.2 Dielectrophoresis.....	56
4.2.1 Dielectrophoretic Force.....	56
4.2.2 Torque and Alignment .....	59
4.3 Experimental Setup.....	62
4.4 Assembly of CNT structures .....	63
4.4.1 Assembly of CNT fibrils between two facing electrodes.....	64

4.4.2 Assembly of CNT structures according to field configuration.....	68
4.5 A systematic Study on the effects of parameters.....	70
4.5.1 Frequency of AC electrical field.....	70
4.5.2 Ionic conductivity of suspending medium .....	72
4.5.3 Viscosity of suspending medium.....	73
4.5.4 Concentration of the suspention.....	74
4.6 CNT fibrils fabricated by dielectrophoresis .....	75
4.6.1 Fabrications of CNT fibrils.....	75
4.6.2 Applications of CNT fibrils.....	77
4.7 Conclusions.....	79
4.8 References.....	80
<b>Chapter 5 Automation and Optimization of the Fabrication of CNT fibrils.....</b>	<b>82</b>
5.1 Introduction.....	82
5.2 Problems of the Original Experimental Setups and Solutions .....	84
5.3 Automation of the Process.....	87
5.3.1 Experimental setup.....	87
5.3.2 Change in capacitance of the system.....	89
5.3.3 Labview Program.....	91
5.4 Parameter study using the automated experimental setup.....	93
5.4.1 Effects of Waiting time .....	94
5.4.2 Effects of Voltage.....	96
5.4.3 Effects of Retraction speed.....	99

5.5 Summary.....	100
5.6 References.....	102

# **Chapter 1 Introduction**

## **1.1 Structure and Properties of Carbon nanotubes (CNT)**

The extraordinary mechanical properties, unique electrical properties, chemical and thermal stability and especially the nano-metric sizes and tubular shapes of carbon nanotubes (CNTs) have stimulated extensive research activities across the world since their discovery by Sumio Iijima of the NEC Corporation in 1991. [1] The early researches were focused on production and characterization. While more and more intriguing properties were found about CNTs and relatively efficient synthesis methods for producing CNTs with acceptable qualities were developed, investigations focused on application development have increased in numbers.

### **1.1.1 Structure of CNTs**

Few key studies have explored the structure of carbon nanotubes using high-resolution microscopy techniques. These experiments have confirmed that nanotubes are cylindrical structures based on the hexagonal lattice of carbon atoms that forms crystalline graphite. The fundamental building block of carbon nanotubes is the very long all-carbon cylindrical single

wall nanotube (SWNT), one atom in wall thickness and tens of atoms around the circumference (typical diameter  $\sim 1.4$  nm). (Figure 1.1 a) The primary products of the synthesis of SWNTs are aggregates of individual tubes forming structure akin to ropes of fibers, which are called SWNT bundles. Figure 1.1 b shows the cross section a SWNT bundle. Multiwall nanotubes (MWNT) are a collection of several concentric graphene tubules that are interconnected by van der Waals force, and their total diameter ranges from 5 nm to 50 nm. (Figure 1.1 c)

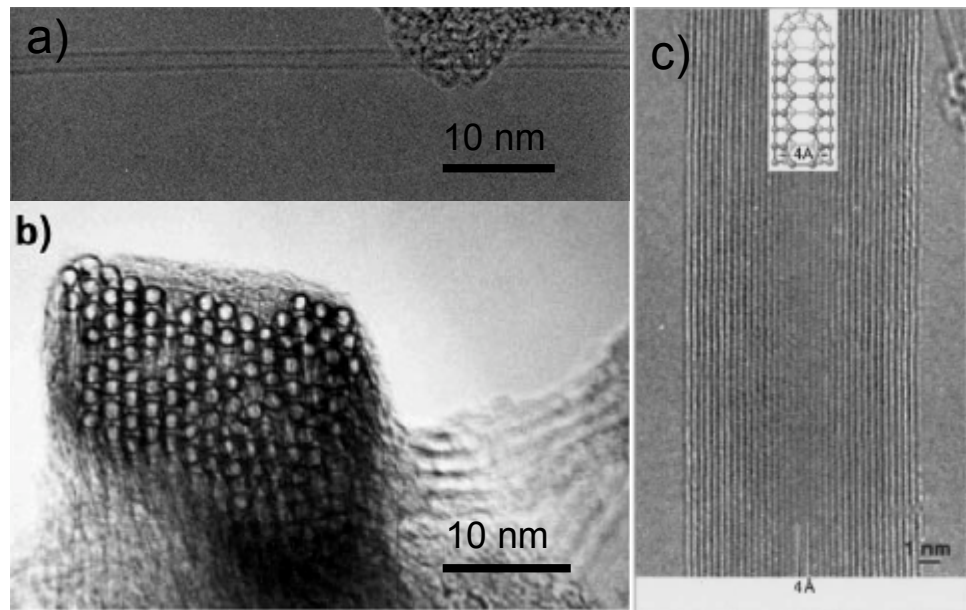


Figure 1.1 High resolution transmission electron microscope pictures of (a) An isolated SWNT [4] (b) Cross section of SWNT bundles. SWNTs produced by laser ablation and arc discharge bundles up because of van der Waals attraction. The cross section forms a triangular lattice structure. The diameter of a bundle is between 10 and 50 nm, corresponding to 30-500 tubes per bundle [3]. (a) MWNT, the inner core can be as small as 0.4 nm [2].

When the graphene sheet is ‘rolled up’ in different angle to form a nanotube, three types of single walled nanotubes are possible. They are called armchair, zigzag and chiral nanotubes respectively. In Figure 1.2, the so-called chiral vector of the nanotube,  $Ch$ , is defined by  $Ch = n\hat{a}_1 + m\hat{a}_2$ , where  $\hat{a}_1$  and  $\hat{a}_2$  are unit vectors in the two-dimensional hexagonal lattice, and  $n$

and  $m$  are integers. Another important parameter is the chiral angle, which is the angle between  $\mathbf{C}_h$  and  $\hat{\mathbf{a}}_1$ . When the graphene sheet is rolled up to form the cylindrical part of the CNT, the ends of the chiral vector meet each other. The chiral vector thus forms the circumference of the CNT's circular cross-section, and different values of  $n$  and  $m$  lead to different CNT structures. Armchair nanotubes are formed when  $n = m$  and the chiral angle is  $30^\circ$  (see Figure 1.2 (a)) Zigzag nanotubes are formed when either  $n$  or  $m$  are zero and the chiral angle is  $0^\circ$  (Figure 1.2 (b)). All other nanotubes, with chiral angles intermediate between  $0^\circ$  and  $30^\circ$  are known as chiral nanotubes (Figure 1.2 (c)). In figure 1.3 (a) shows an armchair SWNT, (b) shows a zigzag SWNT and (c) shows a chiral SWNT.

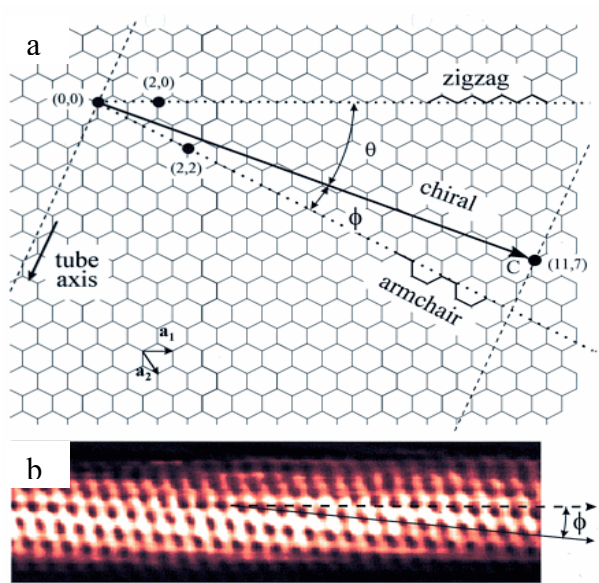


Figure 1.2 Structure of a SWNT related with its chiral vector. (a) A chiral vector  $\mathbf{C}_h = n \mathbf{a}_1 + m \mathbf{a}_2$  is defined on the honeycomb lattice of carbon atoms by unit vector  $\mathbf{a}_1$  and  $\mathbf{a}_2$  and the chiral angle  $\theta$  with respect to the zigzag axis [5], (b) A high resolution scanning tunneling microscopy (STM) image showing the lattice structure of a chiral SWNT. The helical structure is clearly revealed [6].

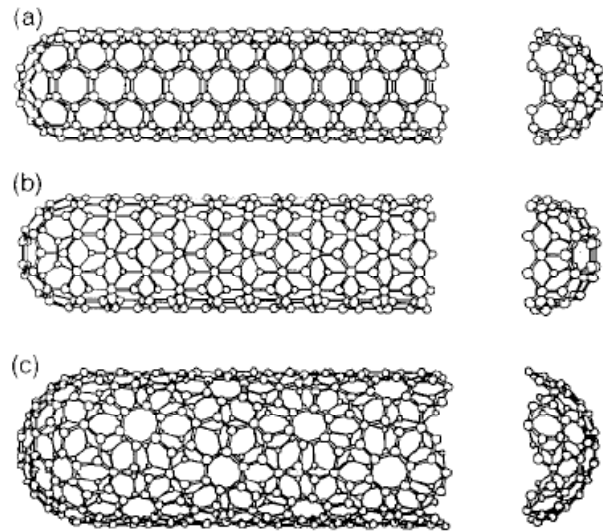


Figure 1.3 Different types of SWNT, (a) an armchair SWNT; (b) a zigzag SWNT; (c) a chiral SWNT [7]

### **1.1.2 Properties of CNTs**

The unique structures of CNTs provide them with many unique properties that attracted tremendous amounts of research and development efforts. The findings have significantly extended our understanding of the fundamental science at the nanometer scale and created the opportunities for future technologies.

First of all, the nanometer size and high aspect ratio structures of CNTs (diameters in nanometers, lengths in microns) together with the unique electronic structure of a graphene sheet make their electronic properties highly unusual. For the perfect tubes, theoretical studies have shown that the electronic properties of the carbon nanotubes are intimately connected to their structure. They can be metallic or semiconducting, depending sensitively on tube diameter and chirality. [8]

From the fundamental physics point of view, SWNTs provide a nearly perfect model system for one-dimensional conductors. Relatively early in the research of nanotubes, Thess *et al.* calculated the resistivity of ropes of metallic SWNTs to be in the order of  $10^{-4} \Omega\text{-cm}$  at 300 K. [2] Which would indicate that the ropes were the most highly conductive carbon fibers known, even factoring in their error in measurement. It is also reported that [9] the stable current density of one arc-produced MWNT was able to reach greater than  $10^7 \text{ A/cm}^2$ . Later, Phaedon Avouris [10] suggested that stable current densities of MWNTs could be pushed as high as  $10^{13} \text{ A/cm}^2$ . Furthermore, electronic transport in metallic SWNTs and MWNTs occurs ballistically (i.e., without scattering) over long tube lengths, enabling them to carry high currents with essentially no heating. [11-14]

Research results suggested an unusually high value thermal conductivity of 6600 W/mK, for an isolated (10, 10) nanotube at room temperature, comparable to the thermal conductivity of a hypothetical isolated graphene monolayer or diamond. [15,16]

The Young's modulus (elastic modulus) of CNTs are calculated to be 1.0 to 1.3 TPa for individual MWNTs and 1.36 to 1.76 TPa nm/d for SWNT of diameter d, while SWNT bundles of 15 to 20 nm in diameter had a modulus of about 100 GPa. [17-22] The maximum tensile strength of a SWNT is close to 30 GPa. On the whole, SWNTs are stiffer than steel and are resistant to damage from physical forces. Pressing on the tip of the CNT will cause it to bend without damage to the tip or the whole CNT. When the force is removed, the tip of the CNT will recover to its original state. [19] Table 1.1 summarizes calculated Young's modulus and tensile strength for (10, 10) SWNT and bundle and MWNT with comparison with other materials.

Table 1.1 Mechanical properties of Nanotubes [23]

	Young's Modulus (GPa)	Tensile Strength (GPa)	Density (g/cm <sup>3</sup> )
MWNT	1200	~150	2.6
SWNT	1054	75	1.3
SWNT bundle	563	~150	1.3
Graphite (in plane)	350	2.5	2.6
Steel	208	0.4	7.8

The porous structure of SWNT bundles and unique electrochemical properties of CNTs also give promising properties as energy storage materials. [24-30]

## 1.2 Applications of CNTs

The unique properties of CNTs produced many potential applications for carbon nanotubes, including conductive and high-strength composites; energy storage and energy conversion devices; sensors; field emission displays and radiation sources; hydrogen storage media; and nanometer-sized semiconductor devices, probes, and interconnects. Some of these applications are now realized in products. Others are demonstrated in early to advanced devices, and one, hydrogen storage, is clouded by controversy. Polydispersity in CNT type, and limitations in processing and assembly methods are important barriers for some applications.

### **1.2.1 Nanoprobes and Sensors**

Scanning probe microscopy (SPM) has become an essential scientific research tool, particularly in the field of nanoscale science and technology. Because of its versatility, SPM has become one of the techniques for the investigation of single molecule phenomena in areas of scientific research from molecular biology to nanoscale fabrication. SPM is also playing a more and more important role in surface characterization for industrial applications. This is particularly important in semiconductor industries when devices approach sizes below 100nm. Some examples for industrial applications are: magnetic force microscopy (MFM) for characterization of magnetic domains in the data storage industry and general surface roughness characterization of ultra thin films. [31]

At the heart of SPM is the interaction between the tip of the scanning probe and a sample surface. The geometry and material properties of the tip on the scanning probe ultimately determine the performance and resolution of the instrument as it is shown in figure 1.4.

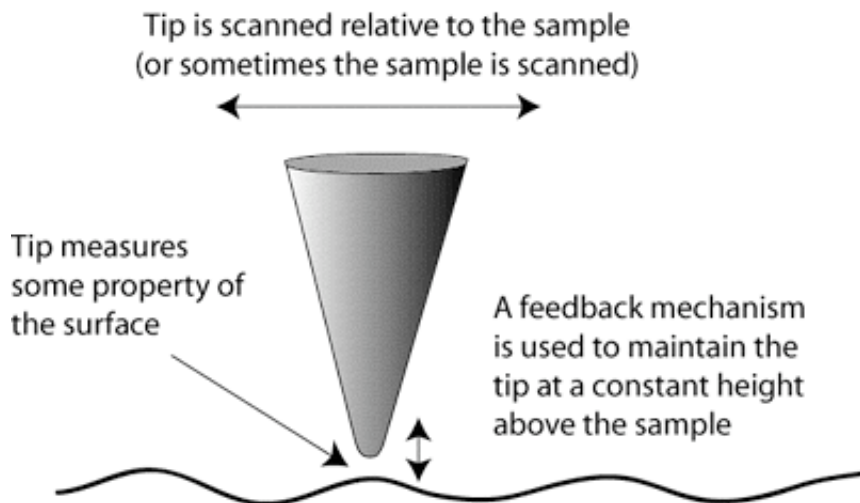


Figure 1.4 Schematics drawing to illustrate the working mechanism of a SPM probe [32]

As described in the property section, CNTs with extremely small sizes, high conductivity, high mechanical strength and flexibility, are ideal starting materials for fabrication of Nanoprobes. One could think of such probes as being used in a variety of applications, such as high-resolution imaging, nano-lithography, nanoelectrodes, drug delivery, sensors and field emitters. The possibility of nanotubes-based field emission will be discussed in the next section. The advantage of CNT probe is its slenderness and the possibility to image features with high aspect ratios, which are almost impossible to probe using the larger, blunter etched silicon or metal tips. MWNTs and SWNT bundles are conducting and can also be used as STM probes. Biological molecules, such as DNA can also be imaged with higher resolution using CNT probes, compared to conventional STM probes. In addition, due to the high elasticity of the CNTs, the probes do no suffer from crashes on contact with the sample surfaces. Any impact will cause buckling of the nanotubes, which generally is reversible on retraction of the tip from the surface. Also because CNTs have much higher resistance to abrasion, CNT probes have much longer life times compared with silicon probes. [33-36]

In addition to the use of CNT probes for high-resolution imaging, it is also possible to use CNTs as active tools for surface manipulation. It has been shown that CNT AFM probes being used in nano-lithography. Ten nanometer lines have been written on oxidized silicon substrates using CNT probe. [37,38]

CNTs can be selectively modified chemically through attachment of functional groups. CNT probes with specially attached functional groups can be used as molecular probes for chemical and biological discriminations on surfaces. Functionalized CNT AFM probes were

used to perform local chemistry, to measure binding forces between protein-ligand pairs and for imaging chemically patterned substrates. [39-40]

### **1.2.2 Field Emitters**

Electron sources are key components of many modern devices and play a central role in information display. Presently, the most widely used electron source is the bulky thermionic cathode, where a metal filament is heated to 1000-3000°C such that a portion of the electron population has sufficient kinetic energy to overcome the work function of the metal (a few electron volts) to be emitted to vacuum level [41]. Field emission is an alternative mechanism of extracting electrons. It is a quantum mechanical phenomenon in which electrons near the Fermi level escape from a solid surface into vacuum by tunneling through a thinned energy barrier under the influence of an external electric field [42]. In contrast to the commonly used thermionic emission based on a hot filament, field emission occurs at room temperature as an instantaneous response to the applied electric field. Because of several attractive characteristics, including no requirement of heating (therefore, no cooling of the system), fast response to electric field variation, resistance to temperature fluctuation and radiation, and an exponential current-voltage relationship, field emission is a preferred electron emission mechanism for many applications such as flat panel displays, portable X-ray tubes, compact microwave amplifier, and high resolution electron microscopy [43].

Field emission is also called Fowler-Nordheim tunneling. Fowler-Nordheim equation ( $I = aV^2 \exp(-b\phi^{3/2}/\beta V)$ , where  $I$ ,  $V$ ,  $\phi$ ,  $\beta$  are emission current density, applied voltage, work function, and field enhancement factor) gives accurate description of this tunneling

phenomena. [44] According to the equation, field emission current density depends on the applied voltages, the emitter's work function and the field enhance factor, which totally depends on the geometry of the emitter. The work function is an intrinsic property of the material that can be lowered by engineering only to a certain degree. However the field enhance factor, which is the slope of the F-N plot, can be tremendously increased by tailoring the geometry of the emitter.

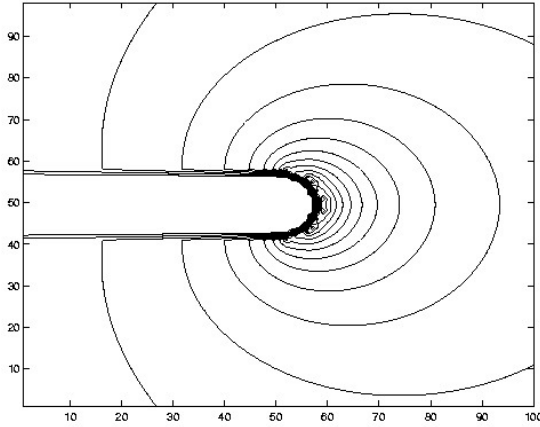


Figure 1.5 Compressed equipotential lines near the sharp protrusion of a metal surface (unit of x and y axis: nm, equipotential spacing: 10V) [45].

Studies have shown that high aspect ratio and sharp end of the emitters both contribute to high field enhance factors. Figure 1.5 shows the concentrated electrical field around the sharp protrusion. CNTs though with relatively large work function (4.8 eV for SWNT) are ideal field emitters, first due to their high aspect ratio and nanometer sized geometry; [46]. Secondly, as described in the property section, CNTs are very good electrical and thermal conductors. The extraordinary electrical and thermal conductivities of CNTs provide them

abilities to carry on high current density for extended period of time without building up too much heat, which will cause degradations of the emitters. [41].

Field emission experiments carried out on individual nanotubes also revealed the excellent emission stability at high current. A single multiwall nanotube emitter was capable of emitting 2  $\mu$ A current for more than 100 hours [47], and catastrophic failure did not occur until the current reached as high as 0.2 mA. Single wall nanotubes generally have a smaller diameter and higher degree of structural perfection than multiwall nanotubes, hence a capability for achieving higher current densities and a longer lifetime [42]. The current-voltage characteristics of an individual clean single wall nanotube showed no evidence of current saturation for emission currents reaching 2  $\mu$ A, corresponding to a current density of  $10^8$  A/cm<sup>2</sup> [48].

CNTs can be used as electron sources in two different types of set-ups, namely single and multiple electron beam devices. One possible application of a single electron beam instrument is an electron microscope that uses an individual CNT or a small CNT bundle as a field emission electron gun to produce a highly coherent electron beam. Conversely, flat panel displays and electron source for X-ray tubes are the most popular example of multiple beam instruments where a continuous or patterned film of CNTs provides a large number of independent electron beams.

The field emission properties of macroscopic CNT film largely depend on the film fabrication techniques, namely the adhesion between CNTs and the substrate and emission

density of the film. [49]. Methods such as electrophoresis, printing, self-assembling were developed to fabricate continuous or patterned CNT films for field emission purpose. [50-52]

### ***1.2.3 Other Applications***

#### **Energy Storage**

Carbon materials have been used as electrode materials in fuel cell and batteries for decades. The efficient of fuel cell and batteries depends on the electron transfer rate at the carbon electrode. While structure and morphology of the carbon material determines the electron transfer rate. The porosity and reactivity of CNTs make them ideal replacement for conventional electrode materials. Both MWNTs [53] and SWNTs [54, 55] are shown to undergo reversible redox reaction with electron donors such as alkali metals resulting in a significantly reduced electrical resistivity [54, 56] and electronic work function [57].

#### **Nanometer sized Electronic Devices**

Electronic circuits cannot continue to shrink by orders of magnitude and provide corresponding increases in computational power, unless radically different device materials, architectures, and assembly processes are developed. Dramatic recent advances have fueled speculation that nanotubes will be useful for downsizing circuit dimensions.

CNTs show exceptional electronic and mechanical properties as described in the property section. They behave like one-dimensional quantum wires that can be either metallic or semiconducting, depending on their chirality and diameter. It is also expected that the CNTs could solve the thermal dissipation problem due to their high thermal conductivity. [58-60]

CNTs can transport terrific amount of electric current without considering doping problem in Si-FETs because the bonds among carbon atoms are much stronger than those in any metal. [61, 62] Recently, several papers have been reported on the CNTs for FETs and CNT-logic applications [63]

### **1.3 Conclusions and dissertation overview**

As discussed above, CNTs with their unique structures and therefore extraordinary properties give hopes of such versatile application possibilities. Their potential applications include electron field emission, gas storage and separation, nanoprobes, chemical sensors, energy storages and high strength composites. However, there are some limitations inherent to the current synthesis and processing methods, which are preventing the true potential of CNTs from being realized. The SWNT generated so far is not a well-defined molecule. It comes with different structures and dimensions, and as a result, different properties. The variations in the “molecular” architecture in principle provide an additional materials design parameter. However, the polydispersity also leads to nonuniform and unpredictable properties. Therefore further study on methods for production and processing of CNTs are desirable to further tune their properties.

And more important lack of bottom up manufacture process that can efficient assemble functional structures and devices using these nano-structured building blocks has been the main hindrance for the applications of CNTs.

The goal of this dissertation is to study the methods for and processing of CNTs, in order to further tune their properties, and most of all, to develop an efficient assembly method of CNTs that allows a fabrication of functional CNT structures. In chapter 2, a brief review is given in currently used synthesis methods. Laser-CVD method is proposed as a new method and some preliminary experimental result is given. In chapter 3, methods for purification and cutting CNTs are discussed. And properties of cut CNTs are studied. In chapter 4, dielectrophoresis as an efficient way to assembly CNTs into functional structures is studies. Among all the structures fabricated by dielectrophoresis, ultra-thin CNT fibril were found to have intriguing application as nanoprobes and field emission point sources. In chapter 5, the fabrication of CNT fibrils by dielectrophoresis is further optimized by automation of the process and parameter studies.

## 1.4 References

1. S. Iijima, *Nature* **354** (1991) 56
2. L. -C. Qin, X. Zhao, K. Hirahara, Y. Miyamoto, Y. Ando, and S. Iijima, *Nature* **408** (2000) 50.
3. Thess, R. Lee, P. Nikolaev, H. Dai, P. Petit, J. Robert, C. Xu, Y. H. Lee, S. G. Kim, A. G. Rinzler, D. T. Colbert, G. E. Scuseria, D. Tomanek, J. E. Fischer, R. E. Smalley, *Science*, **273** (1996) 483.
4. “Image gallery” of a website <http://www.pa.msu.edu/cmp/csc/nanotube.html>
5. M. S. Dresselhaus, G. Dresselhaus, Ph. Avouris (Eds.) “*Carbon Nanotubes: Synthesis, Structure, Properties, and Applications*”, Springer-Verlag, Heidelberg, 2001.
6. J. W. G. Wilder, *Nature* **391** (1998) 59.
7. W. Moore, *Chemistry and Physics of Carbon*, **17**, P. L. Walker, Jr., P. A. Thrower (Eds.) Dekker, new York (1973)
8. W. Liang, *et al.*, *Nature* **411**, 665 (2001)
9. Stefan Frank *et al.*, *Science* **280** 1744 (1998)
10. Anthony Kendall, Thomas A. Adams II, and Elizabeth Pfaff (1999)
11. P. Chen, X. Wu, J. Lin, K. Tan, *Science* **285**, (1999), 91
12. Liu, Y. Y. Fan, M. Liu, H. T. Cong, H. M. Cheng, M. S. dresselhaus, *science* **286**, (1999), 1127
13. Nutenadel, A. zuttel, D. Chartouni, L. Schlapbach, *Solid-State Lett.* **2**, (1999), 30
14. Chambers, C. Park, R. T. K. Baker, N. m. Rodriguez, *J. Phys. Chem. B* **102**, (1998), 4253
15. J. Hone, M. Whitney, A. Zettle, *Synthetic Metals*, **103** 2498 (1999)
16. S. Berber, Y-K Kwon, and D. Tomànek, *Phys. Rev. Lett.* **84** (2000)
17. J. F. despres, E. Daguerre, K. Lafdi, *Carbon* **33**, (1995), 87.
18. S. Iijima, C. brabec, A. Maiti, J. Bernholc, *J. chem. phys.* **104**, (1996) 2089.

19. O. lourie, D. M. Cox, h. D. Wagner, *Phys. Rev. Lett.* **81**, (1998) 1638.
20. J. Muster, M. Burghard, S. Roth, G. S. Dusberg, E. Hernandez, A. Rubio, *J. Vac. Sci. Technol.* **16**, (1998) 2796
21. P. Poncharal, Z. L. Wang, D. Ugarte, W. A. de Heer, *Science* **283**, (1999) 1513
22. R. S. Ruoff, D. C. Lorents, *Bull. APS* **40**, (1995) 173
23. Dekker, *Physics Today*, (1999) 22.
24. P.M. Ajayan and O.Z. Zhou, *Top. Appl. Phys.* **80** (2001), 391
25. B. Gao et al., *Chem. Phys. Lett.*, **307**, (1999), 153
26. J.S. Sakamoto and B. Dunn, *J. Electrochem. Soc.* **149** (2002) A39
27. G. Y. Zhang and E.G. Wang, *Appl. Phys. Lett.* **82**, (2003) 1926
28. J. sloan et al., *Chem. Commun.* (1998) 347
29. C.H. Kiang et. al., *J. Phys. Chem. B*, **103** (1999) 7449
30. M. Terrones et al., *MRS Bull.*, **43** August (1999)
31. M. Meyyappan, *Carbon Nanotubes Science and Applications*, CRC press, (2005)
32. V, H, Morris, A. P. Gunning, and A.R. Kirby, *Atomic Force Microscopy for Biologists*, Imperial college Press, London (1999)
33. Kudo, T. et al. *Advances in Resist Technology and Processing XVIII, SPIE Preceedings*, 4345, (2001), 179
34. C. V. Nguyen et al. *Appl. Phys. Lett.*, **81**, (2002) , 901
35. P. G. Collins, M. s. Arnold, Ph. Avouris, *Science*, **292** (2001), 706
36. P. G. Collins, et al. *Phys. Rev. Lett.*, **86** (2001), 3128
37. J. Cumings, P. G. Collins, and A. zettl, *Nature*, **406**, (2000), 586
38. C.V. Nguyen et al. *J. Phys. Chem. B*, **108** (2004), 1816
39. Q. M. Hudspeth et al. *Surface Sci.*, **515**, (2002), 453

40. T. Arie et al. *J. Vac. Sci. Tech. B*, **18**, (2002), 104
41. N. Yoshida et al. *Jpn. J. appl. Phys.*, **41**, (2002) 5013
42. W. Zhu (Ed) “*Vacuum Microelectronics*” Wiley 2001.
43. Y. Cheng, O. Zhou, *C. R. Physique* **4** (2003) 1021.
44. W. I. Milne, K. B. K. Teo, G. A. J. Amarantunga, P. Legagneux, L. Gangloff, J. -P. Schnell, V. Semet, V. Thien Binh, O. Groening, *J. Mater. Chem.* **14** (2004) 933.
45. R. H. Fowler, L. W. Nordheim, *Proc. R. Soc. (London)* **A119** (1928) 173.
46. R.Gomer, “*Field Emission and Field Ionization*”, Harvard University press, Cambridge, MA 1961.
47. Y. Cheng, PhD dissertation, “*Carbon nanotube based field emission X-ray sources*” 2004.
48. R.Gomer, “*Field Emission and Field Ionization*”, Harvard University press, Cambridge, MA 1961.
49. D. S. Y. Hsu, *Appl. Phys. Lett.* **80** (2002) 2988.
50. S. J. Oh, J. Zhang, Y. Cheng, H. Shimoda, and O. Zhou, *Appl. Phys. Lett.* **84**, (2004), 3738-3740.
51. S. J. Oh, Y . Cheng, J. Zhang, and H. Shimoda,O. Zhou, *Appl. Phys. Lett.*, **82**, (2003), 2521-2523.
52. B. Gao, G.Z. Yue, Q. Qiu, Y. Cheng, H. Shimoda, L. Fleming and O. Zhou, *Adv. Mater.*, **13**(11), (2001), 816-819
53. O. Zhou, R. M. Fleming, D.W. Murphy, C. T. Chen, R. C. Haddon, A. P. Ramirez, and S. H. Glarum, *Science* **263**, (1994) 1744–1747.
54. R. S. Lee, H. J. Kim, J. E. Fischer, A. Thess, and R. E. Smalley, *Nature (London)* **388**, (1997) 255.
55. A. M. Rao, P. C. Eklund, S. Bandow, A. Thess, and R. E. Smalley, *Nature (London)* **388**, (1997) 257–259.
56. L. Grigorian, K. A. Williams, S. Fang, G. U. Sumanasekera, A. L. Loper, E. C. Dickey, S. J. Pennycook, and P. C. Eklund, *Phys. Rev. Lett.* **80**, (1998) 5560–5563.

57. S. Suzuki, C. Bower, Y. Watanabe, and O. Zhou, *Appl. Phys. Lett.* **76**, (2000) 4007–4009.
58. W. Liang, *et al.*, *Nature* **411**, 665 (2001)
59. Z. Yao, C. L. Kane, C. Dekker, *Phys. Rev. Lett.* **84**, 2941 (2000)
60. Z. Yao, C. Dekker, Ph. Avouris, *Top. Appl. Phys.* **80**, 147 (2001)
61. R. Martel, T. Schmidt, H. R. Shea, T. Hertel, Ph. Avouris, *Appl. Phys. Lett.* **73**, 2447 (1998).
62. A. Bachtold, P. Hadley, T. Nakanishi, C. Dekker, *Science* **294**, 1317 (2001)
63. P. G. Collins, M.S. Arnold, and P. Avouris, *Science*, **292**, (2001) 706.

# **Chapter 2 Synthesis of Carbon Nanotubes**

## **2.1 Introduction**

As it is described in last chapter, CNTs have shown so many intrigue properties that attracted tremendous research efforts to study their potential applications. However, not until a reliable synthesis method, which can provide reasonable amount of CNTs with desirable qualities, is found can those potential applications be truly realized. While CNTs synthesized by different methods may have different characteristics that suits for different applications. Therefore, currently used production methods are studied and a new way to produce CNTs is proposed here and some experimental results will be given.

## **2.2 Summary of currently used synthesis methods**

At present there are three basic methods in widespread use for synthesis of both SWNTs and MWNTs, laser ablation (LA), arc-discharge, and chemical vapour deposition (CVD).

### **2.2.1 Arc-discharge**

The first confirmed carbon nanotubes were fabricated using an electric arc discharge between graphite electrodes. [1] This method had been shown to be successful for the preparation of fullerenes in large quantities. [2] It was while examining the fullerene products of arc-discharge products that MWNTs were observed. Shortly after, it was discovered that the addition of certain catalyst metals to one of the electrodes produced deposits rich in SWNTs. [3-5]

The basic arc-discharge method involves establishing a DC electric discharge between a pair of graphite electrodes under an inert helium atmosphere (~500 torr). The electrodes are typically water-cooled graphite rods separated by ~1mm with the cathode being of larger diameter than the anode (8-12mm and 6-8mm respectively). A bias of approximately 10-35 V is applied to the electrodes to establish the discharge; currents of ~60-100A and current densities of ~150A/cm<sup>2</sup> are typically produced. Achieving a stable discharge plasma is the main factor in generating an environment favorable to nanotube growth. The high temperature arc (> 4000 °C) leads to sublimation of material from the anode which is transferred to the cathode and surrounding walls of the apparatus.

When bi-metal mixtures of Co, Ni, Y, and Fe are placed in a hole drilled in the anode, a concentration of 30-50% of SWNT will be found in the cathode deposits. [6-12] It is typical for deposits to be generated at rates of 20-100mg/min, though rates as high as 1.2g/min have been reported. [13] SWNTs produced by arc discharge method usually have high crystallinity due to their high formation temperature in the arc. However the drawback of arc-discharge

method is that the process can only last a few minutes before it is terminated by the instability of the DC arc, which is caused by uneven consumption of the anode and build-up of material on the cathode.

### **2.2.2 Laser Ablation**

Like the arc-discharge method, laser-based synthesis of CNTs began as an extension of a process used for fullerene production. [14] After the first demonstration of using laser ablation to fabricate SWNTs, it has subsequently been used almost exclusively for the synthesis of SWNTs. [15] Figure 2.1 shows the laser ablation experimental setup in our lab for synthesis SWNTs.

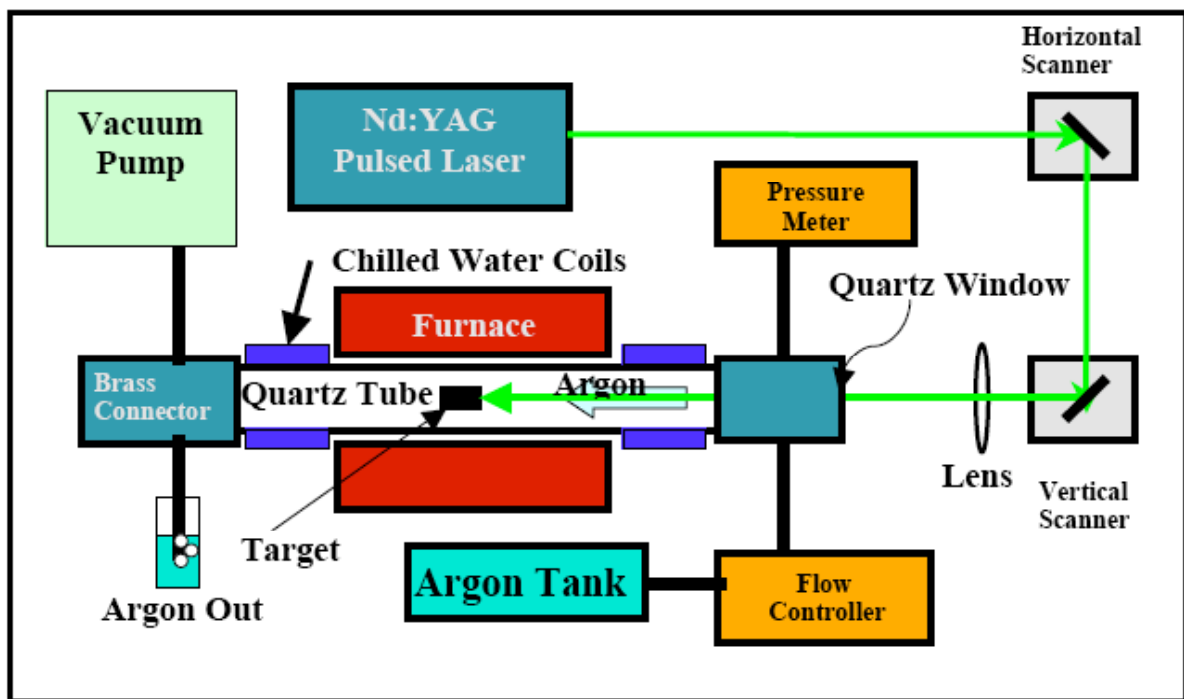


Figure 2.1 Laser ablation system for the synthesis of single wall nanotubes. The focused laser beam scanned over the target surface using an XY raster. The formed nanotubes were carried by Ar and collected in a chill water cooled zone of the quartz tube.

During laser ablation experiment, typically a high power laser beam is used. A target of graphite and transition metal nanoparticles mixture is put in a quartz tube with a quartz window facing the laser beam. The quartz tube is put in a furnace, which is heated up to 900-1200°C (1175 °C in our experiment). The high laser energy densities (50-70J/cm<sup>2</sup>sec) focused on target surface will evaporate the solid target and form high temperature plumes (3500 to 4000 °C), which is a molten mixture of carbon and catalytic particles. The temperature gradient of the plumes and furnace environment will cause the plumes to expand, and SWNTs will form in the plumes. Then the CNTs along with amorphous carbon and residue catalysts formed in the plume will be carried by the flowing of inert gas (Ar flowing at 400 sccm in our setup) to the quartz tube end, that is wrapped by cooling coils, and deposit there. The laser beam is passed through two scanning prism that will raster scan it across the target surface to get an even consumption of the target.

Although the highest production rate of SWNT by laser ablation is 1.5g/h, [16] when conventional setup described above is used, yield is only around 100mg/hr. The SWNTs produced by laser ablation also have high crystallinity due to the high plume temperature. And they usually form bundles of diameter 30-50 nm because of van der Waals attraction among the individual tubes. When individual SWNTs are needed, tremendous efforts need to be taken in order to exfoliate the bundles. It was also found that the SWNT produced by laser ablation is a mixture of nanotubes with random chirality, therefore bulk materials comprise one-third metallic and two-thirds of semiconducting nanotubes. [17]

Theoretically the laser ablation method can provide a continuous production of SWNTs when a big enough target is put into the quartz tube. However after the target is raster-scanned by the laser beam for extended period of time, pits will form on the scanned surface. Therefore, the increased roughness of the target surface will deflect the laser beam, decreased its energy density and slow down the ablation process. For this reason, the laser ablation process usually will be stopped in 12hrs and the target will be taken our and re-polished.

Another draw back of the laser ablation method is that according to the following description, target making is a very time consuming process. (Target making recipe used in our lab: The ablation target was made by compressing the mixture of graphite powder and 0.3 atomic % (each) Ni/Co catalysts. To do this, 74 mg of Ni (Alfa Aesar, average 0.1 $\mu$ m, 99% purity) and 74 mg of Co powder (Alfa Aesar, average 0.1 $\mu$ m , >99% purity) was evenly mixed with 1g of graphite powder (Alfa Aesar, 2-5  $\mu$ m, >99.99% purity) and 5.7g of graphite cement (Dylon Industry, 70% graphite, 30% furfuryl alcohol) in a mortar, and the paste was pressed into a cylindrical pallet with 0.5 inch diameter using a metal mold. The soft graphite pallet was first hardened by compressing it with a pressure of 1 metric ton using the Instron machine. The pallet also was heated slowly and held at 130°C during the compression to remove most of the oily binder material as a liquid form. Once removed from the metal mold, the hardened target was further heated in Ar environment up to 1000°C with a slow ramping speed (100°C/hour), and held at 1000°C for at least 8 hours. During this curing process, the remaining organic material is removed from the target through evaporation and thermal decomposition. The target was cooled and used for laser ablation.)

### **2.2.3 Chemical Vapor Deposition (CVD)**

The basic mechanism of CVD involves the pyrolysis of gas-phase carbon-rich molecules (hydrocarbon) in the presence of catalyst at elevated temperatures, and the subsequent conversion of the carbon-fragments (catalytically decomposed from hydrocarbons) into nanotubes. This general procedure had been used to generate carbon fibers and filaments for many years. [18-21] Until 1993 MWNTs were first synthesis by CVD method. [22]

Describing a generalized CVD-based nanotube synthesis experiment is somewhat difficult since the variations in methods used are much more diverse than those of the arc or laser-based techniques. [23-39] For the most part, CVD synthesis can be divided into two main categories : supported catalyst growth and floating or gas-phase growth. In the supported growth process, the catalyst is prepared in advance and deposited in some way on a support medium. This is inserted into a flow apparatus, typically a tube at atmospheric pressure in a temperature-controlled furnace, where it can be exposed to flowing carbon-rich gas at elevated temperatures (typically 500–1100 °C) for a sustained period of time. Figure 2.2 shows a common supported catalyst CVD setup. For floating-catalyst growth, a high-temperature flow-furnace is still used, however the catalyst and carbon source are injected into the system simultaneously, either in gas phase or as an aerosol, where the subsequent decomposition and reaction can either occur completely suspended in the gas flow or following self-deposition on a surface in the reactor.

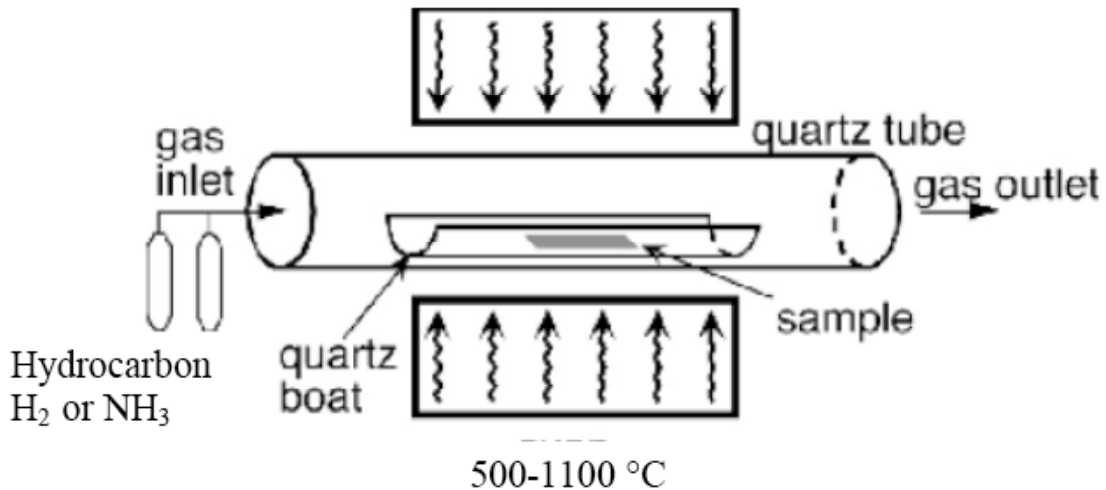


Figure 2.2 Supported catalysts CVD system, catalyst is deposited on a substrate, which is put into a heated up furnace, hydrocarbon is flowed into the furnace. [24]

Supported growth is the most widely used CVD-based method of nanotube synthesis. A Preparing the catalyst in advance provides opportunity to define specific patterns for the CNT growth on the substrate. Plasma enhanced CVD can also provide control over the growth direction of CNTs. The ability to control the position and direction of growth could have significant benefits, including simple routes to achieving nanotube-based electronic devices. Techniques such as photolithography, [27] electron beam lithography, [25] laser etching, [34, 35] and plasma etching have been successfully used to achieve patterned nanotube growth.

Disadvantages of CVD methods are, first of all CNTs grown by CVD methods have relatively poorer quality compared with arc-discharge and laser materials due to their low forming temperature. And catalyst will often be poisoned by pyrolyzed hydrocarbons and the process has to be stopped within 30 minutes. To solve this problem, floating-catalyst techniques have been studied. Fabrication of ultra long SWNTs by floating catalyst methods

was reported.

Overall, Arc-discharge and laser ablation provide CNTs with relatively higher crystallinity, however at very low yield. CVD methods shows the greatest promise as a true industrial scale process, particularly floating catalyst techniques which, in principle, can be operated in a continuous fashion.

## **2.3 The method of Laser-CVD**

### **2.3.1 *The idea of Laser-CVD***

As summarized above, in all the three methods, the growth of CNTs requires carbon source, catalyst and energy to break the carbon rich material and mix carbon and catalyst in atomic level. While both CVD process and Laser ablation process require a heated up furnace with gas flowing through it. CNTs may be synthesized when hydrocarbon is flowed into the laser ablation chamber and pyrolysis in the plume generated by a laser beam hitting on a pure catalyst target. Combining the laser ablation and the CVD methods may provide opportunities to synthesis CNTs with relatively high crystallinity as the laser ablation materials and at high yield as what CVD method provides, and CNTs synthesized in new condition may provide unique characteristics.

### **2.3.2 Experiments and Results**

#### **Experiments**

The experimental setup is shown in Figure 2.3. A laser ablation chamber described above is used. While respectively 5%, 10% methane is added to the flowing inert gas (Ar). And a pure metal rod (Alfa Aesar: Fe rod 99.99% purity, Ni rod 99.99% purity, Co rod 99.99% purity respectively) is placed in the position of laser ablation target. Iron, Nickel and Cobalt were tried respectively to study their catalytic effect on the CNT growth. While an alloy target with two or more kinds of transition metals may provide a better catalytic effect for CNT growth, it is hard to find such alloy rod commercially. And it's hard to make a pallet of mixed metal particles that can sustain the high power Laser beam bombardment without being cracked. The furnace is heated up to 800°C instead of 1150°C. A 10Hz pulsed Nd:YAG (Yttrium-Aluminum-Garnet) laser operating at a wavelength of 532 nm is used. The position of the target was determined according to the focal length of the focusing lens so that a focused laser beam with a diameter of 3 mm can fall on the ablated surface. The pulse intensity was 400 mJ/pulse, which, in turn, corresponded to the average intensity density of  $5.7 \text{ J/cm}^2 \cdot \text{pulse}$ . The target surface was raster-scanned with a beam for a uniform ablation over the entire area.

The furnace is gradually ramped up to 800°C instead of 1150°C. The laser beam was turned on after the furnace reached targeted temperature. Then the furnace and the laser beam were turned off 2 hrs later. The system is cooled down and Soot like materials were found deposited at the end of quartz tube where laser ablation materials usually deposit. The Laser

CVD materials fabricated using different catalyst target and different concentration of hydrocarbon were analyzed by high-resolution transmission electron microscope (HRTEM) and Raman spectroscopy. Results are discussed in the next section.

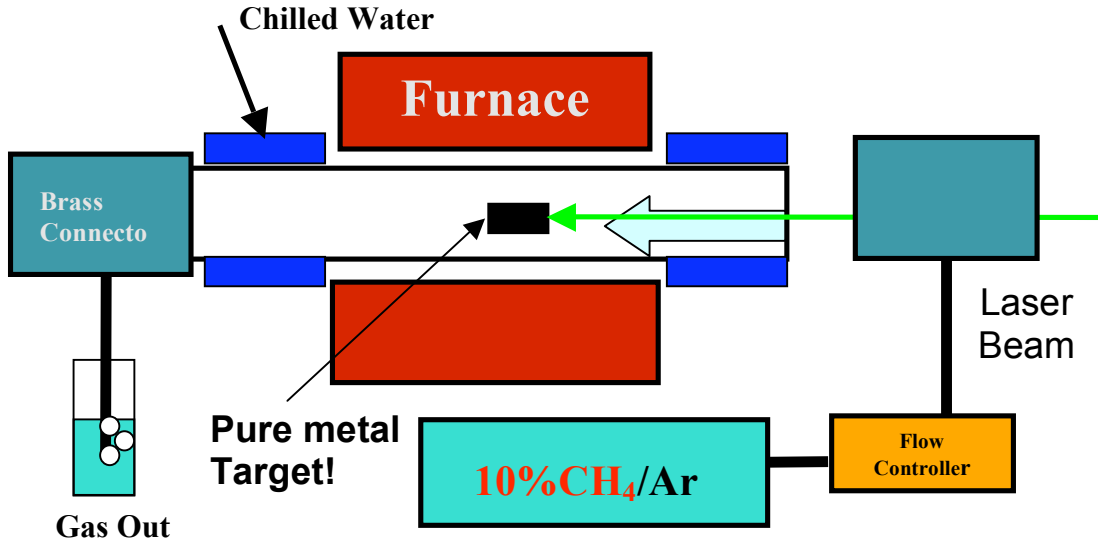


Figure 2.3 Same setup described in Figure 2.1, a cylinder of methane / Ar mixture is used instead of pure Ar gas and a pure metal target is used.

### ***Experimental Results***

The Laser-CVD materials collected from the chamber were studied by TEM and Raman spectroscopy. The yield of the Laser-CVD method is comparable with Laser ablation method but is low compared with CVD method, partially due to the low concentration of hydrocarbon is used. However CNTs are produced by using 5% methane and 10% methane. And results show that, higher the concentration of hydrocarbon, higher the yield and higher the purity of the material. While for sake of safety, concentration of hydrocarbon higher than

10% was not attempted. Gas flow rate was increased from 400 sccm to 800 sccm, while there's no significant increase of the yield. The increase Ar flow may carry the methane and the catalyst particles in the laser plume to the end of quartz tube before their encounter and the pyrolysis of methane in the presence of catalytic particles. Figure 2.4 (b) shows the CNTs made by Laser-CVD method, while pure iron target was used and the hydrocarbon concentration was 10%. Compared with regular laser ablation raw material, the purity of laser-CVD material is still low, however the average bundle size is smaller.

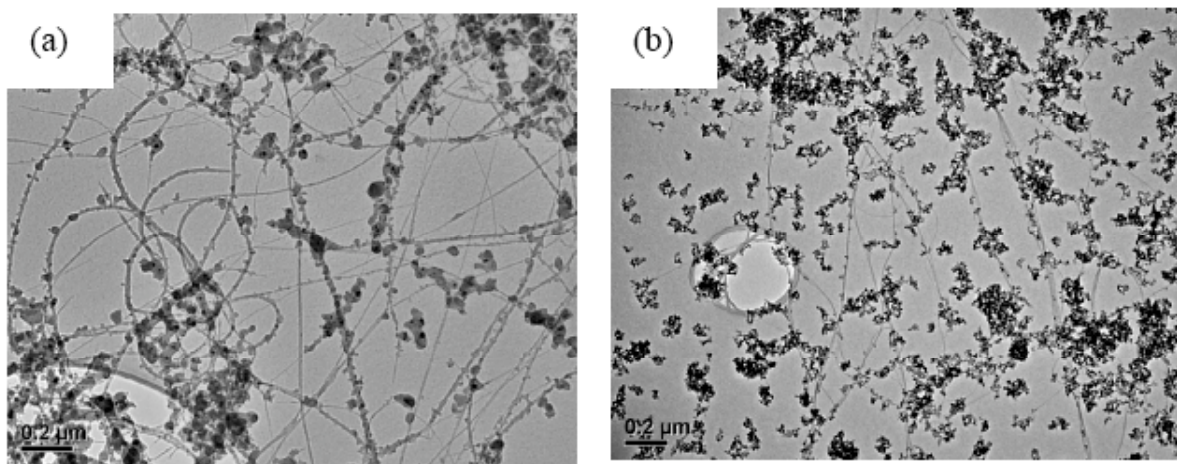


Figure 2.4 TEM images of as synthesized SWNT bundles. (a) SWNTs synthesized by laser ablation method using 0.3% Ni-Co target. (b) SWNTs synthesized by laser-CVD method using iron target (99.99% purity from Alfar Asear), and 10% methane was added to the flowing gas while flow rate was 400 sccm.

And high resolution TEM confirmed that only single walled nanotubes are fabricated by laser-CVD method and the SWNT bundles are smaller compared with regular laser ablation materials. It also shows that many individual SWNTs are found in the laser-CVD material, which is not normally found in laser ablation materials. Around 30 HRTEM images were taken for each sample of three samples fabricated by using different metal target. As shown in Figure 2.5, it is found out that nickel used as catalyst produces SWNTs with best

crystallinity and relatively uniform diameters averaged to 1.5 nm. While when iron is used as catalyst, the SWNTs synthesized also have relatively high crystallinity while with a relatively wider diameter distribution from 0.65nm to 2 nm. When cobalt is used as catalyst by itself, the SWNT thus synthesized have corrugated structures as shown in Figure 2.5 (b).

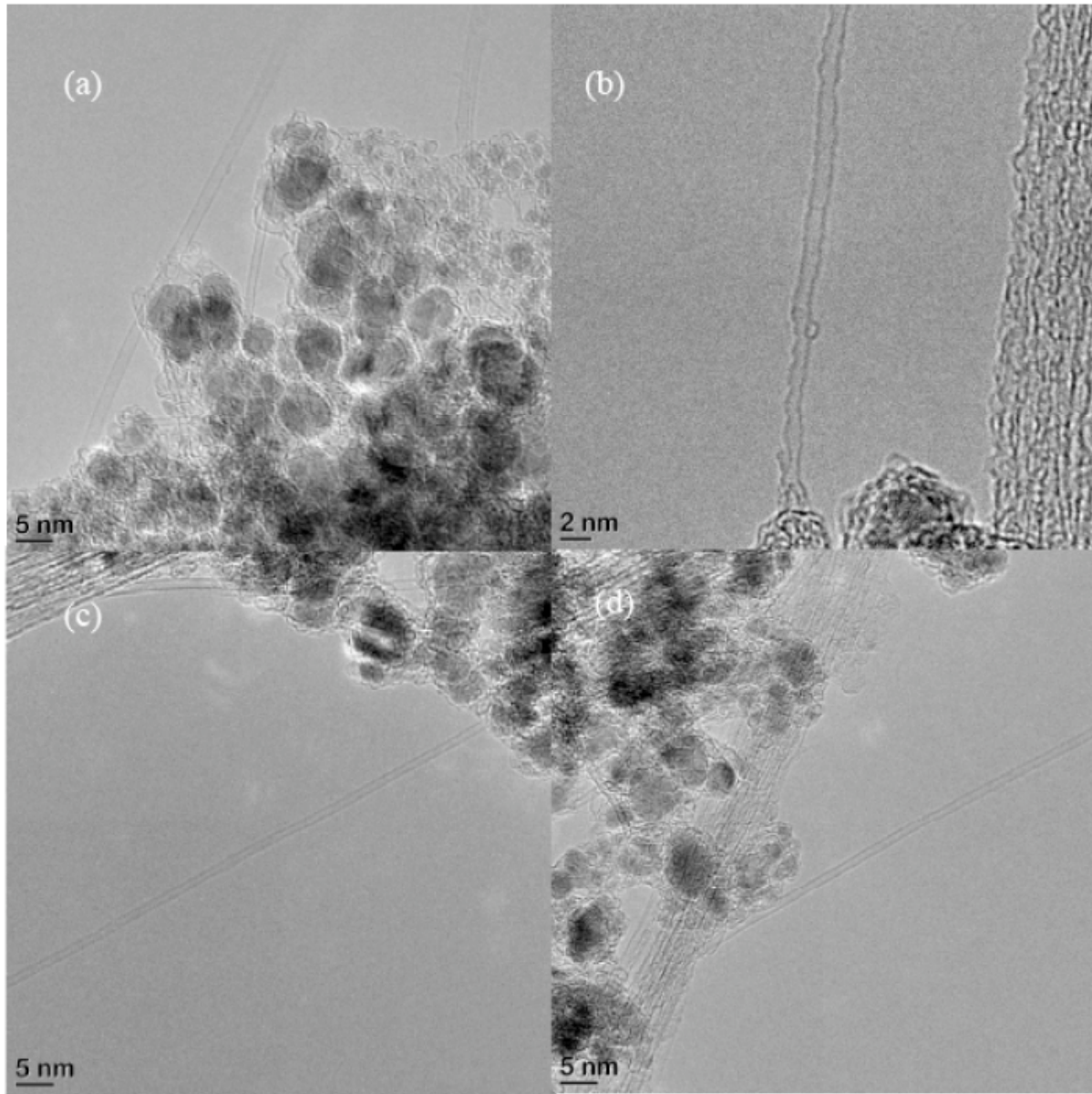


Figure 2.5 HRTEM images of as SWNT synthesized by laser CVD method. (a) iron target (99.99% purity from Alfar Asear) was used; (b) Co target (99.99% purity from Alfar Asear) was used; (c) and (d) Ni target (99.99% purity from Alfar Asear) was used. In all the experiments 10% methane was added to the flowing Ar, while flow rate was 400 sccm

Raman spectroscopy was also used to characterize the SWNTs synthesized by laser-CVD method. The results are shown in Figure 2.6

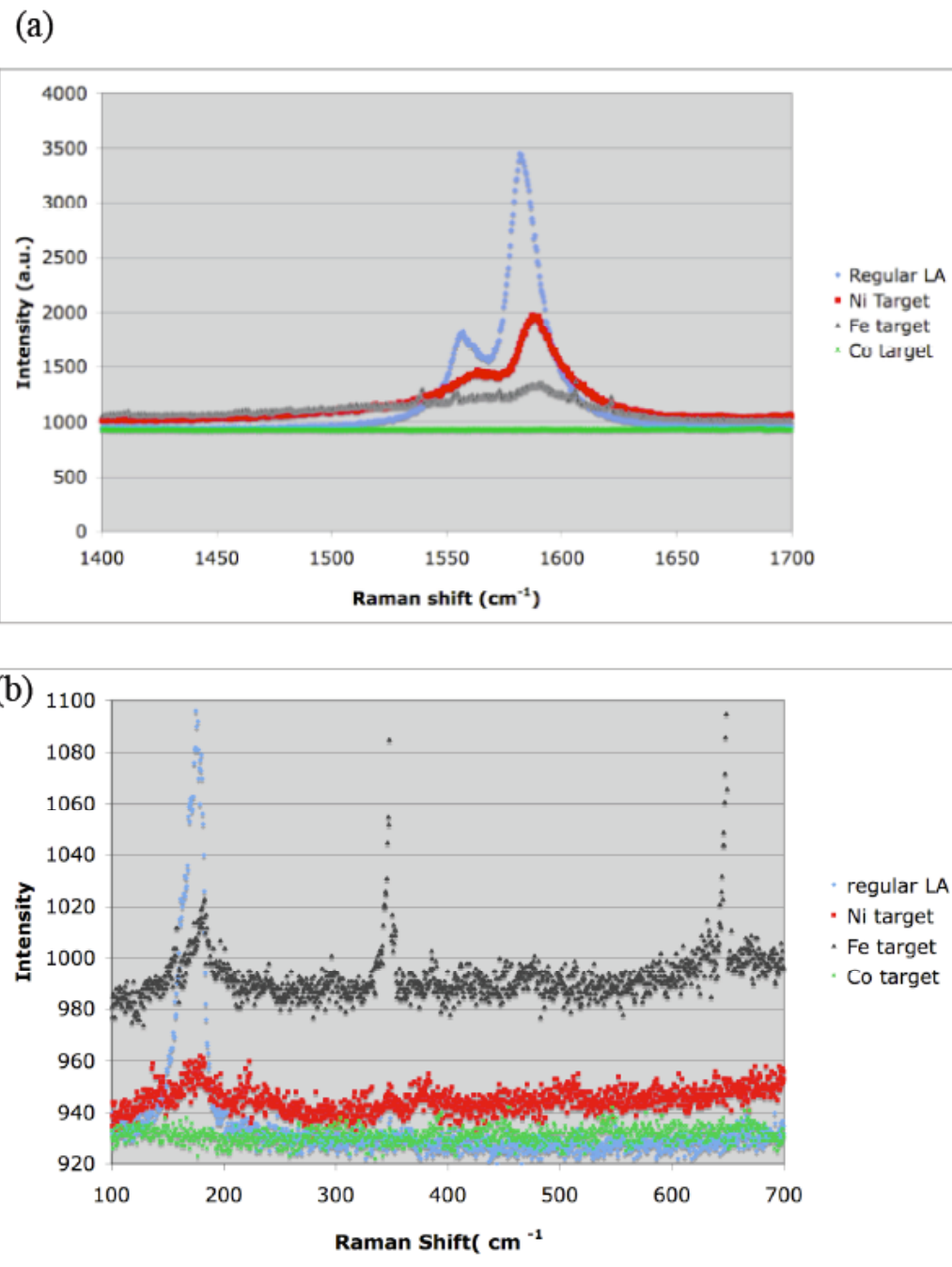


Figure 2.6 Raman spectral of SWNT synthesized by laser ablation method and laser CVD method by using Fe, Ni and Co pure metal rod targets. (a) high wave number G band signal. (b) Low wave number breathing mode signal.

From the raman spectroscopy shown in Figure 2.6, compared with tw when a particulare wavelengh of Laser was used in this study. Of course, there's other factors that affects the intensities of the Raman peaks, including density of the Raman samples prepared, bundle sizes, and the electronical structures of the CNTs in the samples. Due the low yield of this method, the CNTs fabricated may not have practical applications, therefore further study was not carrired on.

## **2.4 Summary**

A summary of the methods currently used to synthesis CNTs are given here. The pros and cons of each method is discussed. Experimental details of synthesis CNTs by laser ablation method were described. The idea of combining laser ablation and CVD method for production of CNTs were porposed. Some experiments were done and the results were discussed.

Overall, the Laser CVD methods provide a new way to synthesis CNTs. All the CNTs synthesised this way are SWNTs when pure nickel, cobalt or iron were used as catalyst. The effects of hydrocarbon carbon concentration and gas flow rate were studied, however due safty reason, higher concentration of hydrocarbon was not researched. Nickel and Iron ,when used as catalysts, provide CNTs growth with better crystallinity, compared with Cobalt. The yield of the Laser CVD method is low when low concentration of hydrocarbon was used, and further applications of materials synthesised by this method is not studied.

## 2.5 References

1. S. Iijima, *Nature* **356**, (1991), 56-58
2. W. Kartschmer, O. L. Lamb, K. Fostiropoulos, D. R. Huffman, *Nature* **347** (1990), 354-358
3. P.M. Ajayan, S. Iijima, *Nature* **358**, (1992), 23
4. S. Iijima, T. Ichihashi, *Nature* **363**, (1993), 603
5. D.S. Bethund, C.H. Kiang, M.S. de Vries, G. Gorman, R. Savoy, J. Vazquez, R. Beyer, *Nature* **363**, (1993) 605
6. P.M. Ajayan, J.M. Lambert, P. Bernier, L. Barbedette, C. Colliex, Planeix, J.M. *Chem. Phys. Lett.* **215**, (1993), 509–517.
7. C.H. Kiang, W.A. Goddard III, R. Beyers, J.R. Salem, D.S. Bethune, *J. Phys. Chem.* **98**, (1994) 6612–6618.
8. S. Seraphin, D. Zhou, *Appl. Phys. Lett.* **64**, (1994) 2087–2089.
9. J.M. Lambert, P.M. Ahayan, P. Bernier, J.M. Planieix, V. Brotons, B. Coq, J. Castaing, *Chem. Phys. Lett.* **226**, (1994) 364–371.
10. Kiang, C.H.; Goddard III, W.A.; Beyers, R.; Bethune, D.S. *Carbon* **33**, (1995) 903–914.
11. Lambert, J.M.; Ajayan, P.M.; P. Bernier, *Synth. Met.* **70**, (1995) 1475–1476.
12. Journet, C.; Maser, W.K.; Bernier, P.; Loiseau, A.; Lamy de la Chapelle, M.; Lefrant, S.; Deniard, P.; Lee, R.; Fischer, J.E. *Nature* **388**, (1997) 756–758.
13. Y. Ando, S. Iijima, *Jpn. J. Appl. Phys.* **32** (2000), L1342-L1345
14. H.W. Kroto, J.R. Heath, S.C. O'Brien, R.F. Curl, R.E. Smalley, *Nature* **318**, (1985), 162-163
15. T. Guo, P. nikolaev, A. Thess, D.T. Colbert, R.E. Smalley, *Chem. Phys. Lett.* **243**, (1995) 49-54
16. P.C. eklund, B.K. Pradhan, U.J. Kim, Q. Xiong, J.E. fischer, A.D. friedman, b.C. Holloway, K. Jordan, M.W. Smith, *Nano Lett.* **2**, (2002) 561-566
17. X. P. Tang, A. Kleinhammes, H. Shimoda, L. Fleming, K. Y. Bennoune, C. Bower, O. Zhou, Y. Wu. *Mater. Res. Soc. Symp. Proc.* **593** (1999) 143.

18. P.L. Walker, J.F. Rakiszawski, G.R. Imperial, *J. Phys. Chem.* **63**, (1969), 133-140
19. W.R. Ruston, M. Waezee, J. Hennaut, J. Waty, *Carbon* **7**, (1969), 47-57
20. D. Robertson, *Carbon* **8**, (1970) 365-374
21. T. Baird, J.R. Frayer, B. Grant, *Nature* **233**, (1971) 329-330
22. M.J. Yacaman, M.M. Yoshida, L. Rendon, J.G. santiesteban, *Appl. Phys. Lett.* **62**, (1993) 202-204
23. C.J. Lee, D.W. Kim, T.J. Lee, Y.C. Choi, Y.s. Park, W.S. Kim, Y.H. Lee, W.B. Choi, N.S. Lee, J.M. Kim, Y.G. Choi, S.C. Yu, *Appl. Phys. Lett.* **75**, (1999) 1721-1723
24. J. Kong, T.T. Soh, A.M. Cassel, C.F. Quate, H. Dai, *Nature* **395**, (1998) 878-881
25. S. fan, M.G. Chapline, N.r. Franklin, T.W. Tombler, A.M. Cassell, H. Dai, *Science* **283**, (1999) 512-514
26. D. Xu, G. Guo. L. Gui, Y. Tang, Z. Shi, Z. Jin, Z. Gu, W. Liu, X. Li, G. Zhang, *Appl. Phys. Lett.* **75**, (1999) 481-483
27. S. Huang, A.H.W. Mau, *Appl. Phys. Lett.* **82** (2003) 796-798
28. K. H. Lee, J. M. Cho, W. Sigmund, *Appl. Phys. Lett.* **82**, (2003) 448-450
29. M.P. siegal, D.L. Overmyer, P.P. Provencio, *Appl. Phys. Lett.* **80**, (2002) 2171-2173
30. C.L. Cheung, A. Kurtz, H. Park, C.M. Lieber, *J. Phys. Chem.. B* **106**, (2002) 2429-2433
31. B.Q. Wei, Z.J. Zhang, P.M. Ajayan, G. Ramanath, *Carbon* **40**, (2002) 47-51
32. C.J. Lee, J. Park, *Appl. Phys. Lett.* **77**, (2000) 3397-3399
33. O.A. Nerushev, S. Dittmar, R.-E. Mrjan, F. rohmund, *J. Appl. Phys.* **93**, (2003) 4185-4190
34. M. Terrones, N. Grober, J. Olivares, J.P. Ahang, H. Terrones, K. Kordatos, W.K. Hsu, J.P. Hare, P.D. Townsend, K. Prassides, a.K. Cheetham, H.W. Kroto, D.R.M. Walton, *Nature* **388**, (1997) 52-55
35. N. Grobert, m. Terrones, S. Trasobares, K. Kordatos, H. Terrones, J. Olivarez, J.P. Zhang, Ph. Redlich, W.K. Hsu, C.L. Reeves, D.J. Wallis, Y.Q. Zhy, J.P. Hare, A.J. Pidduck, H.W. Kroto, DR.M. Walton, *Appl. Phys. A* **70**, (2000) 175-183

36. Y. Gao, J. Liu, M. Shi, S.H. Elder, J.W. Virden, *Appl. Phys. Lett.* **74**, (1999) 3642-3644
37. Ch. Emmenegger, P. Mauron, A. Zuttel, Ch. Nutzenadel, A. Schneuwly, R. Gallay, L.
38. Schlapbach, *Appl. Surf. Sci.* **162**, (2000) 452-460
39. X.H. Chen, S.Q. Feng, Y. Ding, J.C. Peng, Z.Z. *Thin Solid Films* **339**, (1999) 6-9
40. C. Emmenegger, J.-M. Bonard, p. Mauron, P. Sudan, A. Lepora, B. Grobety, A. Zuttel, L. Schlapbach, *Carbon* **41**, (2003) 537-547

# **Chapter 3 Processing of Carbon Nanotubes**

## **3.1 Introduction**

As synthesized carbon nanotube materials (raw materials) contain significant amount of impurities, including amorphous carbon, graphitic particles and metal catalysts as shown in a TEM picture in Figure 3.1(a). Purification is often needed when high purity CNTs are required. As produced CNTs after purification have different length distribution and in the case of SWNTs, different bundle sizes also, which are determined by the synthesis method. Further processing such as wet etching, heat treatment and chemical functionalization provide another dimension to tailor the properties of CNTs so that they can be utilized in various kinds of applications. For example, in applications where CNTs with certain length distribution are desirable, methods are developed to etch them into a shorter length distribution in a controllable way. And when accessibility to the interior spaces of the CNTs is important for their applications in energy storage and fuel cells, ability to tailor their end openness is closely studied. And high temperature annealing of chemical treated CNTs may increase their crystallinity and enhance their properties as high current field emitters.

### **3.2 Purification and cutting of Carbon Nanotubes**

#### ***3.2.1 Purification of Carbon Nanotubes***

Different methods for purification are used for different types of CNTs. In this dissertation study SWNTs made from laser ablation method in our group are mainly used due to the accessibility of the equipment and the relative reliable quality of these laser ablation materials. While small amount of CNTs were needed in this research, the relatively low yield of laser ablation method did not impose difficulties. As described in chapter 2, in the laser ablation target only 0.3 wt% of catalyst particles were added, which means catalyst particles do not compose major part of the impurities in the raw material. Therefore acid is not needed in the purification process and methods are particularly developed to separate amorphous carbon, graphitic particles and C<sub>60</sub> from SWNTs.

The purification schemes that have been developed usually take advantage of the differences in the aspect ratio [1] and oxidation rate between the nanotubes and the impurities [2,3]. Although the majority of the impurity phases can be eliminated by a combination of filtration and oxidation treatment, these processes also damage the structural integrity of the nanotubes by creating defects on the graphene shells [4].

A combination of hydrogen peroxide (H<sub>2</sub>O<sub>2</sub>) reflux and filtration [5] is an effective way to remove most of the impurities without causing much damages to the nanotube compared to, for example, sonication in more potent oxidation agent such as Nitric acid [4]. In this process,

amorphous carbon impurities are preferentially oxidized during the hydrogen peroxide reflux, and their oxidation products are separated from CNTs by filtration. C<sub>60</sub> impurities are also removed by dissolution in carbon disulfide.

Detailed purification process was schematically described in Figure 3.2. 500mg of as produced CNT containing soot was first well dispersed in 400 mL methyl alcohol by bath sonication for 2-3 hours. SWNTs bundles in the raw materials have average length larger than 10 μm, they often tend to entangle and form aggregations in the suspension. This pre-dispersion is to break or soften those entangles, so that a uniform chemical exposure of the material will be achieved. Sometimes, the raw material was also grounded in an electric blender with methyl alcohol to get a uniform dispersion. Then the methyl alcohol is removed by filtering the solution through 2μm pore-size PTFE (poly-tetrafluoro-ethylene) membrane filter (Milipore, Isopore filter). Before the total evaporation of the methanol and re-entanglement of the CNTs, they were placed in 300mL of 20% H<sub>2</sub>O<sub>2</sub> in a round bottom flask. The flask was placed in a heat mantle to keep the solution at 100°C for the oxidization of amorphous carbon by H<sub>2</sub>O<sub>2</sub>. The flask neck was connected to the condenser circulated with chill water to keep the fluid refluxing. After 8 hours' reaction, the solution was allowed to cool to room temperature. At this point, most amorphous carbon initially surrounding CNT ropes is oxidized, but the oxidation products remain dissolved in the solution.

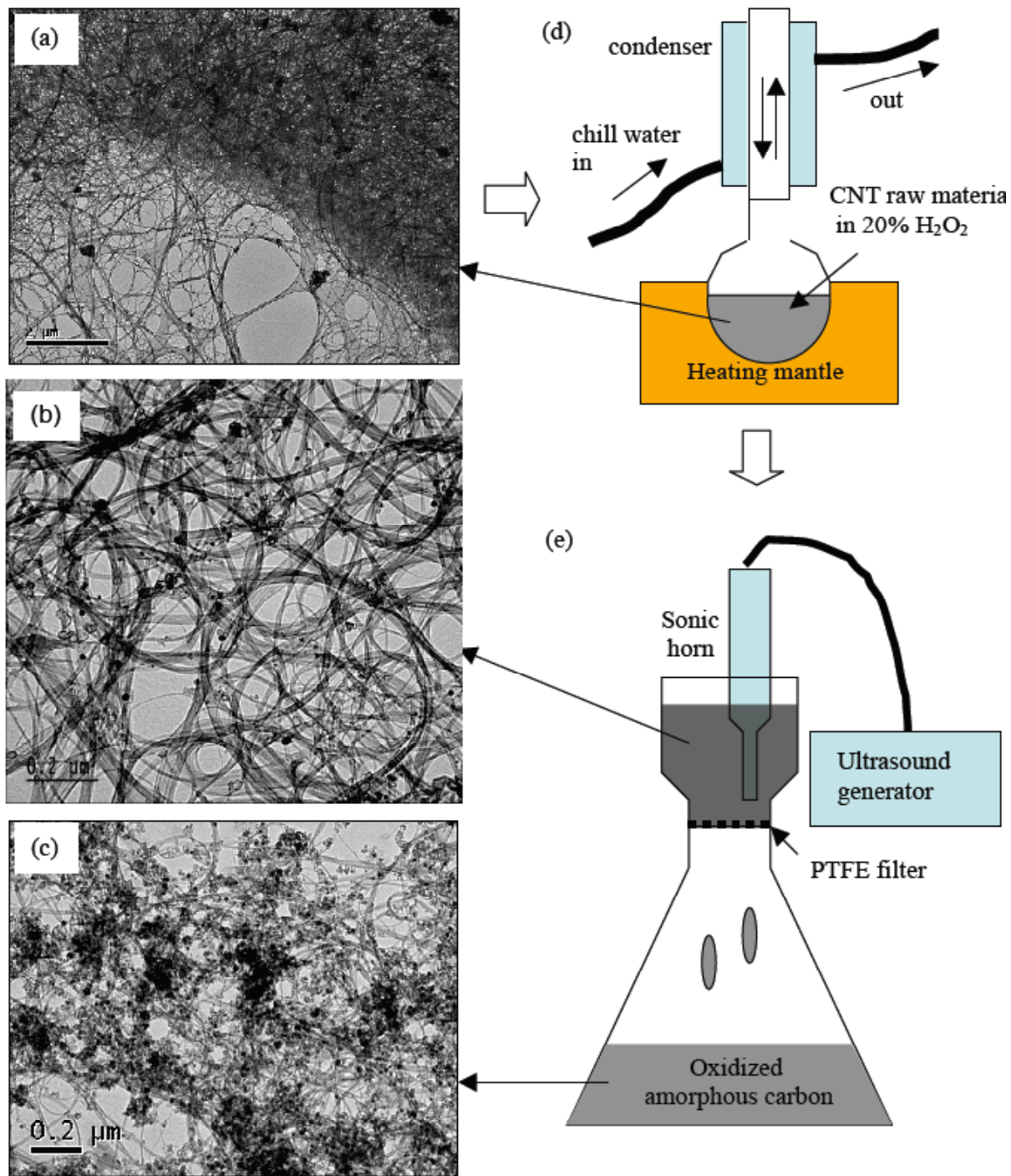


Figure 3.1 Purification of SWNTs produced by laser ablation. (a) A TEM picture of as synthesized SWNTs shows entangled SWNT bundles surrounded by amorphous carbon and catalyst particles. (b) Purified SWNT bundles with purity higher than 90%. (c) The impurities along with some SWNT bundles was filtered through the membrane with the aid of an ultra sonic horn; (d) Illustration of H<sub>2</sub>O<sub>2</sub> reflux system. The SWNT raw material was oxidized for 8 hours using 20% H<sub>2</sub>O<sub>2</sub> in water. The heat mantle was operated at 100°C. (e) Filtration System.

a sonic wave generating horn was placed inside the solution to keep the CNTs suspended in the medium without sinking down onto the membrane surface to clog the pores and at the same time to separate the oxidized amorphous carbon, isolated catalyst particles and small graphitic particles from the nanotubes. By repeating this process several times until the solution coming down through the filter membrane is almost clear, most oxidation product of amorphous carbon could be removed. During the same process, small amount of isolated catalyst particles are also removed, but some of them attached to the CNTs and covered with graphitic shell were hard to remove without further oxidation using different oxidation chemical reactions.

At the last step, CNTs are suspended in Carbon disulfide and methyl alcohol mixture. Then the suspension is filtered with the aid of the sonic wave generation horn to purify C<sub>60</sub> in the material. Purified CNT film is collected from the surface of the membrane filter and dried in a convection oven overnight. X-ray diffraction (XRD) and TEM measurement using a LEO EM 910 TEM indicate that the purified samples contain ~ 90% SWNT bundles over 10 µm in length and 30-50nm in bundle diameter. (Figure 3.1 (b)) The average SWNT diameter was estimated to be 1.4 nm by x-ray and Raman measurements [7].

### **3.2.2 Cutting of Carbon Nanotubes**

Even though the purified CNTs are free of most amorphous carbon impurities, they remain long and entangled. It is difficult to align or assemble pristine SWNTs with large aspect ratios ( $10^3$  - $10^4$ ) into well controlled patterned structures with a small dimensions. And it is difficult to use the long spaghetti like CNT bundles as nanoprobes even though they are

assembled. Therefore, reducing the CNT bundle length in a controlled way is often desirable. The cutting of CNTs also opens their end tips, allowing the guest species to diffuse into the interior spaces of nanotubes.

The nanotubes can be shortened by ball-milling [8,9], mechanical cutting [10], and chemical etching [11-13]. Narrower length distribution is always desired in all kinds of applications for short cut CNTs. In this respect, chemical etching is believed to produce better results than ball-milling or mechanical cutting because of the homogeneous nature of a solvent-based process [14]. In chemical etching, purified CNTs are sonicated in concentrated acid so that chemical oxidation can be initiated from the sidewall defects as well as the tips, where the reactivity is higher [14].

To cut CNTs by wet chemical etching, 100 mg of purified and dried CNTs are first placed in a mortar. To get uniform exposure of CNTs to strong acid, CNTs were pestled with the help of several droplets of strong sulfuric acid (98% Assay). When uniform slurry is obtained, the slurry is transferred to a flask and more sulfuric acid is added until the total volume reaches 60mL, then 20 mL of concentrated Nitric acid (78% assay) was added to the mixture. The flask containing CNTs and acid mixture was placed in the water sonication bath. Sonication duration varied depending on the desired average length of CNTs. The average length of SWNT bundles was consistent within a narrow error bar with repeated experiments when the same ultrasonic bath was used. Therefore, an empirical relationship between the bundle length and the etching time could be established using a low power ultrasonic bath (Fisher model FS15, operating power 60W) (Figure 3.3). For the laser ablation SWNTs, to

get 2  $\mu\text{m}$  bundle length, 21 hours of sonication is needed, while for 0.5  $\mu\text{m}$ , 30 hours is needed. The etch time and length distribution relations also depend on the quality of the starting material. When cutting CVD grown small diameter MWNTs, much less time is needed to get similar length distribution. After the desired etch time, the acid-CNT solution was diluted 10 times with deionized water to prevent further oxidation. The diluted acid mixture was then filtered through a PTFE membrane filter with 0.5  $\mu\text{m}$  size pores. Shortened CNTs were collected from the surface of the membrane filter, and dispersed in 300 mL of deionized water to rinse away the residual acid. After repeated filtration and dilution in deionized water, approximately 20 mg (in case of 21 hour etching) of shortened CNTs were collected from the surface of the membrane filter and dried in a convection oven over night. The TEM pictures in Figure 2.4 shows rigid rod-like SWNT bundles of average length 1.5  $\mu\text{m}$  and 0.5  $\mu\text{m}$ , respectively.

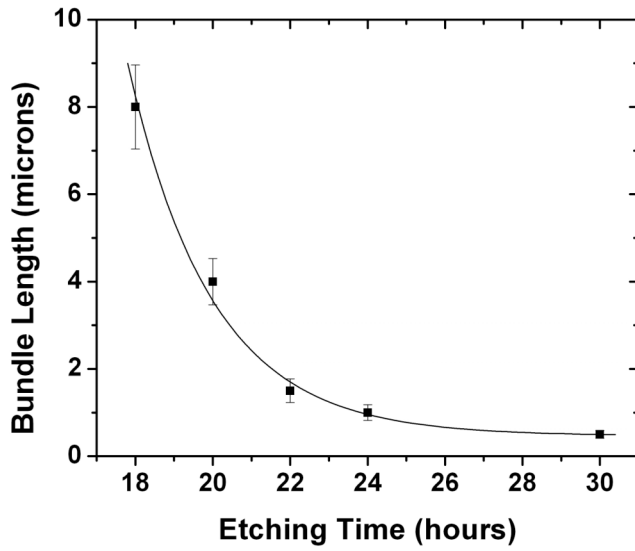


Figure 3.2 Experimentally observed relationship between the average bundle length and the processing time. This relationship was determined for SWNTs produced by laser ablation process [11].

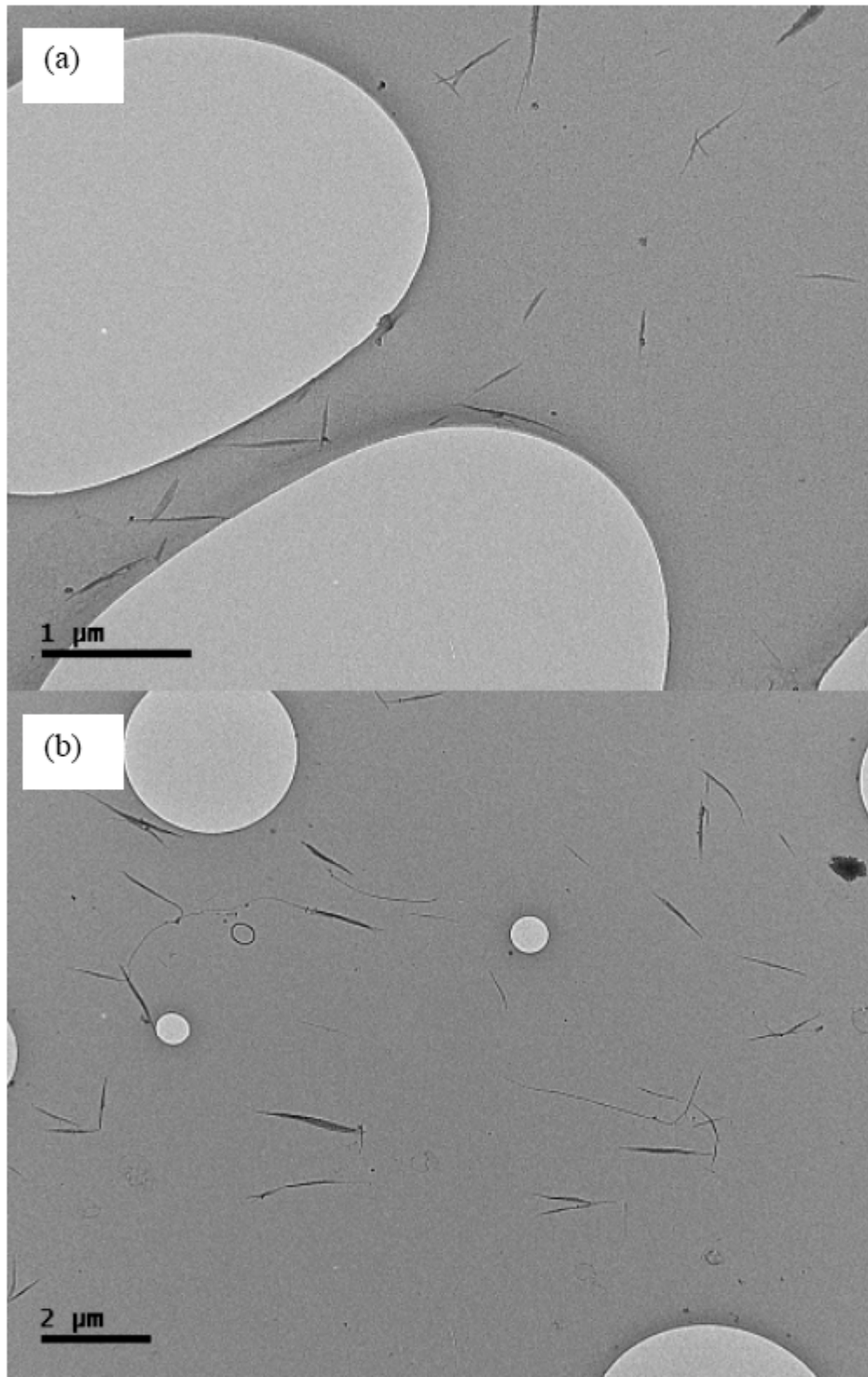


Figure 3.3 TEM pictures of shortened SWNT bundles to average length a. 0.5  $\mu\text{m}$  and b. 1.5  $\mu\text{m}$ . The tubular structure was not damaged during the chemical etching.

### **3.2.3 Properties of Acid Treated Carbon Nanotubes**

Except for the desired length distributions and the rigid-rod morphology, these strong acid oxidized CNTs have other interesting properties.

#### ***Open Ended Structure (Accessibility to interior space)***

As described in the fist chapter, the porosity and reactivity of the carbon nanotubes (CNTs) make them attractive host materials for storage of neutral species and electron donors [15]. Experimental and theoretical results have shown relatively high storage capacities alkali metals [16,17], suggesting potential applications for fuel cells and rechargeable batteries. One of the key parameters that determine the applicability of the CNTs for energy storage is the amount of materials/charges that can be stored per unit weight. This is determined in part by the accessibility of the interior spaces of the CNTs for diffusion. Experiments of lithium intercalation [17] have shown that the lithium/carbon ratio increases from  $\text{LiC}_6$  to  $\text{LiC}_3$  after the CNTs are etched in strong acid [17]. Similar results have also been observed for other guest species such as methane [18] and  $\text{C}_{60}$  fullerenes[19]. The large increase is attributed to diffusion of additional Li ions into the interior spaces of the SWNTs through the open ends and possibly the defective sides on the sidewalls. Opening of the tube ends in oxidizing environment have been reported in several studies. The effects of exposing CNTs to different oxidizing agents from mild oxidizing gas [20-22] to strong acids [23,24] have been investigated.

Here the end structure of acid treated CNT bundles is studied carefully by high resolution TEM (HRTEM). Low resolution TEM image for the batch of strong acid oxidized SWNT

bundles is shown in figure 3.4 (a). While a HRTEM image of the bundle ends is shown in Figure 3.4 (b). The outer surfaces of the bundles were coated with amorphous carbon, which was presumably produced by the etching process. The ends of the SWNT bundles have a tapered morphology suggesting that the etching process starts both laterally and longitudinally. The detailed structure of the individual SWNTs was not resolved because the abundance of the amorphous carbon.

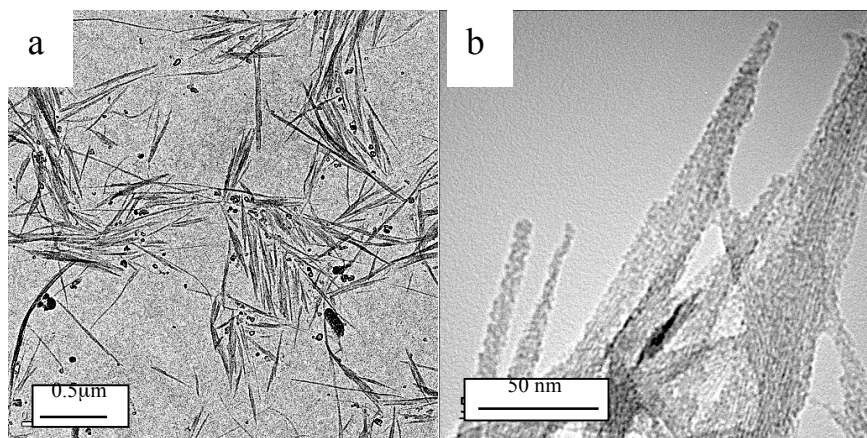


Figure 3.4: a) Low resolution TEM image of acid treated SWNT bundles before annealing to show the average bundle length is about 1 $\mu$ m, the scale bar is 0.5 $\mu$ m; b) High resolution TEM image of acid treated SWNT bundles, showing blurred edge of the bundles, indicating that they are wrapped with amorphous carbon after the acid treatment. The tapered ends also suggest that etching process happens both lateral and longitudinal.

The same batch of sample was vacuum annealed at 400°C for 10hr under  $5 \times 10^{-6}$  torr base pressure. Then it was studied by HRTEM. HRTEM images of 20 individual tubes were taken from the sample. The results show that the tips of overwhelming majority of the SWNTs were opened by the oxidation process and remained open after annealing (Figure 3.5). This is consistent with the prior Li intercalation [17] and gas uptake [18] experiments, which showed a large increase of the storage capacity after the SWNTs were etched and annealed at 500 °C

in vacuum [18]. The surfaces of these SWNT bundles have much less amorphous carbon and the bundles have better crystallinity than those before annealing, as shown by the TEM images.

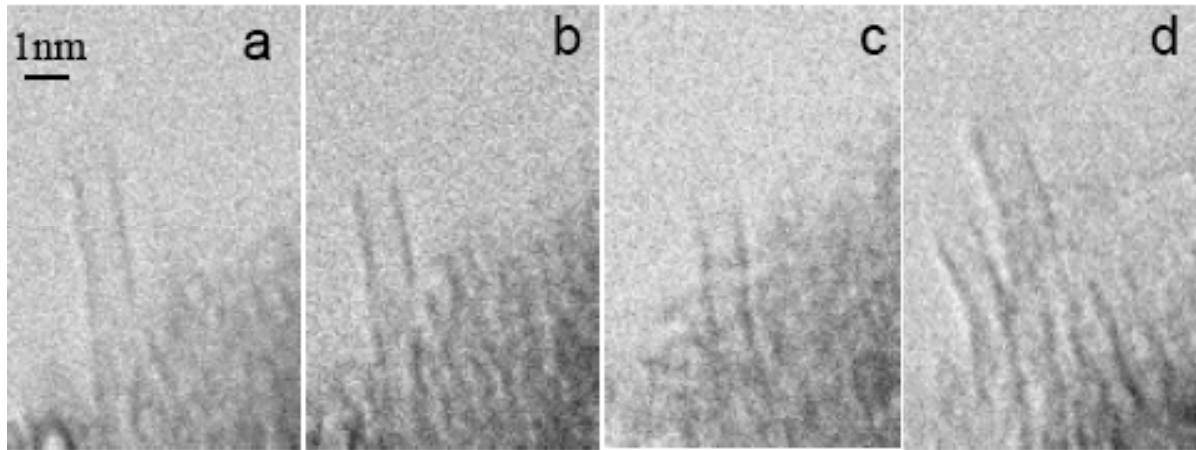


Figure 3.5 HRTEM images of individual SWNTs after oxidation and vacuum annealing at 400 °C for 10hrs. The results show that the ends of the SWNTs stayed open after the 400 °C annealing. (The scale bar is the same for all 4 images)

The reduced aspect ratio of the shortened SWNT bundles was 50-100 depending on the length. This is much lower than the intrinsic aspect ratio  $10^3$ - $10^4$  of pristine nanotubes, but it is still sufficiently high for most applications including field emission. The Raman spectroscopy data also showed unchanged Radial Breathing Mode (RBM) frequency, confirming unchanged intrinsic structure of oxidized SWNTs (Figure 3.6).

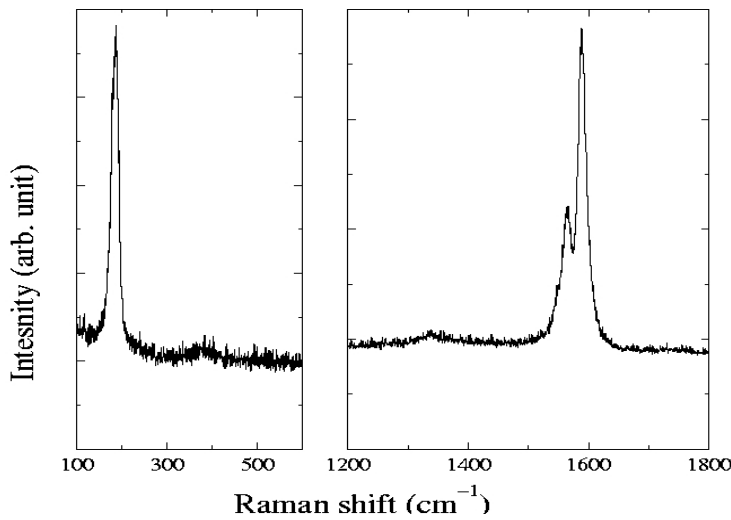


Figure 3.6 Raman spectroscopy data from chemically oxidized SWNTs indicates unchanged frequency of the characteristic RBM mode.

### 3.3 Regraphitization of the Carbon Nanotubes by High Temperature Annealing

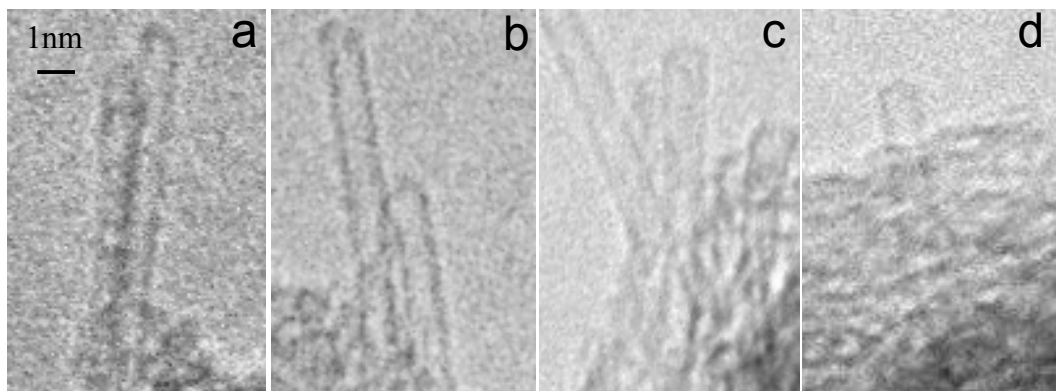
The regraphitization of carbon nanotubes by high temperature annealing was studied here to gain further control over the structure of the processed carbon nanotubes. Although the regraphitization of CNTs has been the subject of several theoretical investigations [25, 26] there is no report on re-graphitization of the defects in bulk CNT materials.

Here we investigated the effects of annealing on the structure of the SWNT tips in *bulk* samples by HRTEM and NMR studies. HRTEM results show the SWNT opened by oxidation (shown in previous section) can be closed by vacuum annealing at a lower than

expected temperature. The observation is confirmed in bulk samples by proton NMR measurements of the amount of ethane uptake at different processing stages. The re-graphitized SWNT tips have a variety of morphologies that are different from the ideal hemispherical structure. The results demonstrate the structure of the SWNTs in bulk quantities can be modified in a controlled fashion to optimize their materials properties.

### **3.3.1 HRTEM Analysis**

After TEM observations the same batch of acid treated SWNTs discussed in last section was annealed at 800°C for 1hr at  $5 \times 10^{-6}$  torr. Figure 3.7 shows the typical TEM micrographs taken from the same sample after annealing at 800°C. The tips of 19 out of the 20 individual SWNTs observed were closed and/or covered with some disordered structures. The closed tube ends were found to have various morphologies instead of the perfect hemispherical structure. For example flat and irregular cap structures were often observed as shown in Figure 3.8 (i). Some of the tips were covered with disordered structures as shown in Figure 3.8 (e)-(h). The exact nature of these structures is unclear. They are possibly chemical groups attached to the nanotube tips or the amorphous carbon formed either during the oxidation process or by contamination formed during TEM observation. Out of the 20 clear images of the individual SWNT tips taken, only one showed an open-ended structure.



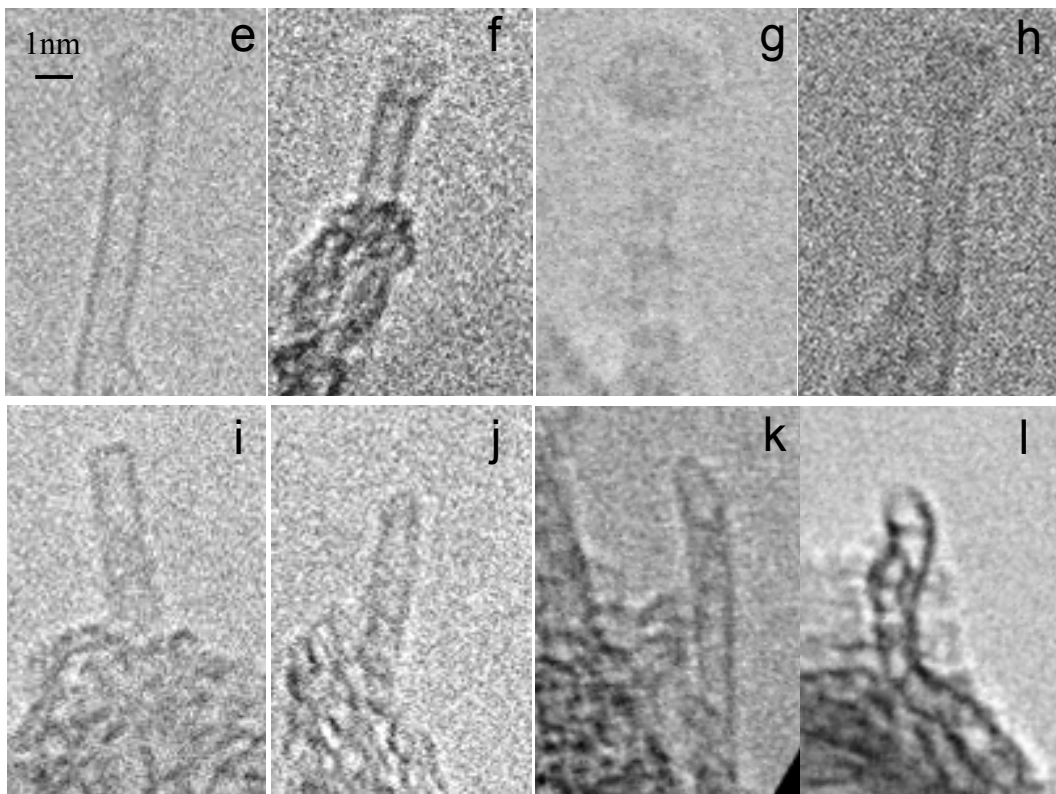


Figure 3.7 HR-TEM images of individual SWNTs after oxidation and annealing first at 400°C for 10hrs then at 800 °C for 1hr. (The figures share the same scale bar.)

### **3.3.2 Gas Absorption Experiment and Results**

Since TEM studies are intrinsically limited by the fact that the number of nanotubes observed is a very small fraction of the total sample, NMR technique was utilized to investigate the effect of oxidation and vacuum annealing on the *bulk* SWNT samples. The hypothesis of this approach is that gas adsorption capacity is correlated to the accessibility of the interior space of the nanotubes which can be modified by oxidation and annealing. This has been confirmed by our previous studies that showed the amount of methane adsorption increased significantly after the SWNTs were etched by oxidation [18].

The SWNT sample was put into a quartz NMR tube connected to a vacuum pump and an ethane cylinder. The experiment was performed at room temperature in the pressure range of 0-0.6MPa of C<sub>2</sub>H<sub>6</sub>. Data were analyzed using the method published in reference [13]. In brief, since the intensity of the NMR spectrum is proportional to the numbers of proton spins in the observed volume, it changes with the gas pressure and the adsorption capability of the SWNT sample. The NMR spectrum at certain pressure is composed of a sharp peak and a broad peak. The sharp peak, which is only proportional to the gas pressure, is attributed to gas molecules in the region of the NMR sample tube unoccupied by SWNTs. The intensity of the broad peak, whose dependence on the gas pressure is plotted in Figure 3.8, shows characteristic behaviors of adsorption.

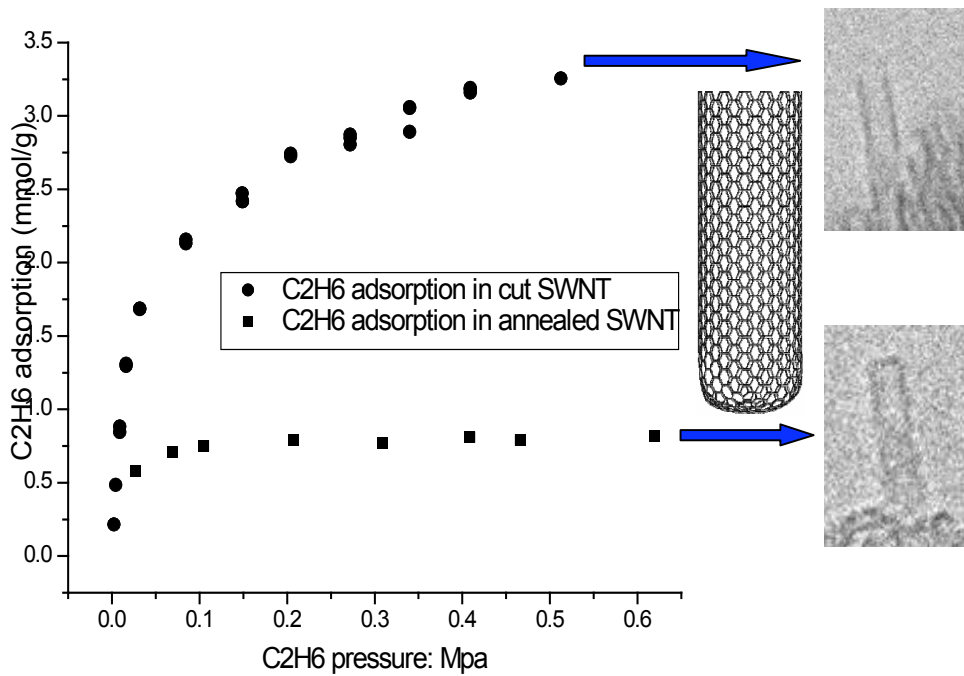


Figure 3.8 Pressure dependence of the intensities of the broad peaks of the <sup>1</sup>H NMR spectra of cut SWNTs before and after 800°C annealing exposed to C<sub>2</sub>H<sub>6</sub> at room temperature. The change in intensity clearly indicate the openness of SWNT tips.

The amount of ethane uptake was measured for the etched sample and the same sample after 800°C annealing obtained from the *in-situ* proton NMR experiment. As shown in Fig. 4, the amount of C<sub>2</sub>H<sub>6</sub> stored in the etched SWNTs reached the level of ~3.5mmol of C<sub>2</sub>H<sub>6</sub> per gram of SWNTs at 0.6MPa which is to be compared with the 0.4 mmol/gram in pristine SWNTs that we reported previously [18]. The adsorption rate after annealing at 800°C dropped significantly to became comparable to that of the as purified pristine SWNTs (with close-end structure). At 0.6MPa, the amount of C<sub>2</sub>H<sub>6</sub> uptake reduced to 0.8mmol/gram. The NMR result also showed that the amount of proton-containing chemical groups such as carboxyl or/and hydroxyl group were reduced significantly after the high temperature annealing.

The NMR result is consistent with the conclusion from the TEM study that the tips of most of the SWNTs were closed after annealing at 800°C. This re-graphitization temperature is lower than the temperature predicted by theoretical calculations [13, 25]. First-principles molecular dynamics simulations show that open-end SWNT closes spontaneously into graphitic dome with no residual dangling bonds at 2000K-3000K [25]. A recent electron field emission study showed that the SWNT tip can be opened under high emission current and closed again when the current is decreased at an estimated tip temperature of 1600K induced by the emission current.

The low re-graphitization temperature observed in the present experiment might be due to the present of amorphous carbon and other hydrocarbon chemical groups created by the oxidation process. The difference shown (in section 3.2) between the etched sample and the

sample heat treated at 400°C has also indicated the migration of amorphous carbon along the tube wall. The forming of a flat cap structure was simulated using the Cerius2 software by introducing pentagons and atomic carbon to an open end (10, 10) SWNT. After relaxation was allowed this structure was found to be metastable, though energetically less stable than perfect hemispherical caps.

### **3.4 Summary**

In summary, the methods of purifying CNTs and cutting them into desired length distributions by using strong acid mixture are discussed here. The end structures of the acid treated material and the same batch of material after heat treatment was studied carefully by using HRTEM and NMR study of gas absorption. The results presented here demonstrate that the structure of macroscopic quantity of SWNTs can be modified to fine-tune their materials properties such as their morphology and the storage capacity of the guest species. Although individual opened SWNT tips have been reported before, this combined TEM and NMR study shows for the first time that tips of SWNTs in bulk quantities can be uniformly opened by oxidation and closed by vacuum annealing at a surprisingly low temperature. The results provide a guideline on how the SWNTs should be processed for potential energy storage applications.

### 3.5 References

1. K. B. Shelimov, R. O. esenaliev, A. G. Rinzler, C. B. Huffman, R. E. Smalley, *Chem. Phys. Lett.* **282** (1998) 429.
2. T. W. Ebbesen, P. M. Ajayan, H. Hiura, K. Tanigaki, *Nature* **367** (1994) 519.
3. K. Tohji, T. Goto, H. Takahashi, Y. Shinoda, N. Shimizu, B. Jeyadevan, I. Matsuoka, Y. Saito, A. Kasuya, T. Oshuna, K. Hiraga, Y. Nishina, *Nature* **383** (1996) 679.
4. M. Monthoux, B. W. Smith, B. Burteaux, A. Claye, J. E. Fischer, D. E. Luzzi, *Carbon* **39** (2001) 1251.
5. O. Zhou, B. Gao, C. Bower, L. Fleming, H. Shimoda, *Mol. Cryst. Liq. Cryst.* **340** (2000) 541.
6. Soojin Oh's Dissertation
7. X.P. Tang, A. Kleinhammes, H. Shimoda, L. Fleming, C. Bower, S. Sinha, O. Zhou, and Y. Wu., *Science* **228** (2000) 492.
8. B. Gao, C. Bower, J. Lorentze, L. Fleming, A. Kleinhammes, X. P. Tang, L. E. McNeil, Y. Wu, and O. Zhou, *Chem. Phys. Lett.* **327** (2000) 69.
9. N. Pierard, A. Fonseca, Z. Konya, I. Willem, G. van Tendeloo, J. B. Nagy, *Chem. Phys. Lett.* **335** (2001) 1
10. I. Stepanek, G. Maurin, P. Bernier, J. Gavillet, A. Loiseau, R. Edwards, O. Jaschinski, *Chem. Phys. Lett.* **331** (2000) 125
11. H. Shimoda, B. Gao, X. P. Tang, A. Kleinhammes, L. Fleming, Y. Wu, and O. Zhou, *Phys. Rev. Lett.* **88** (2002) 015502
12. P. M. Ajayan, T. W. Ebbesen, T. Ishihashi, S. Iijima, K. Tanigaki, H. Hiura, *Nature* **362** (1993) 522.
13. J. Liu, A. G. Rinzler, H. Dai, J. Hafner, A. R. Bradley, P. Boul, A. Lu, T. Iverson, A. K. Shelimov, C. B. Huffman, F. Rodriguez-Macias, Y. Shon, R. Lee, D. T. Colbert, R. E. Smalley, *Science* **280** (1998) 1253.
14. P. M. Ajayan and T. W. Ebbesen, *Rep. Prog. Phys.* **60** (1997) 1025.
15. J.E. Fischer. *Acc. Chem. Res.*, **34**(12) (2002) 1079-1086.

16. R.S. Lee, H.J. Kim, J.E. Fischer, A. Thess, and R.E. Smalley. *Nature*, **388**: (1997) 255-257.
17. H. Shimoda, B. Gao, X.P. Tang, A. Kleinhammes, L. Fleming, Y. Wu, and O. Zhou *Phys. Rev. Lett.*, **88**(1) (2002) 015502.
18. A. Kleinhammes, S.H. Mao, X.J. Yang, X.P. Tang, H. Shimoda, J.P. Lu, O. Zhou, and Y. Wu. *Phys. Rev. B*, **68**(7), (2003) 075418-1-6.
19. Smith B.W. and D.E. Luzzi. *Chem. Phys. Lett.*, **321** (2000) 169-174.
20. S. C. Tsang, P. J. F. Harris, M.L. H. Green. *Nature* **362**, (1993) 520
21. P. M. Ajayan, T. W. Ebbesen, T. Ichihashi, S. Iijima, K. Tanigaki, H. Hiura, *Nature* **362**, (1993) 522
22. Hiura, H; Ebbesen, T (1997). U.S. Patent **No.5,698,175**. Washington, DC: U.S. Patent and Trademark Office.
23. J. Sloan, J. Hammer, M. Z. Sibley, M. L.H. Green, *Chem. Commun.*, (1998) 347
24. J.C. Charlier; X. Blasé; A. De Vita; R. Car; *Applied Physics A*. **68** (1999) 267
25. K. A. Dean; B. R. Chalamala *J. Vacuum Society Techonlogy B* **21(2)**, (2003) 868
26. H. Geng, X. B. Zhang, S. H. Mao, A. Kleinhammes , H. Shimoda ,Y. Wu, O. Zhou *Chemical Physics Letters* **399** (2004) 109–113

# **Chapter 4 Manipulation and Assembly of CNTs by Dielectrophoresis**

## **4.1 Introduction**

In the previous chapters, it is described clearly that carbon nanotubes (CNTs) have become an important class of materials for both fundamental studies and technological applications [1]. Considerable progress has been made recently in understanding the formation mechanism and in developing synthesis routes for fabrication of homogeneous CNTs with controlled structure and morphology and in further process procedure to tune their properties. However eventual utilization of these novel materials in the wide range of applications such as sensors, electron field emitters and microelectronics, requires new processes for controlled assembly and integration, which is current lacking.

Dielectrophoresis is a versatile technique widely applied in biological systems [4] It is also often used to manipulate and separate colloidal particles based on the interaction between the alternating-current (AC) field and the induced dipole moments [2, 3]. Recently it has been utilized to orient, purify and align CNTs, [5-7] to make CNT interconnects, [8-10] and even

to separate metallic SWNTs from semiconducting SWNTs. Here a close study on the possibilities of assembly CNTs into functional structures by dielectrophoresis is carried on. Effects of some experimental conditions including the viscosity, ionic conductivity of the medium, and the frequency and amplitude of the AC field are systematically studied. The feasibility of fabricating CNT structures connecting differently patterned electrodes were researched; And CNT fibrils attached to sharp tips, which have versatile applications, were fabricated.

## 4.2 Dielectrophoresis

### 4.2.1 Dielectrophoretic Force

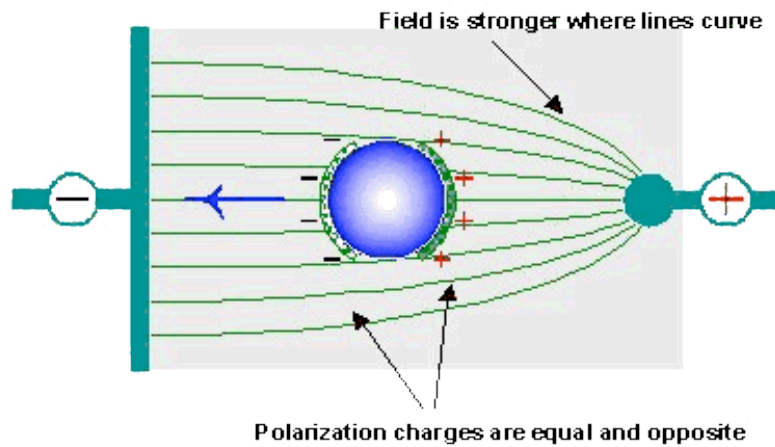


Figure 4.1 Illustration of Dielectrophoresis. [11]

When a neutral particle is placed in an electrical field that is spatially inhomogeneous, equal and opposite charges are induced on the particle by the electrical field. Because the field

strength is different on the two sides of the particle, a net force acts on the particle. This is termed as dielectrophoresis. (Figure 4.1)

The dielectrophoretic force  $F(t)$  on a particle is given by the following general expression [12]:

$$\vec{F}_{DEP} = (\vec{m}(t) \bullet \nabla) \vec{E}(t) \quad (1)$$

where  $m(t)$  is the polarizability of the particle and  $E(t)$  is the electrical field. A CNT or bundle can be considered as a rod shaped particle with very large aspect ratio. When a rod shaped particle is placed in the electrical field, it will experience a torque, which tends to align one of the particle's axes with the field. The rod will align so that all components of torque are zero. The magnitude and orientation of the torque depend on the frequency of the applied field and the properties of the particle and the medium. The orientation of a rod shaped particle can be controlled by the conductivity of the medium and the frequency of the applied field<sup>3</sup>. The dielectrophoretic force on a rod whose major axis is parallel to the electric field is given by equation (2) [12].

$$\vec{F}_{DEP} = \frac{2\pi abc}{3} \varepsilon_m \operatorname{Re} \left\{ \frac{\varepsilon_p^* - \varepsilon_m^*}{\varepsilon_m^*} \right\} \nabla \vec{E}^2 \quad (2)$$

Where  $a,b,c$  are the dimensions and  $\varepsilon_p^*$  is the permittivity of the rod.  $\varepsilon_m^*$  is the permittivity of the medium.  $\varepsilon^*$  is given by equation (3)

$$\varepsilon^* = \varepsilon - j(\sigma/\omega) \quad (3)$$

Where  $\sigma$  is conductivity, and  $\omega$  is the frequency of the AC field. From these equations, permittivity, conductivity of the suspending medium and the frequency of AC field are shown to be critical parameters. And the properties of CNTs are not variables in our experiments when certain types of CNTs are used.

From equation (2), when the permittivity of the particle is larger than that of the medium, dielectrophoretic force is positive and the particles will move to areas with high electrical field concentration. While when the permittivity of the particle is smaller than that of medium, negative dielectrophoresis will happen, where particles move to areas with low field concentration. This phenomenon is widely used in biology to separate live and dead cells, because they have different ion concentrations in their plasma. And it can potentially be used to separate metallic and semiconducting SWNTs when they are exfoliated into individual tubes by the aid of surfactants. [13] Experiments with successful results were reported, [14] however there are still doubts on the interpretation of the results. [15-17]

In our study, purified and etched SWNT bundles described in last chapter were used. No surfactant was used to exfoliate the CNT bundles. Therefore semiconducting and metallic tubes are contained in one bundle and the whole bundle appears to be metallic. In the following studies, only positive dielectrophoresis is considered and CNTs are all assumed to have a tendency to align along the electrical field and to move towards areas with high electrical field concentrations. [18]

#### 4.2.2 Torque and Alignment

Particles possessing any kind of polarization anisotropy will experience a torque that tends to align the particle with some preferred axis parallel to the applied electric field. [3] A freely suspended insulating ellipsoid always tends to align itself with its longest axis parallel to the imposed field. This alignment behavior is completely independent of the relative magnitudes of its permittivity or the permittivity of the suspending medium. However when CNT bundles suspended in DI water are subjected to AC field, as conducting particles they may exhibit a frequency dependent orientational effect called an orientational spectrum. There always will be a pair of turnover points, where the particle changes its orientation. And if this pair of points do exist, parallel orientation (where long axis parallels the direction of the electric field) is always favored at the lowest and highest frequencies; The particle first changes from parallel to perpendicular orientation and then back to parallel as frequency is increased. [3]

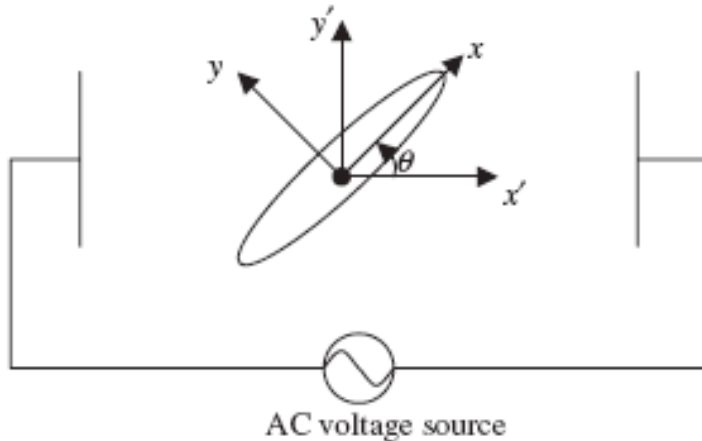


Figure 4.2 Illustration of an elongated particle suspended in AC field. [19]

Figure 4.2 shows a rod shaped particle put into an AC field with angle  $\theta$  between its long axis and the direction of the electrical field. If the particle is considered as a lossless particle

(with no conduction or dielectric conduction), the time averaged alignment torque with respect to z-axis is given by equation (4) [19]:

$$\frac{3\langle T^e \rangle^z}{2\pi ab^2 E_0^2 \epsilon_m} = C_s \frac{\sin(2\theta)}{2} \quad (4)$$

Where a, b are the dimensions of the particle,  $E_0$  is the amplitude of the applied field and  $C_s$  is the nondimensional torque and will be referred to as torque constant. And  $C_s$  can be approximated in equation (5) when the particle has very large aspect ratio:

$$C_s = \frac{a^2}{b^2 \ln(2a/b)} \quad (5)$$

From equation (5), it is clear that a negative value of  $C_s$  will ensure that the parallel orientation be a stable orientation. Otherwise a positive value of  $C_s$  ensures that perpendicular orientation be the stable orientation.

To solve the rotation equation by balancing the alignment torque and a resistant force caused by the viscosity of the medium, the order of magnitude of the rod's responding time to the alignment torque is given by equation (6).

$$t_R = \frac{12\eta a^2 K_s}{b^2 E_0^2 \epsilon_m |C_s|} \quad (6)$$

Where  $\eta$  is the viscosity of the suspending medium and  $K_s$  is a shape factor and can be approximated in equation (7) when the particle has large aspect ratio:

$$K_s = \frac{1}{3 \ln(2a/b)} \quad (7)$$

For alignment of the particles to happen, the responding time need to be small so that effects caused by Brownian motion of the particle can be ignored; [19] However much larger than

the pitch time of electrical field, otherwise the particle will oscillate about the mean orientation. That means  $t_R$  is much larger than  $1/\omega$  and this condition can be approximated in expression (8) when the particle has large aspect ratio [19]:

$$\frac{12\eta\omega}{E_0^2\epsilon_m} \gg 1 \quad (8)$$

There's a threshold value of the AC frequency, only when AC frequency is larger than the threshold value, expression (8) is valid, and then alignment may happen. This threshold value can be lowered by increasing the viscosity of the medium. This is a very simple model, which assumes CNTs as lossless particles, as it is used in reference [19]. This model is explained here to shine some light on the experimental results that will be discussed later.

### 4.3 Experimental Setup

Patterns for electrodes arrays used in this study were first designed by using the program Corel Draw, and then printed out on transparencies, which is later used as photo masks. Glass substrates were rinsed in ethyl alcohol, acetone, and methyl alcohol respectively and then cleaned in UV-Ozone chamber for 30 minutes. The cleaned substrates were spin coated with a layer of photoresist in the clean room. And the mask was used to selectively expose the layer of photoresist. Then the photoresist was developed to get the negative pattern of desired electrode arrays. The pattern substrates were put into thermal evaporation chamber

with a chromium basket and a gold bolt included. Then the chamber was pumped down to desired vacuum by the aid of a liquid nitrogen cold trap. A 20 nm of Chromium was first deposited on the substrate, and then followed with a layer of gold with 100 nm thickness. The chamber was cooled down and the substrates were taken out. Photoresist was lifted off by sonicating the substrates in acetone.

Then a patterned electrode array was connected with a function generator. The experimental setup for in situ manipulation and observation is shown in Figure 4.3.

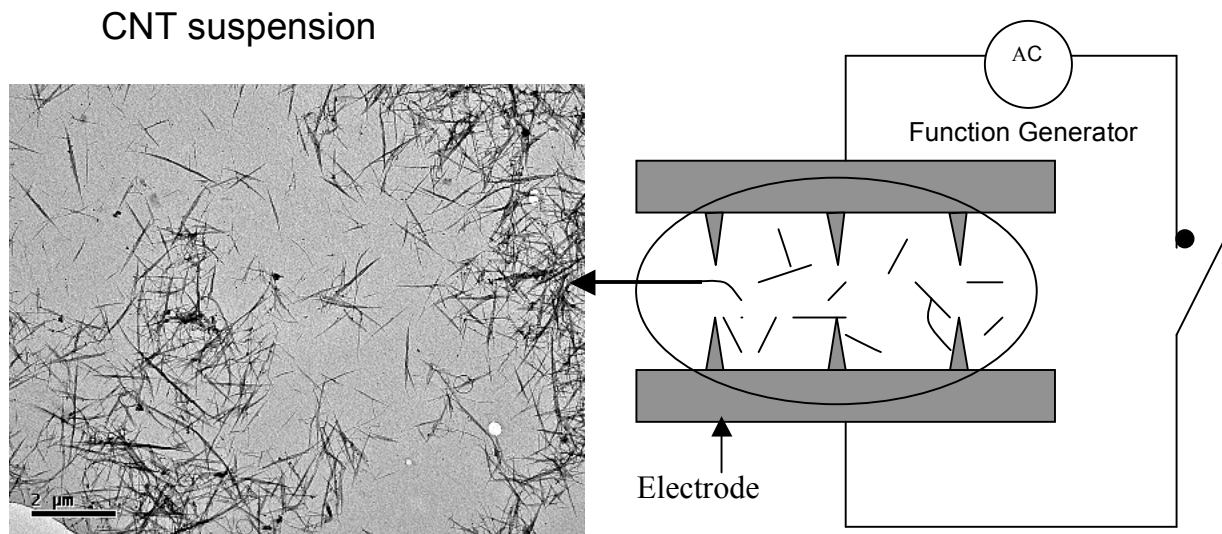


Figure 4.3 Illustration of Manipulation of CNTs on a patterned gold electrode array by dielectrophoresis. Left side is a TEM image of the CNT suspension used in this study.

Purified and etched SWNTs described in last chapter were dispersed in deionized water at the concentration of 0.1mg/ml. A droplet of the CNT suspension was applied on top of the electrode array. The AC field of 200V/cm was then applied. The movement of the CNTs was recorded by a CCD camera attached to an optical microscope.

#### 4.4 Assembly of CNT Structures

The idea of assembly CNT structures by dielectrophoresis was inspired by the work done on assembly of gold nanoparticles between two planar electrodes in AC field. [18,19] Gold nanoparticles were found to assemble from protrusions on the planar electrodes and wires of those particles will grow in the direction of highest field intensity. Planar gold electrodes with gap distance of 5mm on glass substrates were prepared according to reference [20]. After a droplet of CNT suspension delivered between the electrodes and AC field about 5V/mm was applied, Figure 4.4 shows the optical image of the assembled CNT structures.

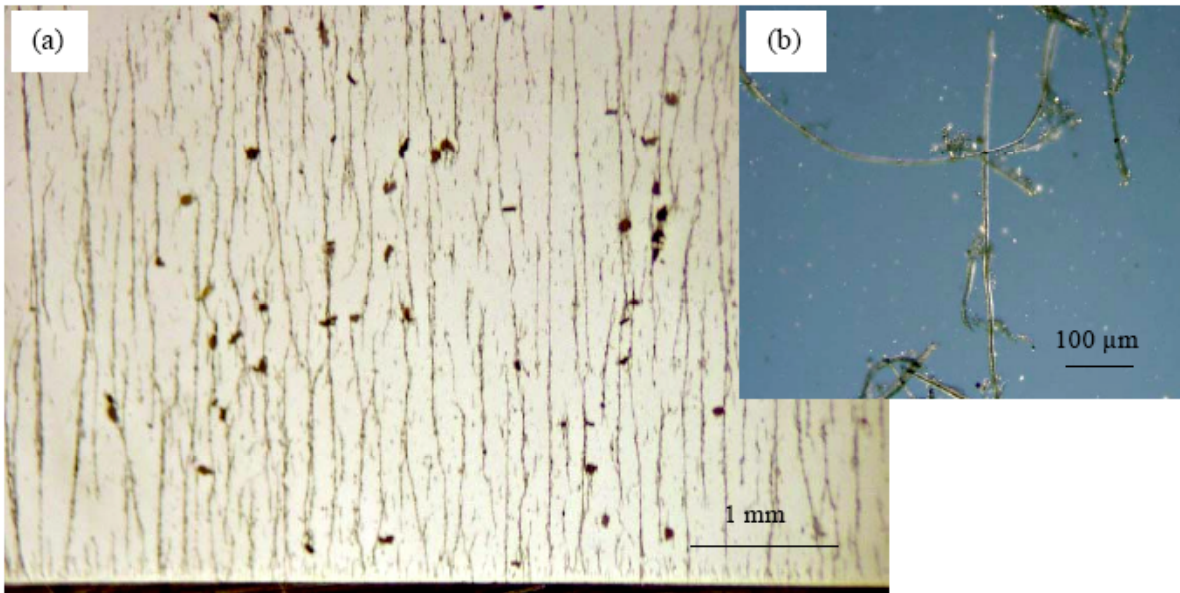


Figure 4.4 CNT structures formed between two planar electrodes. 25 V/mm of AC field was applied. (a) In situ optical image; (b) polarized light optical images of fibrils picked from the substrate.

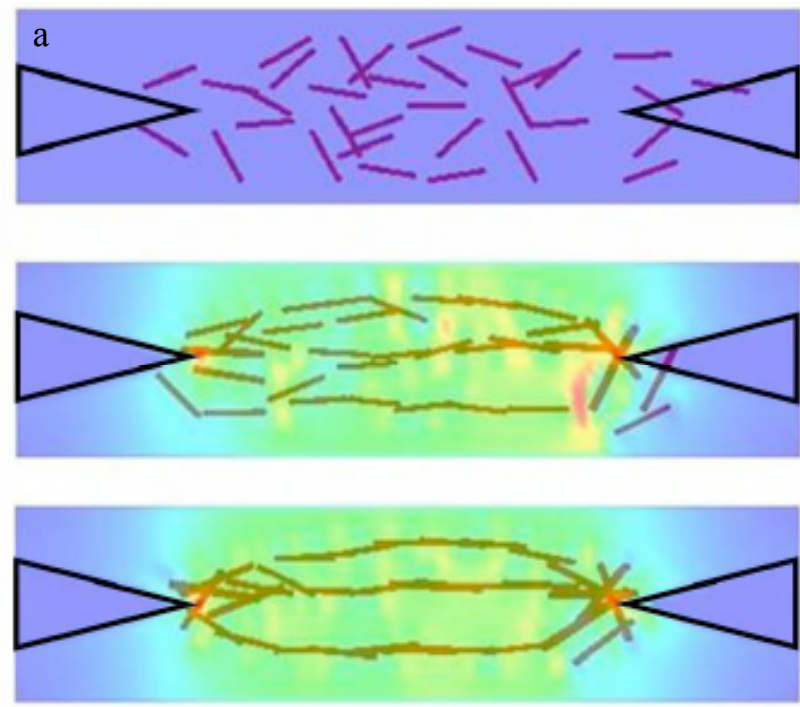
Fibrils like structures were formed along the electrical field. CNT suspension is different from the mono-dispersed homogeneous gold particle suspensions. The dark particles shown in the images are aggregations of CNTs and some impurities. Figure 4.4 (b) shows the polarized light optical image of fibrils picked up from the substrate. Smooth CNT fibrils with diameter around 1  $\mu\text{m}$  were formed.

#### ***4.4.1 Assembly of CNT Fibrils between two Facing Electrodes***

Planar electrodes provide unpredicted and uncontrolled protrusions where fibrils will start to form. When intentional designed electrode arrays were fabricated, CNT fibrils will be assembled in controlled positions on the substrate. Figure 4.5 shows that when protruded electrode arrays were used, CNTs will assemble into fibrils, which automatically connect two facing protruded electrodes. Figure 4.5 (a) shows the theoretical simulation. [25] Figure 4.5 (b) shows a serial of images taken from a movie, which recorded the assembly process of CNT fibrils that connect facing electrodes. And Figure 4.5 (c) illustrated the assembly process by highlighting the fibrils grown in each step. After the 100Hz AC field with strength of 2.5V/mm was applied on the opposing electrode arrays, some CNTs were found to start to assemble on the apex of the protruded electrodes. However CNT fibrils were also found to form in the middle of the gap. The explanation for this assembly away from electrodes is that the assembled fibrils has a lower state of energy than individual CNT bundles flowing in the suspension. There are calculations shows that under AC field the net dipole moment of two conductive spheres in contact is 2.4 times larger than the sum of two identical, non-interacting spheres. For chains of more than two spheres, the particle interactions become

even more pronounced. [3] And when the dipole is parallel with the electrical field, the dipole's potential energy is negative and proportional to the dipole moment. Therefore in AC field, it is energy favored that particles stay in contact with each other and form a wire like structure.

Those fibrils formed in the middle of the gap are still subjected to the dielectrophoretic force and will move to areas of high field concentration, which are the vicinities of the ends of fibrils grown from the protruded electrodes. At the same time all the fibrils are growing longer by themselves when CNTs in the suspension move towards their ends and attach to them. Eventually continuous fibrils connecting two opposing protrusions will form. One interesting phenomenon is that when two fibrils formed on the same pair of protrusion are both connecting the two protrusions, they will attract each other and form a thicker bundle. One explanation is that when the electrical connection is formed, current will flow through the two fibrils, and the magnetic force generated by the flowing current will attract the two fibrils and merge them together.



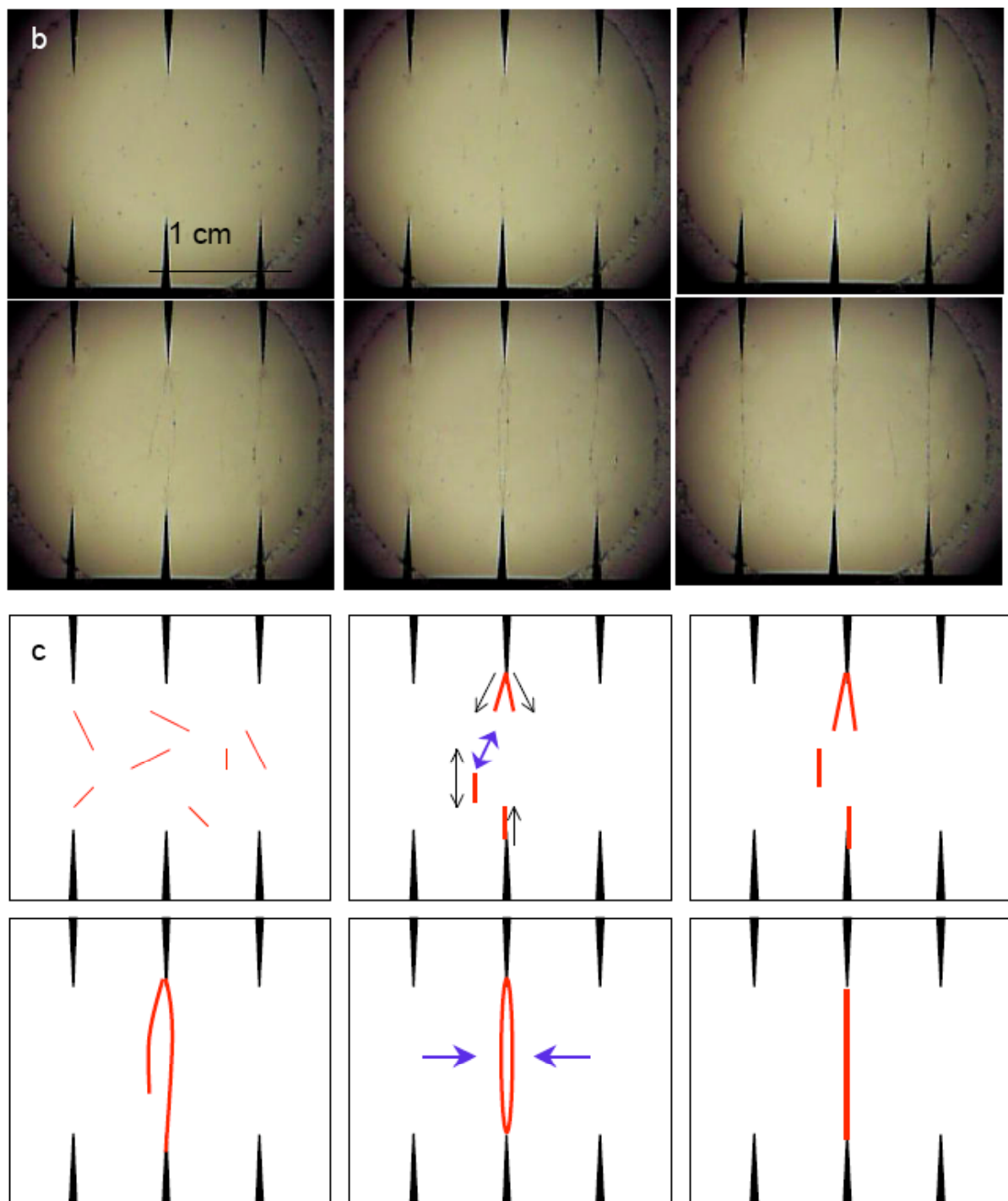


Figure 4.5 (a) Simulation of assembly process of CNTs between facing protruded electrodes; (b) shows several frames from a recorded movie revealing the CNTs at different stages of the assembly process under AC field. In (c) a schematic is drawn according to the optical images.

#### 4.4.2 Assembly of CNT Structures according to Field Distributions

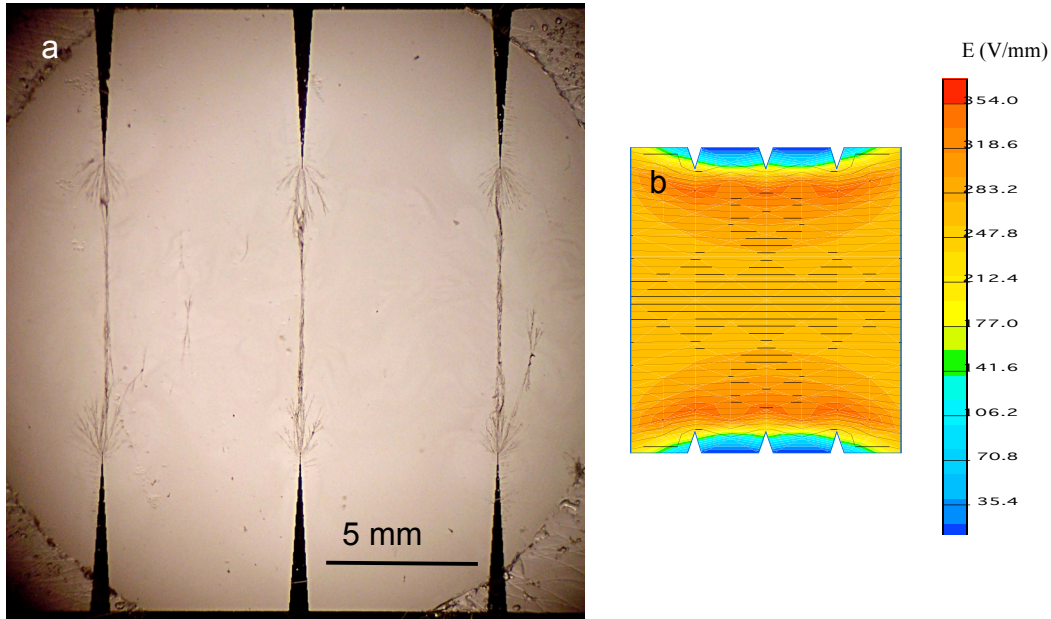


Figure 4.6 (a) Optical image of CNT fibrils assembled on facing electrode arrays. (b) Electrical field distribution of electrode array used in (a).

From the above experiments, the final assembly of CNT structures were found to have close relationships with the electrical field configuration of the electrode arrays. In Figure 4.6 (a), it clearly shows that at the end of protruded electrode CNT fibril were assemble and aligned along the electrical field direction, which is perpendicular to the equipotential lines shown in Figure 4.6 (b). The electrical field distributions of different electrode array configurations were studied by quick field. Then they were fabricated and used to get controlled assembly of CNTs. Figure 4.7 shows the assembled CNT structures by using different electrode arrays. When high frequency (10 MHz) AC field was used, CNTs were found to form refined and very well aligned structures along the electrical field directrion.

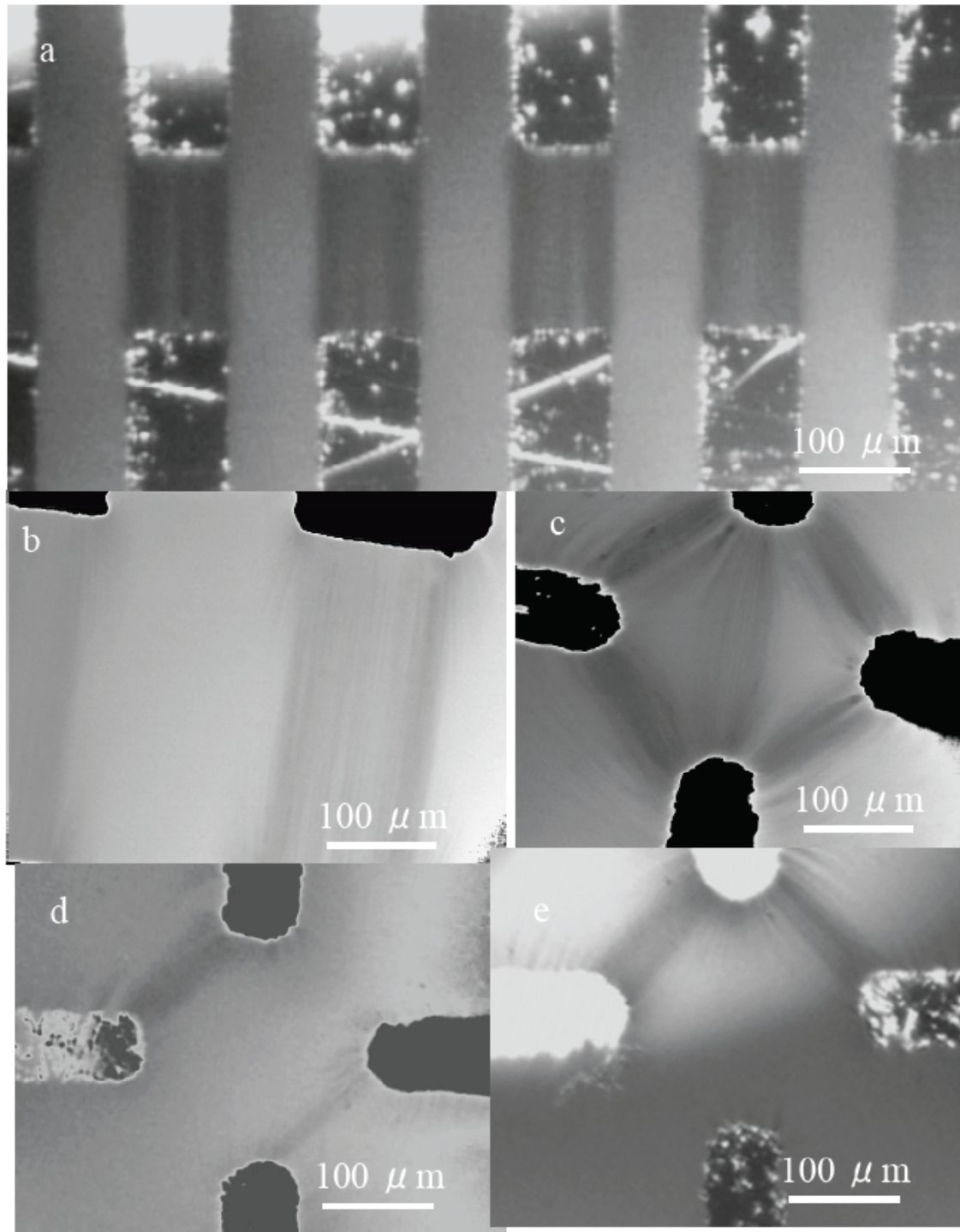


Figure 4.7 Different CNT structures fabricated by using different electrode array configurations. (a), (b) protruded electrodes with flat front facing each other, CNT structures were found to form exactly between the facing electrodes and CNT bundles within the structure are parallel to the electrical field; (c),(d),(e) Same set of electrode array, while when different electrical connection were used, different CNT structures can be fabricated.

## 4. 5 A Systematic Study on the Effects of Parameter

### 4.5.1 AC Field Frequency.

The experiment was conducted by applying a 2V AC field across two opposing metal electrodes that were in contact with a droplet of the CNT suspension. The AC field was turned on till the CNTs were assembled into a stable structure. The experiment was repeated

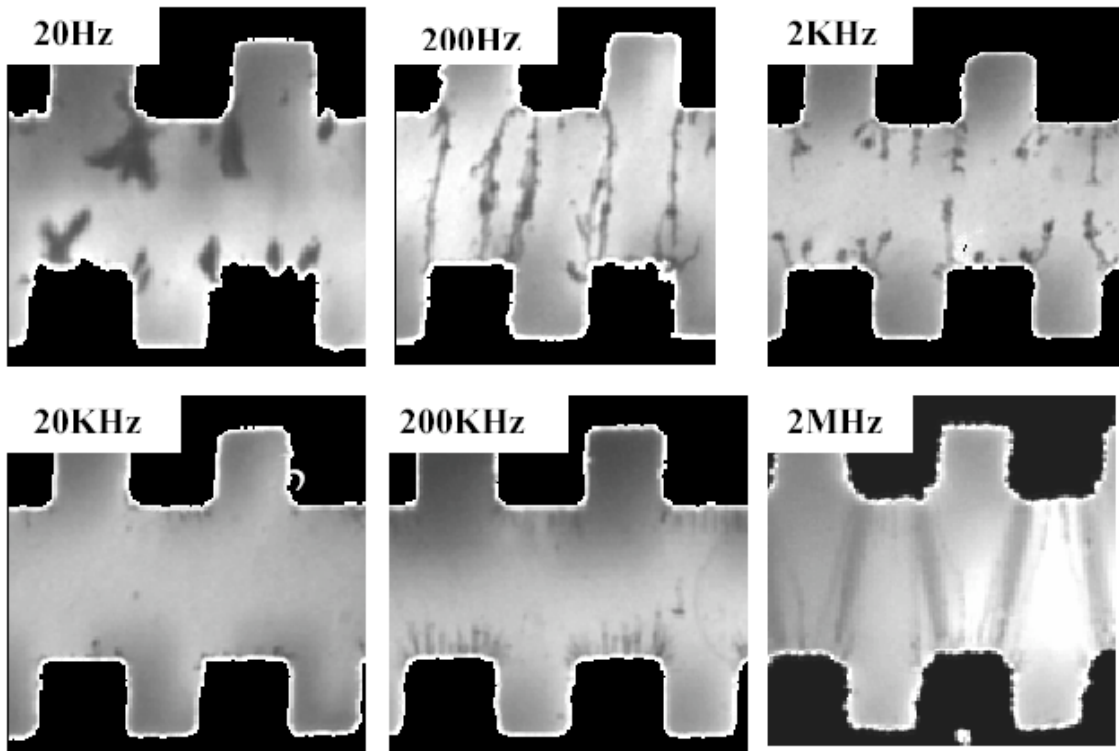


Figure 4.8 A series of optical images showing different CNTs structures formed under AC field with different frequency.

using different AC frequencies varying from 20Hz to 2MHz. For consistence, CNT suspensions from the same batch were used in all experiments. The results are shown in

Figure 4.8. It was found that under low frequency (20Hz) CNTs moved to the electrodes rapidly without aligning to the field direction and formed irregular patterns around the electrodes. When the frequency was increased to 2MHz, finer CNT structures were aligned along the AC field direction. In the middle frequency range (20KHz to 200KHz), the CNTs were found to have very low mobility and especially in the frequency range of 20K to 150K. No CNT structure was assembled even after the field was on for extended period of time.

Electrolysis of water under very AC field with very low frequency may caused the irregular and rapid assembly of CNT structures, because bubbles and flowing of the suspending liquid were observed.

As it was discussed in section 4.2.2 that, when a particle with ohmic loss is placed in the AC field, it may exhibit an orientational spectra, which are marked by a pair of critical frequencies where the particle abruptly changes from one stable orientation to another. CNTs have very large aspect ratio, their cross section dimension may be as large as a few tens of nanometers. And the polarizability of along the cross section direction is also fairly small. While the dielectrophoretic force a particle sees depends on its polarizability along the electrical field and the difference in the intensity of the electrical field along the electrical field that opposite part of the particle see. Therefore when a CNT bundle is perpendicular to the electrical field, the DEP force it sees will be so small that it's negligible. While at the same time the resistance force will be much large. No assembly was seen in the middle range of the AC frequency may very be explained by the orientation of the CNT bundles. If in the

middle range of frequency, stable orientation for CNT bundles are perpendicular to the AC field, then they can't see large enough DEP force, therefore no assembly was observed.

#### ***4.5.2 Ionic Conductivity of the Medium.***

The conductivity of CNT suspension was tuned by adding NaCl/water solution into the suspension. Experimental results showed that highly ordered CNT structures were fabricated in the suspending medium with low conductivity. However, when the conductivity of the medium increased the CNT structures formed became less ordered and when it reached 2S/m no CNT structures was observed. Experimental results are recorded in Figure 4.9. One explanation for this phenomenon maybe that the ions in the suspension screened the electrical field, therefore CNTs bundles failed to move according to field. Also adding free ions into the suspension, changes the zeta potential of the CNT bundles suspended in water, and from images taken when ionic conductivity reached 2S/m, coagulations of CNTs can be observed.

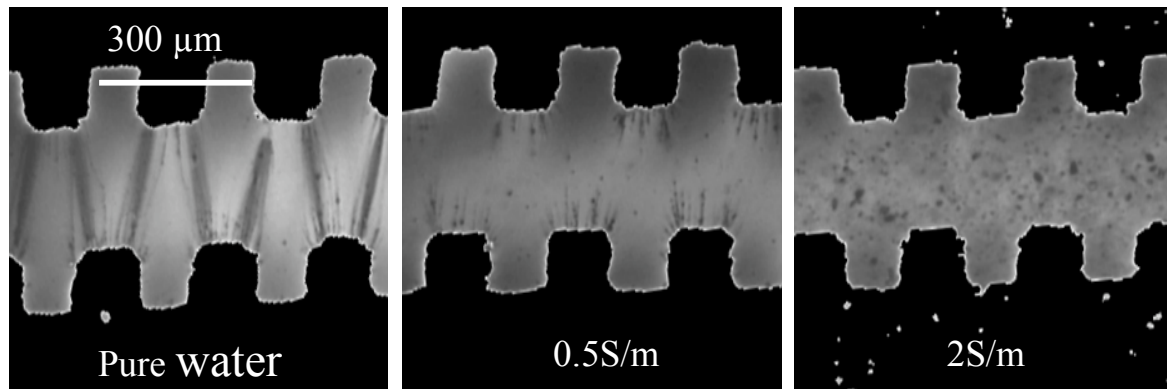


Figure 4.9 A series of optical images showing different structures CNTs formed under the same AC field but different ionic conductivity of the medium.

#### ***4.5.3 Viscosity of the Suspension.***

The viscosity of the medium was changed by adding glycerol into the suspension. Glycerol was mixed with the standard suspension at 1:1 ratio, which gave the medium six times the viscosity of pure water. The frequency dependent experiment was repeated using this more viscous medium. Figure 4.10 shows that under low frequency range (below 200 Hz), the adding of glycerol also prevented the electrolysis of water under AC field of low frequency, therefore prevented bundles moving rapidly and coagulate around edges of electrodes; The more ordered CNT structures observed under low frequency can also be explained by expression (8). Increased viscosity of the suspending medium lowered the minimum frequency required for alignment to happen.

While under frequency higher than 200 Hz, no CNT structure was observed after the field was turned on for extended period of time.

The addition of glycerol may also change the permittivity of the suspending medium therefore complicated the condition. More careful analysis and calculations need to be done to clearly explain this set of experimental data.

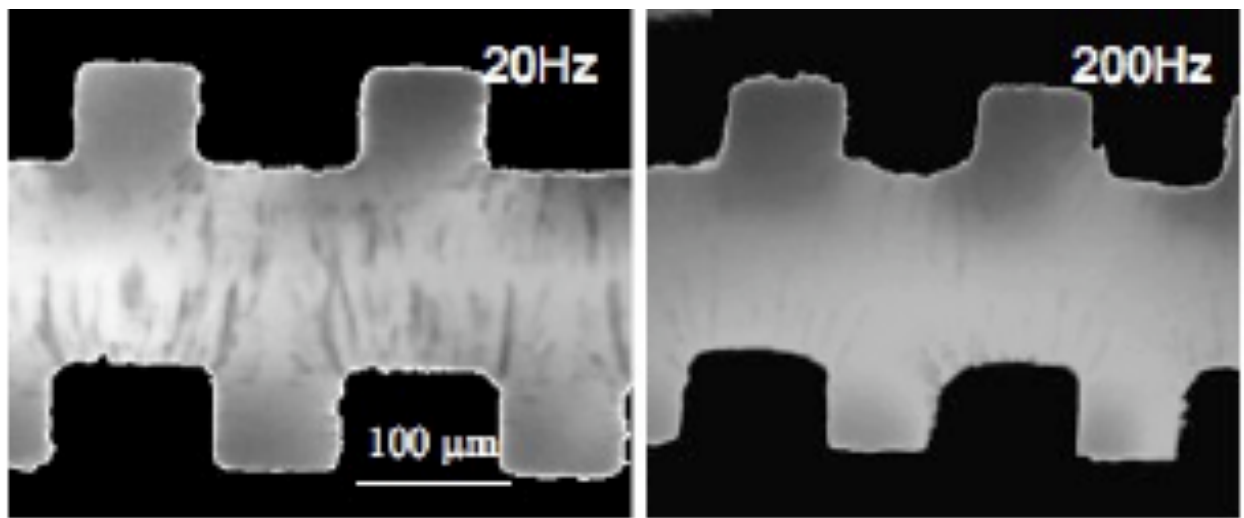


Figure 4.10 Optical images showing CNT structures form in viscous medium under different frequencies.

#### ***4.5.4 Concentration of the Suspension***

CNT structures were fabricated by using electrode arrays with the same configuration. While CNT/ DI water suspensions with different concentrations from 0.25mg/ml to 1mg/ml were applied to electrode arrays and 10MHz AC field with the same amplitude was used. By using CNT suspensions with different concentrations, CNT structures with different density can be fabricated. In Figure 4.11, it shows that by vary the CNT suspension concentration, different CNT coverage between two facing electrode can be achieved.

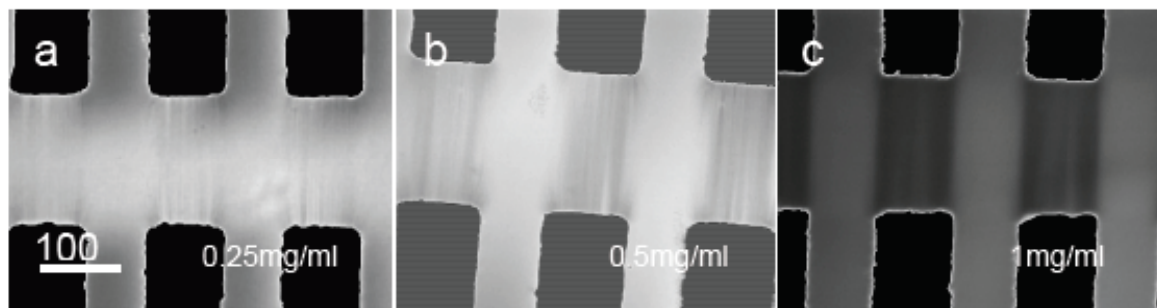


Figure 4.11 Optical images of CNT structures assembled on electrode arrays with the same configuration, under the same AC field, while with CNT suspension of different concentrations.

## **4.6 CNT Fibrils fabricated by Dielectrophoresis**

CNT structure can also be assembly by using electrodes with three dimensional configurations. Among all the CNT structures assemble under AC field, thin fibrils assembled on sharp probes were found to be of great interest [21-23].

### ***4.6.1 Fabrication of CNT fibrils***

When a sharp probe is used as one electrodes, while a flat or ring shaped electrode, which has a relatively much larger area and provide and less concentrated electrical field, is used as counter electrode. A non-uniform electrical field with large field strength gradient can be created. Particles suspended under this field will be subjected to a large dielectrophoretic force. As it was discussed in previous sections, CNTs used in our experiment always experience positive dielectrophoresis. Therefore, they will assemble around the sharp probe area. When the sharp probe is withdrawn from the suspension, the meniscus form around the probe end will compress the assembled CNTs and form well packed CNT fibrils. The whole process can be observed under an optical microscope. Figure 4.12 illustrated the dielectrophoresis process for assembly of CNT fibrils. [21] While Figure 4.13 shows the scanning electron microscopy (SEM) images of the CNT fibrils fabricated by this method. CNT fibrils with relatively controlled thickness and length can be fabricated this way

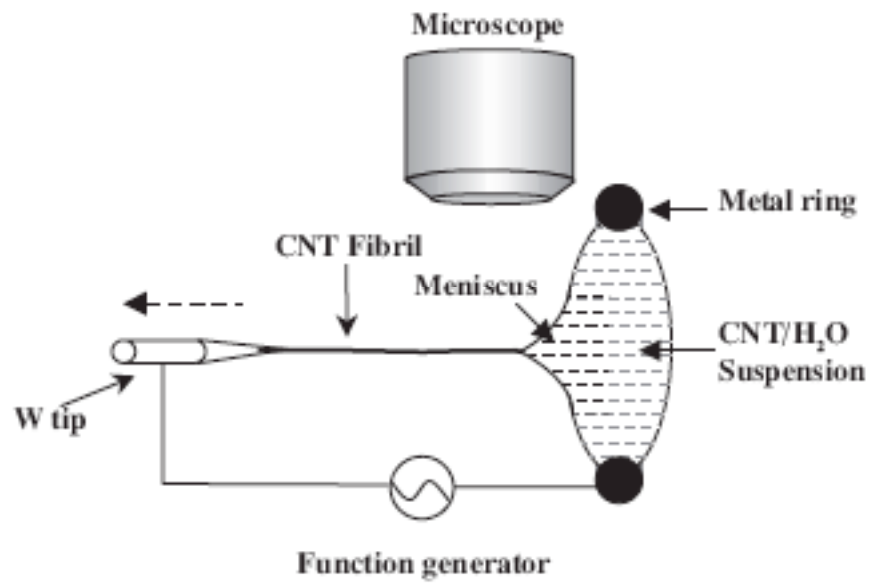


Figure 4.12 Schematic illustration of the dielectrophoresis process for assembly of CNT fibrils [21]

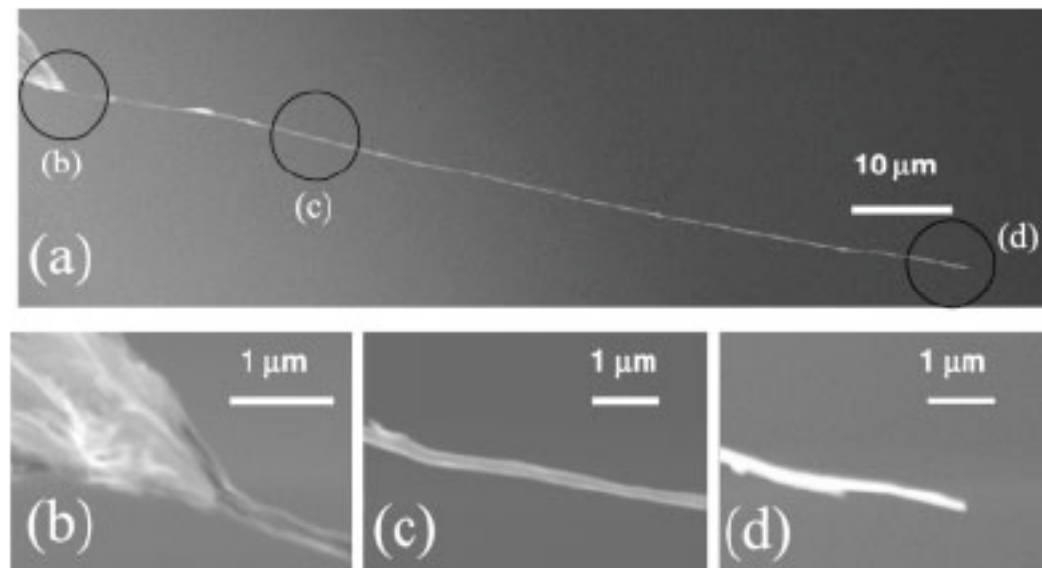


Figure 4.13 SEM images of CNT fibril assembled on the apex of an etched tungsten probe. (a) overall morphology; (b) The interface between the fibril and the W probe; (c) A mid segment of the fibril; (d) The end of the fibril. The concentration of the suspension used was 0.01mg/ml. [22]

#### **4.6.2 Application of CNT fibrils fabricated by Dielectrophoresis**

The CNT fibrils fabricated this way was found to have versatile applications. When a commercial atomic force microscope (AFM) probes was used as the probe electrodes, CNT fibrils will grow onto the apex of the probe. The attached CNT fibrils can provide the commercial silicon probes with improved lateral resolutions, excellent wear resistance, therefore longer life time and possibilities to probe high aspect ratio structures. [23,26, 27]

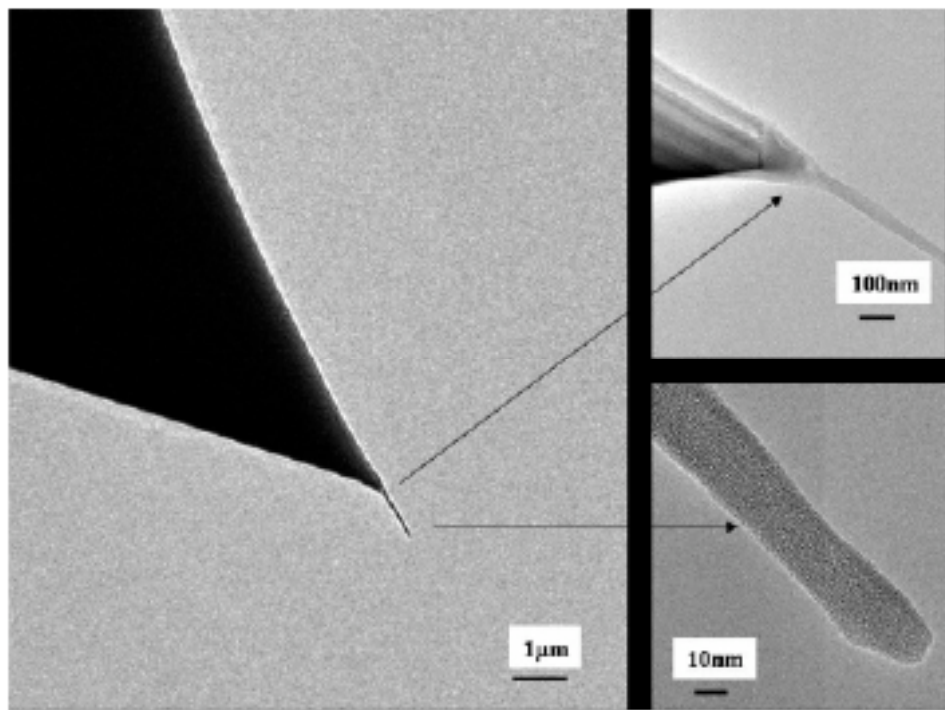


Figure 4.14 SEM images of CNT fibrils attached to commercial AFM probes by dielectrophoresis process. The SWNT bundle has a diameter of 20 nm near the tip and has conical geometry. [23]

Experiments have been done to demonstrate the probing depth of the CNT probes thus produced. An epoxy-based SU8 negative photoresist with a known pattern fabricated by photolithography was imaged using a conventional laboratory AFM (Digital Instruments NanoScope IIIa) operated in the tapping mode. A crosssection SEM image of the photoresist with 4.5-μm-deep trenches is shown in Figure 4.14 a. Figure 4.14 b and c shows the height

profiles measured from the same sample using a conventional Si AFM probe and the CNT probe, respectively. As shown in the Figure, a nearly vertical sidewall ( $87^\circ$ ) was mapped by the CNT probe but not by the conventional AFM probe. SEM shows that the CNT probe remained intact after the measurement.

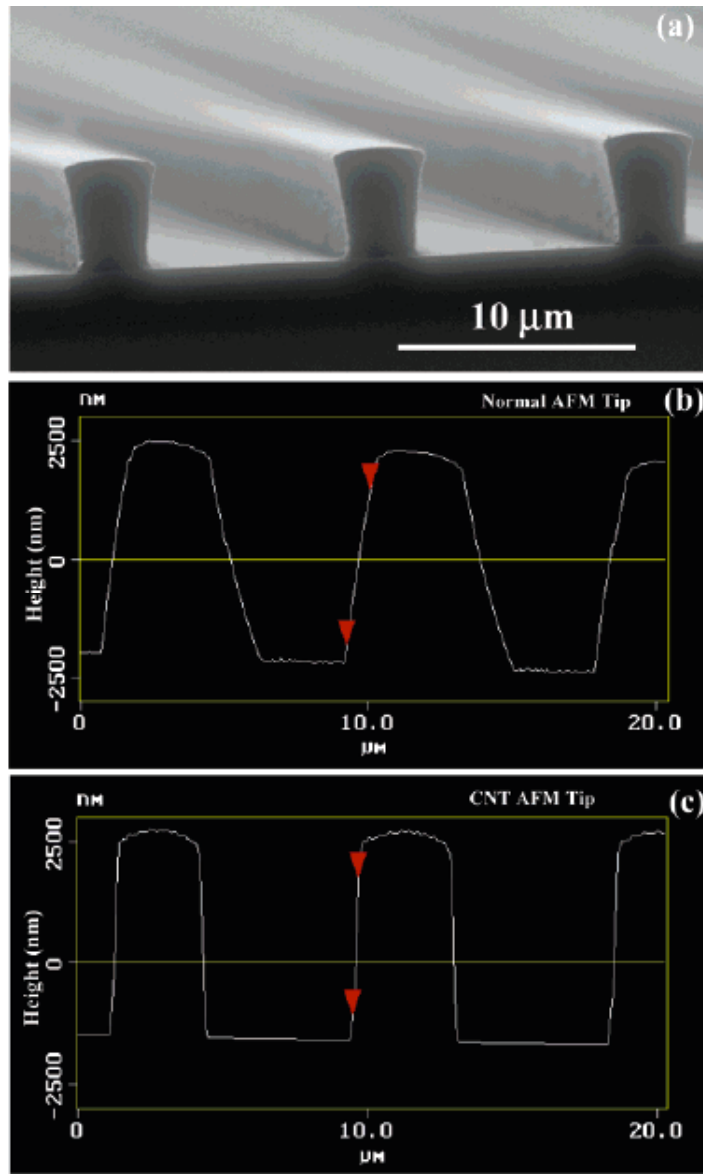


Figure 4.15 (a) Cross-sectional SEM image of a photoresist with 4.5- $\mu\text{m}$ -deep trenches used to test the CNT AFM probe. (b and c) Height profiles measured from the same sample by a conventional Si AFM probe and the CNT probe, respectively. As shown, a nearly vertical sidewall ( $87^\circ$ ) was mapped by the CNT probe but not by the conventional AFM probe. The CNT probe remained intact after the measurement. [23]

Field emission properties of the CNT fibrils assembled on tungsten probes were also studied. [24] Their capability of delivering currents that exceed  $10^5$  A/cm<sup>2</sup> in density and their strong adhesion to the metal supports give them potential to be used as field emission electron sources for precision vacuum electronic instruments such as electro microscopes.

The same method can also be used to assemble magnetic nanowires onto the apex of AFM probes to fabricate magnetic force microscopy (MFM) probes. [28]

#### **4.7 Conclusion**

Dielectrophoresis as a versatile technique was used to assemble CNTs into electrical interconnects, electron field emitters, and ultra-thin conducting fibrils. The relationship between the electrical field distribution and the CNT structures thus fabricated were studied. The versatile applications of ultra-thin CNT fibrils were explored and discussed.

The electrodynamics of the dielectrophoresis was discussed. The effects of external AC electrical field frequency on the mechanical motion of CNTs suspended in liquid media with different ionic conductivities and viscosities were investigated. Rough explanations of the experimental data were attempted by using the theories currently available. However to explain the observed phenomena clearly, more details need to be taken into consideration, and better theoretic model need to be used, and precise calculations need to be done.

#### 4. 8 References

- 1 *Synthesis, Structure, Properties, and Applications.* Topics in Applied Physics. Vol. 80. 2000, Springer-Verlag: Heidelberg.
- 2 H.A. Pohl, *Dielectrophoresis.* 1978, Cambridge: Cambridge University Press.
- 3 T.B. Jones, *electromechanics of Particles.* 1995, Cambridge: Cambridge Univ. Press.
- 4 M.P. Hughes, *Electrophoresis,* 2002(23): 2569-2582.
- 5 K. Yamamoto, S. Akita, and Y. Nakayama, *J. Phys. D: Appl. Phys,* 1998. **31:** L34.
- 6 X.Q. Chen, T. Saito, H. Yamada, and K. Matsushige, *Appl. Phys. Lett.,* 2001. **78**(23): 3714-3716.  
M.Diehl, S. N. Yaliraki, R. A. Beckmann, M. Barahona, J
- 7 M.S. Dresselhaus, G. Dresselhaus, and P. Avouris, *Carbon Nanotubes.* R. Angew. Chem. 2002, 114, 363-366
- 8 L. A. Nagahara, I. Amlani, J. Lewenstein, R. K. Tsui, *Appl. Phys. Lett.* 2002, 80, 3826-3828
- 9 R. Krupke, F. Hennrich, H.b. Weber, D. Beckmann, O. Hampe, S. Malik, M. M. Kappes, H.v. Lohneysen, *Apl. Ahys. A* 2003, 76, 397-400
- 10 R. Krupke, F. Hennrich, H. B. Weber, M. M. Kappes, H.v. Lohneysen, *Nano Letters,* 2003, 3, 1019-1023
- 11 [www.dielectrophoresis.org](http://www.dielectrophoresis.org/) /PagesMain/DEP.htm
- 12 H. Morgan, N. G. Green. *Journal of Electrostatics* 42, 1997, 279-293
- 13 M. J. O'Connelll, S.M. Bachilo, C. B. Huffman, V.C. Moore, et. al. *Science* **297** (2002), 593
- 14 R. Krupke, f. Hennrich, H.v. Lo'hneysen, M.M. Kappes, *Science* **301**, (2003), 344
- 15 S. Baik, M. Usrey, L. Rotkina, M. Strano, *J. Phys. Chem. B* **108** (2004) 15560-15564
- 16 R. Krupke, F. Hennrich, *J. Phys. Chem. B* **109** (2005) 17014-17015
- 17 L.M. Ericson, P. E. Pehrsson, *J. phys. Chem. B* **109** (2005) 20276-20280
- 18 K. H. Bhatt and O. D. Velev *Langmuir,* **20**(2), (2004), 467-476

- 19 H-Y. Hsu, N. Sharma, R. S. Ruoff, N. A. Patankar, *Nanotechnology* **16**, (2005) 312-319
- 20 K. D. Hermanson, S. O. Lumsdon, J. P. Willams, E. W. Kaler, O. D. Velev , *Science* **294** (2001), 1082-1-86
- 21 O. Zhou, H. Shimoda, B. Gao, S.J. Oh, L. Fleming, G.Z. Yue, *Acc. Chem. Res.* **35**, (2002), 1045-1053.
- 22 J. Tang, B. Gao, H. Geng, O. D. Velev, LC. Qin, O. Zhou. *Adv. Mater.* **15**, No.16, (2003), 1352-1355
- 23 J. Tang, G. Yang, Q. Zhang, A. Parhat, B. Maynor, J. Liu, LC. Qin, O. Zhou. *Nano. Lett.* **5**, No.1 (2005), 11-14
- 24 J. Zhang, J. Tang, G. Yang, Q. Qiu, LC. Qin, O. Zhou, *Adv. Mater.* **16**, No. 14, (2004), 1219-1222
- 25 W. K. Liu, E.G. Karpov and H.S. Park. “Nanomechanics and Materials: Theory, Maltiple Scale Analysis and Applications”, John Wiley and Sons, ISBN 0-470-01851-8, (2006)
- 26 T. Larsen, et al. *Appl. Phys. Lett.* **80**, (2002) 1996-1998
- 27 Binnig, G.; Quate, C. F.; Gerber, C. H. *Phys. ReV. Lett.* **56**, (1986) ,930.
- 28 G. Yang, J. Tang, S. Kato, Q. Zhang, L.C. Qin, M. Woodson, J. Liu, J.W. Kim, P. T. Littlehei, C. Park, *Appl. Phys. Lett.* **87**, (2005) 123507

# **Chapter 5 Automation and Optimization of the fabrication process of CNT Fibrils**

## **5.1 Introduction**

The applications of ultra-thin CNT fibrils have been discussed in last chapter. The CNT AFM probes have been shown to give higher spatial resolution, possibilities to probe structures with high aspect ratios and to have significantly longer life times [1,2] And the excellent field emission properties of the CNT fibrils assembled on tungsten probes also give them potentials to be used as field emission electron sources for precision vacuum electronic instruments such as electro microscopes.

Several methods have been developed to either mount or directly grow CNTs on the apex of a sharp probe. Picking up individual CNT or bundles and “glue” them onto the apex of AFM probes by passing a current between the probe and CNT [3,4], by magnetic force [6] or by simply applying glue onto the AFM pyramid [5] have produced some of the early CNT probes. All these method need the aid of electron microscope or AFM imaging. Such techniques are in general time consuming and are not viable for the production of

commercial quantities. CNTs can also be grown directly on the apex of a commercial AFM probe that is selectively deposited with catalysts by the chemical vapor deposition (CVD) technique. [7] This approach can potentially lead to batch production of entire wafers of CNT AFM probes. [8] However this method has shown its limitations by the nonuniformity of the lengths and angles CNTs thus grown. [9] To control the length of the CNTs grown, a technique has been developed to etch CNTs on individual AFM tips by an electrical pulse.[9]

We have previously talked about the fabrication of CNT fibrils on sharp probes by dielectrophoresis. Although dielectrophoresis has been demonstrated to be an efficient method to assemble nanotubes and nanowires on the apex of sharp probes with relatively controlled length and orientation. A precise control over the assembly process is lacking by using the original manual experimental setup. However short length and small diameters are highly desirable for decreasing thermal vibrations and increasing the probe resolution.

There's report about attaching individual MWNTs onto AFM probes [10]. Parameters like the amount of CNT suspension used, the concentration of the suspension and distance between the probe tip and the counter electrode were precisely controlled to gain a precise control over the dielectrophoretic process. However not much success was gained, because they failed to control the assembly time precisely and the assembly speed is very rapid. A numerical simulation was done<sup>18</sup>, and it found that the CNT's position in the suspension and its arrival time at the apex of the probe were critical parameters for the assembly process.

Therefore, methods are researched to control the dielectrophoretic process instantaneously and automatically. Possible ways to detect the wetting of probe end by the suspension electronically were studied. Electronically devices were used and computer programs were

written to control the whole process in a precise way once the wetting is detected.

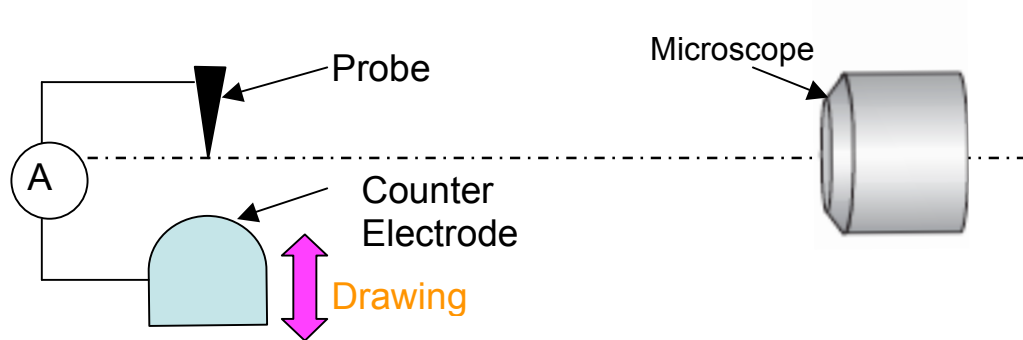
## 5.2 Problems of the Original Experimental Setup and Solutions

The process of fabricating CNT fibrils by dielectrophoresis was described in last chapter. The original experimental setup is illustrated in Figure 5.1. A sharp probe and counter electrode with relatively much larger area was used. The CNT suspension was contained in the counter electrode. An optical microscope was used to observe the whole process. The counter electrode was put on a manual linear stage, and it was aligned with the microscope so that the when a droplet of suspension is put into the electrode, the highest point can be in focus. The probe was mounted on a three dimensional stage. Then it was aligned with the microscope. The highest point of the suspension was first focused; Then the suspension was moved down and out of the imaging area. Finally the probe end was focused by using the translational stage without turning the focusing knob of the microscope. The microscope was connected with a CCD camera and the images were cast on a computer screen. After the alignment, the counter electrode was slowly elevated until the surface of the suspension was seen on the screen. Then the suspension was elevated more carefully. Until the probe end was seen to be wetted by the suspension, the suspension was retracted as soon as it can be achieved by human hand. In the whole process the function generator is on continuously. Dielectrophoresis starts from the moment when the probe is in contact with the suspension, and ends at the moment when the suspension is totally retracted from the probe. Due to the surface tension, the counter electrode need to travel a certain distance before the probe is out

of contact with the suspension.

It is very hard to get a clear focus on the highest point of the suspension. Quite often the probe end and the surface of the suspension were not in the same focal plane. And this makes very hard to judge when the probe end is wetted by suspension. The suspension sometimes was elevated far beyond the critical point, where it wets the probe end, without being noticed. The dielectrophoresis process is a very rapid process, quite often when the probe is pulled out of the suspension, there's already a CNT fibril attached to it with length too long than it is desired. To get finer control over the process, an automatic experimental setup is needed to detect the wetting instantaneously and electronically and to give very precise control over the assembly time and retraction speed.

## Side View



## Top View

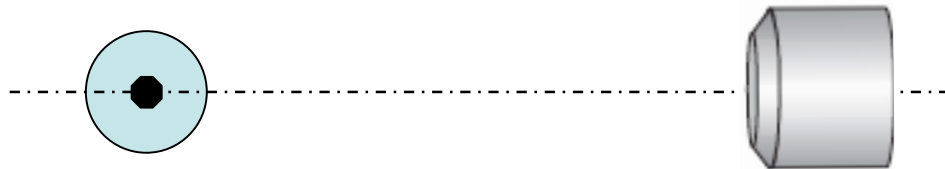


Figure 5.1 Schematics of the manual experimental setup for fabrication of CNT fibrils by dielectrophoresis.

In the automated experimental setup, the change in the system capacitance was monitored by a capacitance meter and utilized as an indicator to detect the wetting of the tip by the suspension. A programmable linear translational stage was used to control the retraction of the suspension and a computer controllable relay was added to isolate the function generator from and loop and time the process very precisely. Then all the devices and apparatus involved are linked to a computer and a lab-view program was written to control them accordingly.

Automation of the dielectrophoretic process will not only provide finer control over the length and diameter CNT fibrils thus fabricated, also provide opportunities to study and optimize the fabrication process due the precise control over the parameters. Overall it also improves the fabrication efficiency of the CNT fibrils. When the wetting is detected electronically, optical image of the probe is not required and the production of CNT AFM probes in scale of a whole wafer becomes possible.

The fluctuation of the concentration of the CNT suspension also makes it difficult to control the assembly process precisely. Because even when the same suspension was used each time the probe won't see the same concentration of CNTs with the same distance to it. Studies still need to be done to further improve the homogeneity of the suspension. However, it is thermal dynamically impossible to eliminate the local concentration fluctuation. Therefore even when automatic experimental setup is used, the fabrication is still a statistical process. Therefore a systematic study of the effects of parameters is need to find out empirical relationships may guide the fabrication process and give us more control over the process.

## 5.3 Automation of the Fabrication Process

### 5.3.1 Experimental Setup

The experimental setup is illustrated in Figure 5.2. A sharp probe (commercial AFM probe or etched tungsten tip) is mounted on a holder, which is attached to a manual 3-D translational stage. Aligned with the end of the probe, a metal bowl is attached to a motorized 1-D translational stage (Newmark system, Microslide Series, 20nm step resolution). A function generator (Wavetek, Model 270) is connected to the probe and the metal bowl using a relay. A HP model 4280 capacitance meter is used to monitor the system capacitance. The motorized linear stage, function generator, capacitance meter and relay are all connect with a PC and can be controlled by a Labview program.

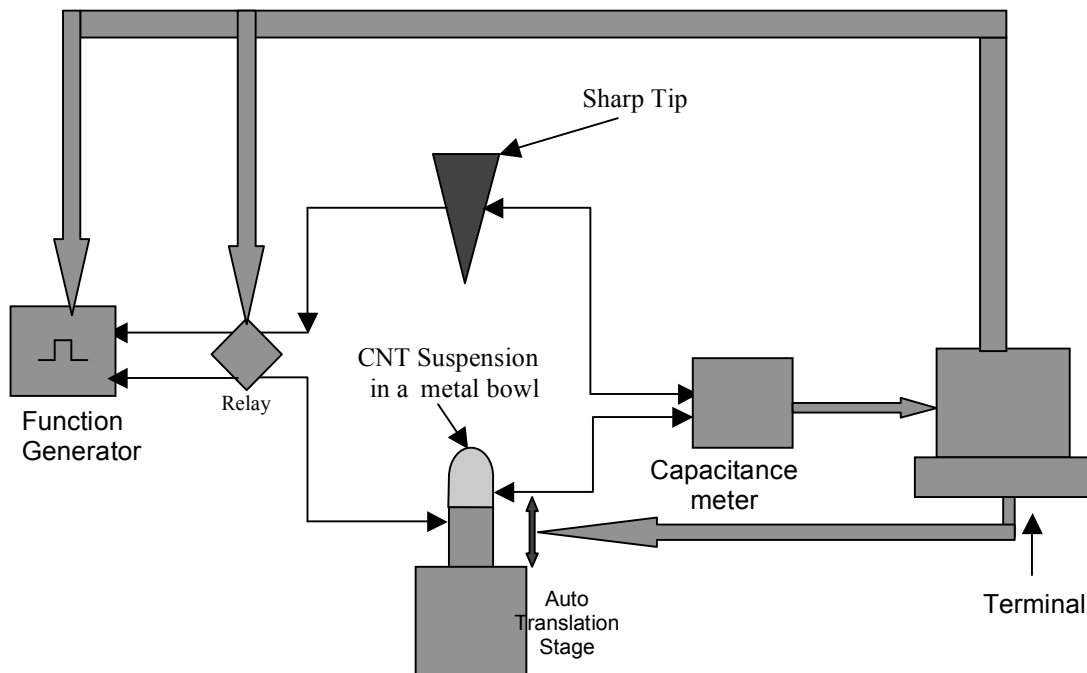


Figure 5.2 Schematic illustration of the automatic experimental setup used to fabricate CNT fibrils by dielectrophoresis.

Small-diameter multi-walled carbon nanotubes (MWNT) used in this experiment were produced by CVD method. (Figure 5.3 (a)). The as produced materials were sonicated in hydrochloride acid to remove catalyst support. Then the CNTs were oxidized to desirable length using strong acid. The oxidation process is described in chapter 3. The length of CNTs used in this study ranges from 0.5 to 1  $\mu\text{m}$ . Around 50% of the CNTs have uniform length about 0.6 to 0.7  $\mu\text{m}$ . Then the CNTs were dispersed in DI water in a certain concentration (Figure 2b). When the suspension of concentration 0.1mg/ml was centrifuged at 15000 rpm for an hour and precipitate discarded, the supernatant (shown in Figure 2c) is considered standard suspension in our experiments. A droplet of CNT suspension was put into the metal bowl. The relay is in off position originally and the capacitance between the probe and the metal bowl is constantly monitored.

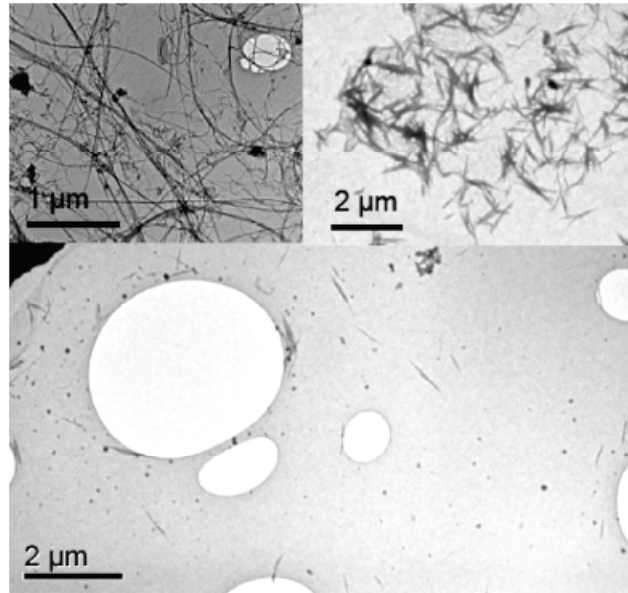


Figure 5.3 TEM images of CNTs used in this study. (a) Purified long carbon nanotubes; (b) Short nanotube suspension before centrifuge; (c) Short nanotube suspension after centrifuge.

### 5.3.2 Change in Capacitance of the System

Due to complicated wiring of the system and irregular shapes of both electrodes, the capacitance can only be roughly modeled in Figure 5.4. From equation (1) a jump in the slope of the capacitance versus distance curve is expected when the probe moves towards the metal bowl and approaches the suspension surface due to the difference in permittivity of water and that of air.

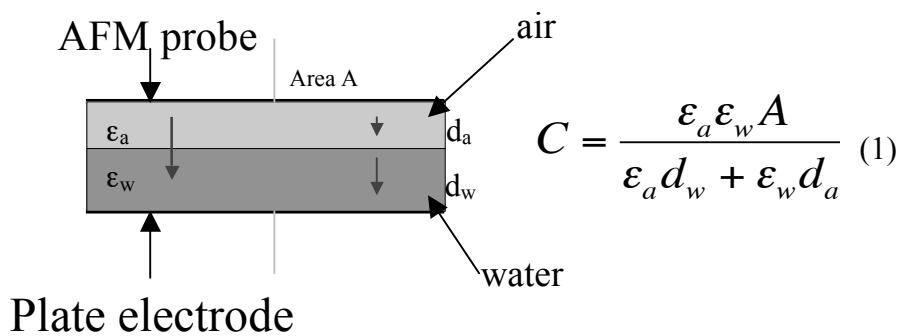


Figure 5.4 A model used to study the change in capacitance of the system. Where  $\epsilon_a$  is the permittivity of air and  $\epsilon_w$  that of water;  $d_a$  is distant from probe end to the surface of the suspension and  $d_w$  is depth of the suspension.

The plate electrode is moving gradually towards the probe by micro steps. The change in system capacitance is  $\Delta C = \frac{\Delta d_a}{80\epsilon_0 d_a^2}$  before the probe reaches the suspension and becomes  $\Delta C = \frac{\Delta d_w}{\epsilon_0 d_w^2}$  after it reaches the suspension. The change in system capacitance predicted by this model is plotted in figure 5.5 (a), While the experimental result is plotted in figure 5.5 (b)

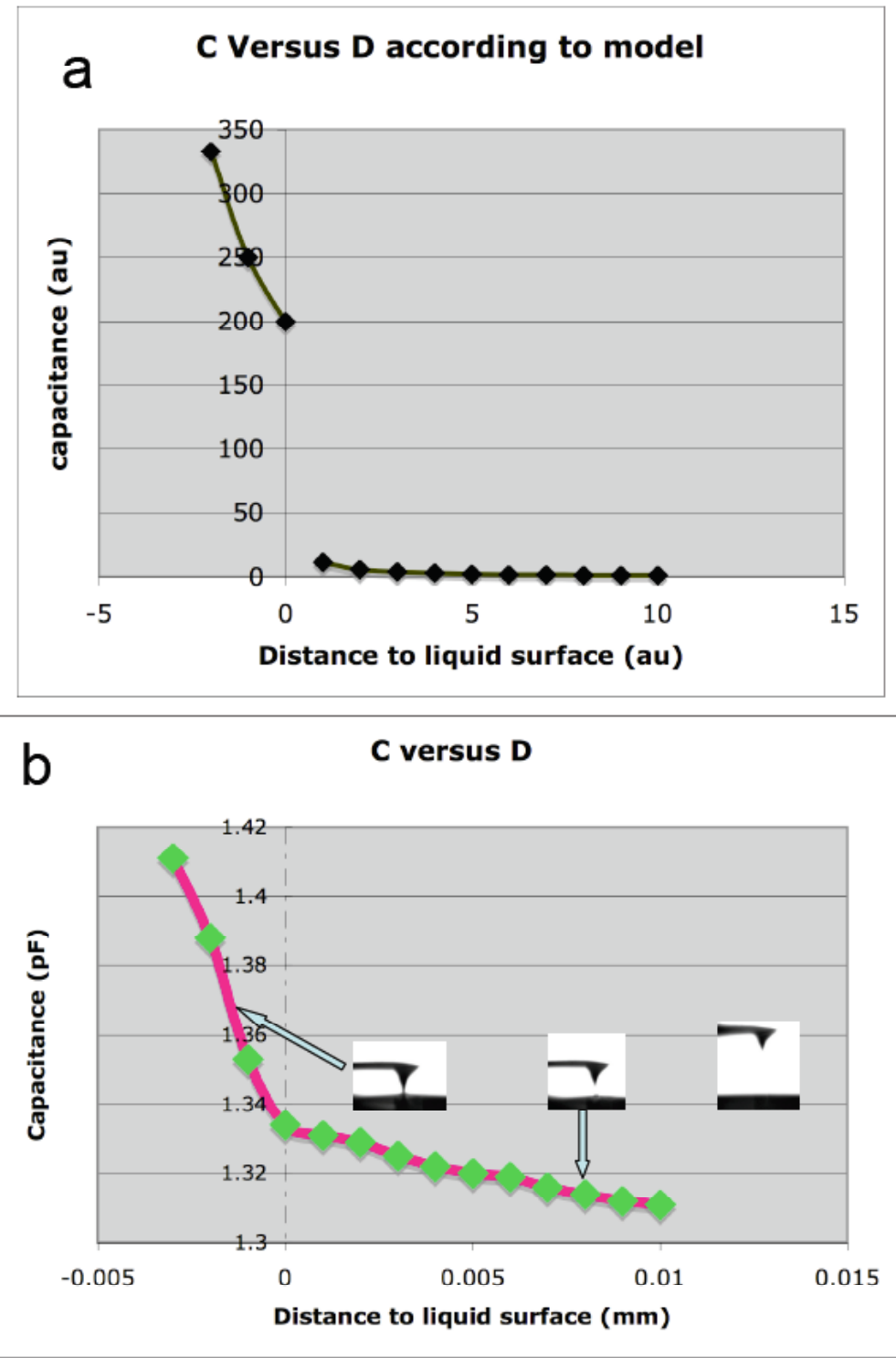


Figure 5.5 Change in system capacitance while the probes move towards the suspension.  
 (a) Capacitance versus distance curved predicted by the model in figure 5.4; (b) Capacitance versus distance curves measured in experiment.

A huge jump of the system capacitance, at the moment the probe moves the micro-step and reaches the suspension, is predicted by the model. However a relatively gradual change is measured during experiment. The discrepancy is caused by the difference in geometry. When the two electrodes are both flat panels, there will be a huge increase in capacitance when the moving electrode reaches water surface. However in our experiment, the moving electrode is a sharp probe. When it reaches the water surface, the actual surface area that is in contact with the water is very small. Therefore no huge increase is observed at this point. However due to the wetting of probe by the suspension there's still a detectable change in the system capacitance. And the model also predicted the change in the slope of the curve before and after the moving electrode approaches water surface. This change will be utilized in our experiment.

### ***5.3.3 Lab View Program***

A lab view program is written to realize the automation of the fabrication process. A probe is first mounted on the stage, and a droplet of suspension is put into the metal bowl, which is used as a counter electrode. The function generator is turned on with almost zero output and was connected to the loop using a relay. The relay was set on off position originally. Then the program is started. The motorized translational stage is designed to move by micro-steps as accurate as 20nms per step. The system capacitance is measure after every step the stage moves, then the data is transferred to the computer to be compared with the previous data. When a abrupt change in the system capacitance is detected, the motorized stage is stopped. At the same the function generator is included in the circuit by turning on the relay. Then the computer set the function generator to output desired amplitude, frequency and wavefunction

of the AC field. Certain time is allowed for dielectrophoresis of CNTs before the suspension was retracted from the probe at certain speed for certain time, then retracted to zero position at the maximum speed. Simultaneously, the relay is turned off the whole process is terminated. A microsecond precision of the time allowance and 20nm/sec precision of retraction speed is realized by using the automatic setup. The program flow chart is shown in figure 5.5

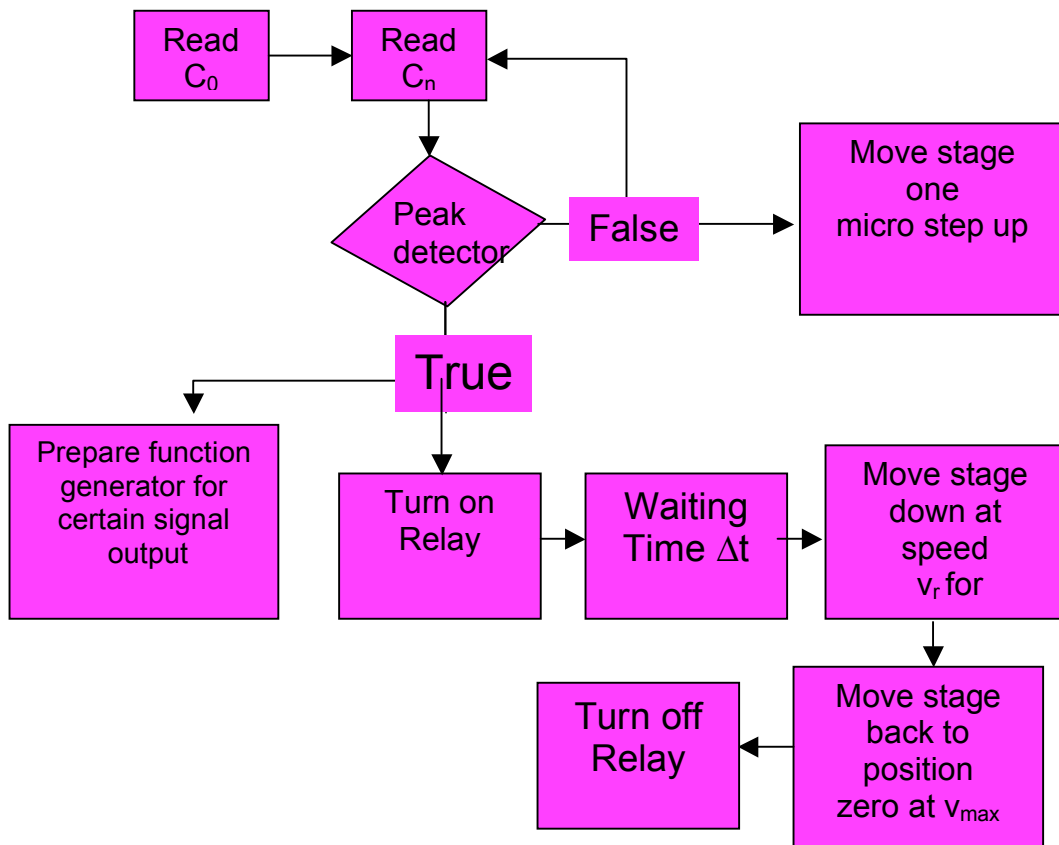


Figure 5.5 Flow chart of the Lab View program, by which the automation of the fabrication process is realized.

## **5.4 Parameter Study using the Automated Experimental Setup**

The automated experiment setup provides the possibility for a more precise control over several parameters that are essential for the CNT assembling process under the AC field. This also makes a systematic study of the parameters possible.

The length and thickness of CNT fibrils fabricated by dielectrophoresis largely depend on local supply of CNTs around the probe area when the probe is drawn from the suspension. Because during the assembling process, those CNTs surrounding the probe end will be pressed by the meniscus formed around the probe and attach to the probe when the probed is pulled from the suspension. While the local concentration of the CNTs depends on the time allowed ( $\Delta t$ ) the CNTs in the bulk suspension to move towards the probe area and the moving speed of the CNTs, which depends on the gradient of the field strength and dipole moment of CNTs. When the suspension is retracted slowly, a continuous growth of CNTs fibrils can be observed. The thickness of the fibrils thus grow is often related with the retraction speed of the suspension.

Parameters such as time allowance for the dielectrophoresis of CNTs ( $\Delta t$ ), retraction speed ( $V_r$ ) and voltage of the AC field ( $V_{AC}$ ) are studied and the empirical relationships between this parameters and the length and thickness of the CNT fibrils are plotted.

### 5.4.1 Effects of Waiting Time ( $\Delta t$ )

In Figure 5.6 the effects of  $\Delta t$  are shown. In all the following experiment the standard suspension was used. Applied AC field has an amplitude of 2 volt, and the probe was withdrawn from the suspension right after  $\Delta t$ . In (a1) to (a4) the probe was retracted as soon as it approached the suspension and the relay was snap on and then off in a few milliseconds. By using standard suspension only 1/3rd of probes are found to have CNTs attached on them. The fibrils are believed to be composed of individual bundles of CNTs, because their length is in the range of individual CNT bundle length used in this study. Therefore fibril lengths vary according to the average length of starting materials. In (b1) to (b4) the probe was retracted 2 second after it was wetted by the suspension. Average length of attached fibrils is found to be 1.5 to 2  $\mu$ ms. In (c1) to (c4) 5 second waiting time was allowed before the assembling process was terminated. Fibril lengths were more uniform and average to 3.5  $\mu$ m.

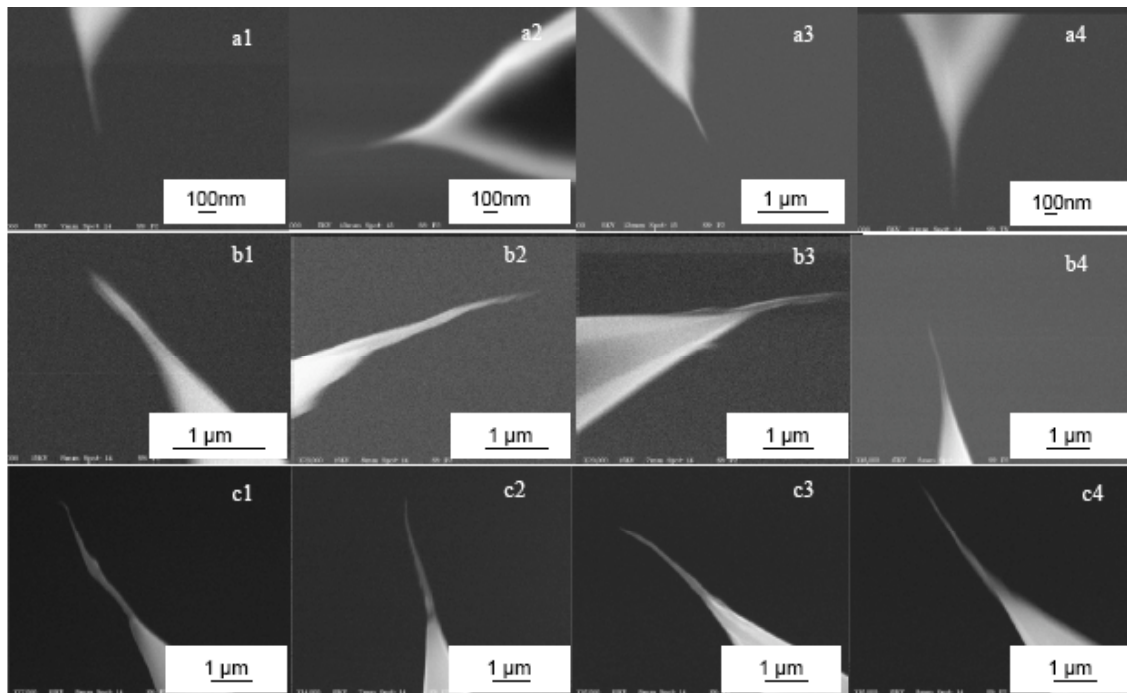


Figure 5.6 SEM images of CNT fibrils grown on commercial AFM probes while different  $\Delta t$  is applied. (a)  $\Delta t$  equals to zero, the probe is retracted right after it reaches the suspension;

(b)  $\Delta t$  equals to 2 second, (c)  $\Delta t$  equals to 5 second. The same CNT suspension and AC voltage was used. The probe was retracted after the waiting at maximum speed.

The experimental result clearly shows that there is a dependence of fibril length on the waiting time. When no waiting time is allowed, only CNTs in the vicinity of the probe will be attached to the probe when the probe is drawn from the suspension. And due to the low concentration of the suspension used, quite often there is no CNT attached to the probe when the probe is withdrawn from the suspension. In one third of cases individual CNT bundles will attach to the probe. Therefore the average length depends on the starting material.

While when longer waiting time is given, fibrils with longer and more uniform length were fabricated. One possible explanation is that when waiting time is long enough, local concentration is high enough to overrule the local concentration fluctuation of the suspension, therefore provides a more uniform supply of CNTs. The average length of CNT fibrils versus waiting time is plotted out in Figure 6d. The average length is found to be almost linear proportional to the waiting time while the waiting time is shorter than 5 seconds. However waiting time up 10 seconds was tried, when the standard CNT suspension and maximum retraction speed were used, CNT fibrils no longer than 4  $\mu\text{m}$  were fabricated. There seems to be a saturation of the waiting time effects. This may indicate that local concentration of CNT suspension has reached saturation. And when the probe is withdrawn from the suspension at maximum speed, the local CNTs are depleted, however CNTs in the bulk suspension don't have the time to move to the local area and attach to the end of the fibril.

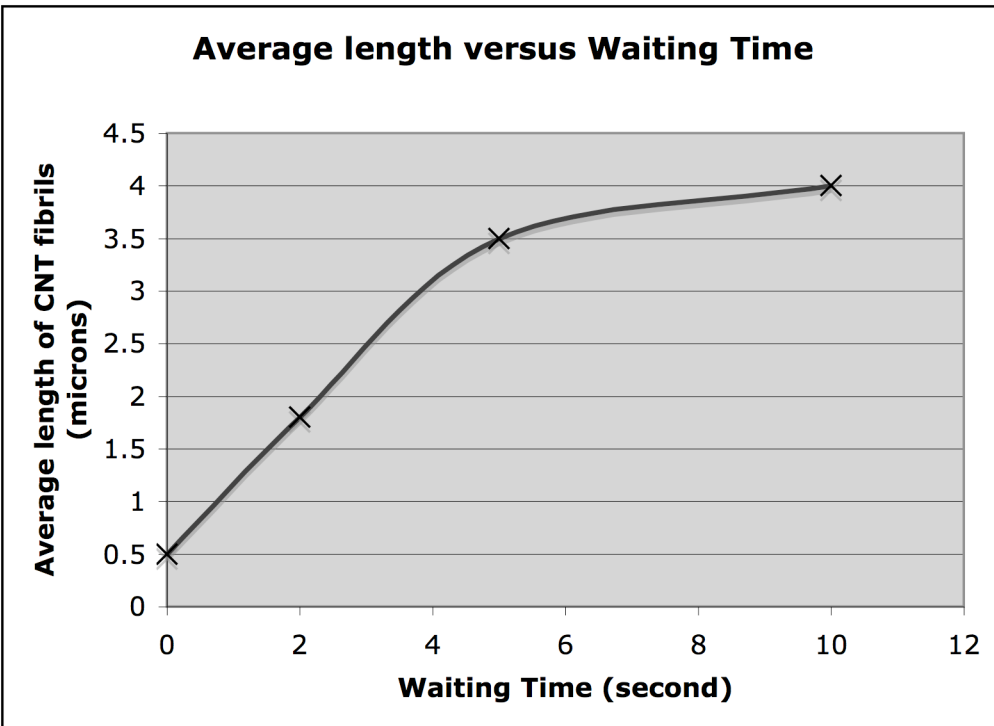


Figure 5.7 Average lengths of CNT fibrils plotted against waiting time. The average lengths were proportional to  $\Delta t$  when  $\Delta t$  is shorter than 5 second, then the average length changes little when  $\Delta t$  was further increased.

#### **5.4.2 Effects of Retraction Speed ( $V_r$ )**

When the probe is drawn from the suspension at a speed lower than some threshold value, a continuous growth of the fibril can be achieved [11]. The retraction speed actually can be interpreted as waiting time allowed per unit length of the movement of the probe. The thickness of CNT fibrils is found to depend on retraction speed. Figure 7 shows the experimental results. In (a) a  $V_r$  of  $1\mu\text{m/sec}$  was used; In (b) a  $2\mu\text{m/sec}$   $V_r$  was used. In (c)  $V_r$  of  $1\mu\text{m/sec}$  was used first then changed to  $2\mu\text{m/sec}$ . A clear correlation of the fibril thickness and the  $V_r$  was observed.

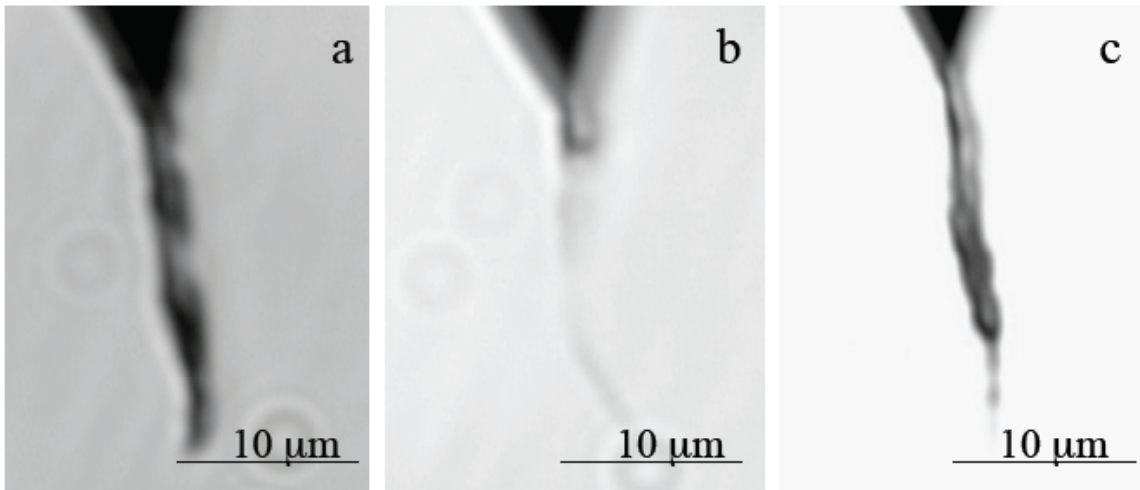


Figure 5.8 Optical images of CNT fibrils fabricated when different retraction speeds were applied. (a)  $V_r$  of  $1\mu\text{m/sec}$  was applied; (b)  $V_r$  of  $2\mu\text{m/sec}$  was applied; (c)  $V_r$  of  $1\mu\text{m/sec}$  was first used then was changed to  $2\mu\text{m/sec}$ , a continuous growth of CNT fibrils with different thickness was observed. The same CNT suspension, initial waiting time and AC voltage was used.

A clear correlation of the fibril thickness and the  $V_r$  was observed. The fibril thickness versus  $V_r$  is plotted in Figure 5.9 (a). In the figure 5.9 (b) the fibril thickness is plotted against the inverse of  $V_r$ , the relationship is found to be almost linear. When retraction speed gets higher than  $3\mu\text{m/sec}$ , no continuous fibril can be fabricated.

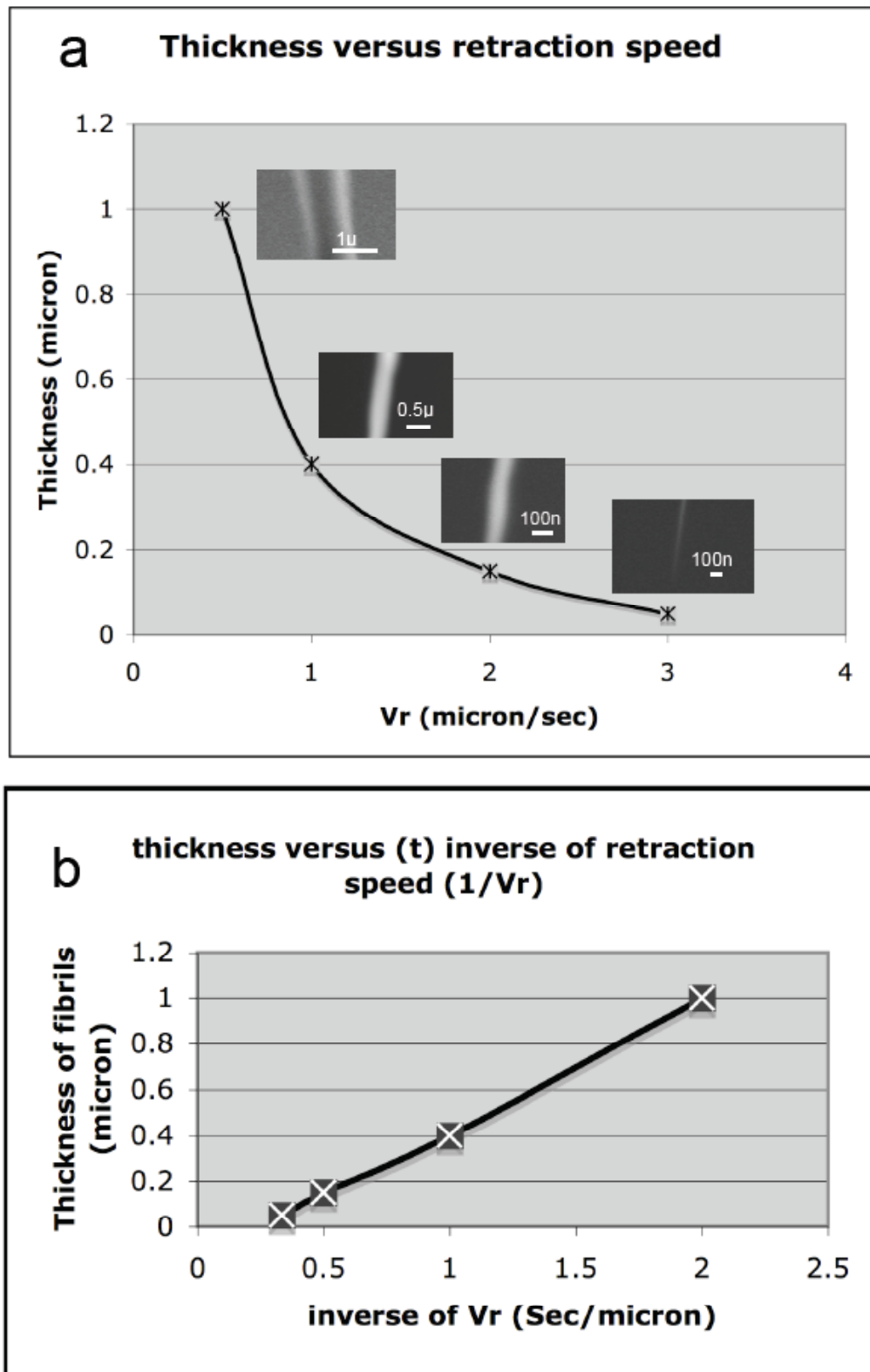


Figure 5.9 Fibril thickness plotted again retraction speed (a) and inverse of retraction speed. (b)

### ***5.4.3 Effects of AC Voltage ( $V_{AC}$ )***

The effects of voltage applied between two electrodes are also studied. The results are shown in Figure 8. In (a1) to (a3) a 2V AC field amplitude was used. Only thin and clean probes were fabricated. In (b1) to (b3) an amplitude of 5V was used. Some of the CNT fibrils were found to be thin and clean, however thick tips as in b1 were also fabricated. In (c1) to (c3) 10V was used, most probes fabricated this way were found to be rugged, which indicate involvement of particles and thicker CNT bundles.

The dielectrophoretic force applied on CNTs and particle impurities in the suspension, which determines the moving speed of CNTs and particles, increases when the dipole moments and the field strength gradient increases. In our experiment, when the voltage is increased, the configuration of the electrodes remain unchanged because the same metal bowl and commercial AFM probes with the same radii were used, therefore though the field strength is increased accordingly, the field strength gradient remained unchanged. Although CNTs with larger polarizability therefore larger dipole moment moves faster than particles, when high voltage is applied, particles acquire large enough dipole moment and will move fast enough and reach the probe area within the allowed period of time.

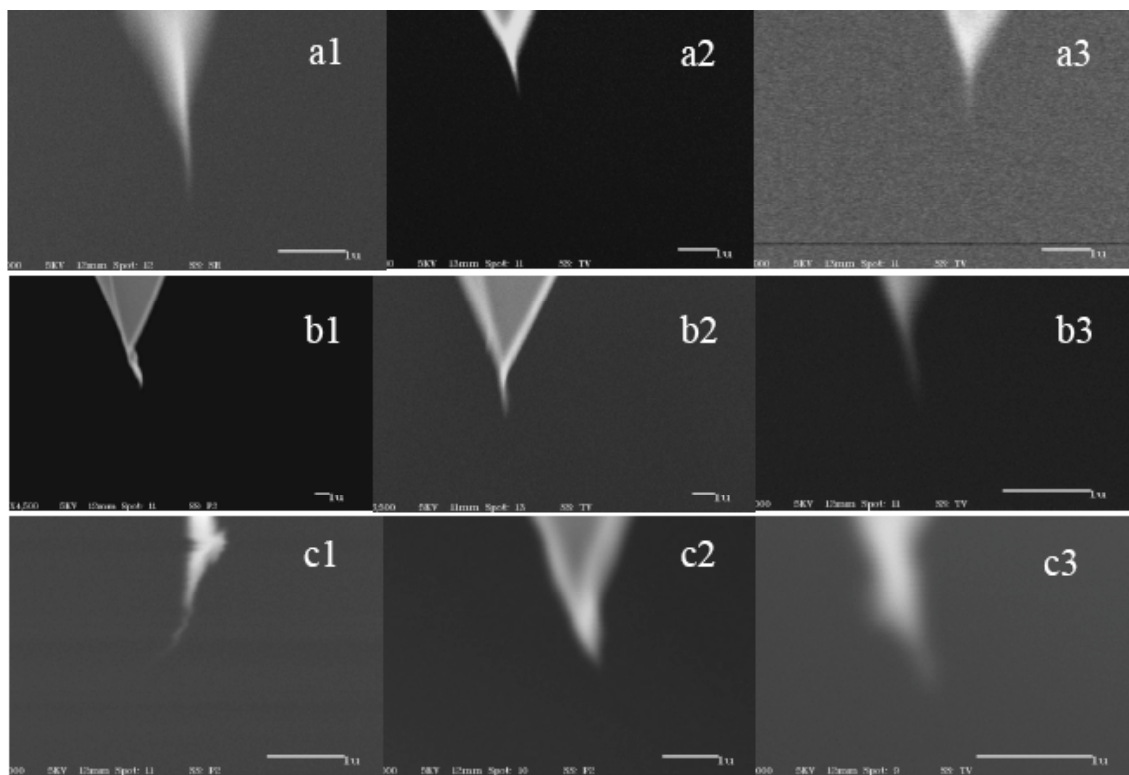


Figure 5.10 SEM images of CNT fibrils grown on commercial AFM probes. (a) AC field of 2 V was applied; (b) AC field of 5 V was applied; (c) AC field of 10 V was applied. The same CNT suspension was used and the probe was retracted from the suspension at maximum speed right after it reached the suspension.

## 5.5 Conclusion

In conclusion, to realize automation of the CNT fibrils fabrication process by dielectrophoresis, A programmable capacitance meter is used to monitor the change in system capacitance, and the abrupt change in system capacitance when the probe is wetted by

the suspension is used to detect the wetting process; A motorized translational stage is used to control the motion of the suspension electronically; A programmable function generator is connected to the probe and counter electrode by a relay to precisely control the assembly time.

A precise control over the fabricated process is gained. However the whole process is still a statistical process due to the concentration fluctuation of the CNT suspension. Therefore, effects of essential parameter such as time allowance, retraction speed and applied voltage were studied; And empirical relationships between these parameters and the length, thickness of the CNT fibrils thus fabricated were plotted. Under the guide of these empirical relationships, finely control over the length and thickness of the CNT fibrils is gained.

## **5.6 References:**

1. T. Larsen, et al. *Appl. Phys. Lett.* **2002**, 80, 1996-1998
2. Binnig, G.; Quate, C. F.; Gerber, C. H. *Phys. Rev. Lett.* **1986**, 56, 930.
3. Dai, H. et al. *Nature* **1996**, 384, 147.
4. Akita, S. et al. *J. Phys. D: Appl. Phys.* **1999**, 32, 1044.
5. Hafner, J. H. et al. *J. Phys. Chem. B* **2001**, 105, 743.
6. Hall, A. et al. *Appl. Phys. Lett.* **2003**, 82, 2506.
7. Hafner, J. H.; Cheung, C. L.; Lieber, C. M. *Nature* **1999**, 398, 761.
8. Dai, H.; C. F. Q.; Chen, R. J. Carbon Nanotubes and Methods of Fabrication Thereof Using a Liquid-Phase Catalyst Precursor. U.S. Patent 6,401,526, 2002.
9. Wade, L. A. et al. *Nano Lett.* **2004**, 4, 725-731.
10. H. W. Lee, et al. *Review of Scientific Instruments* **2005**, 76, 046108
11. J. Tang, et al. *Adv. Mater.* **2003**, 15, No.16, 1352-1355